

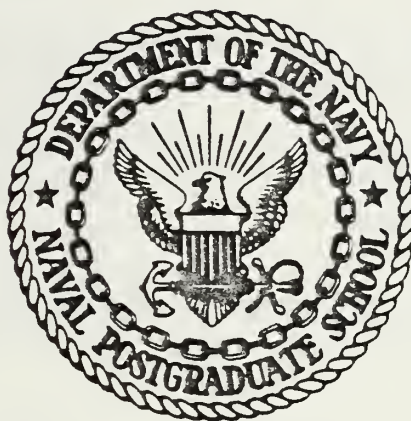
DESIGN CONSTRUCTION AND EVALUATION  
OF A TEM TRANSMISSION CELL  
FOR FIELD PROBE CALIBRATION

Stavros Ioannis Mpoukis



# NAVAL POSTGRADUATE SCHOOL

## Monterey, California



# THESIS

DESIGN CONSTRUCTION AND EVALUATION  
OF A TEM TRANSMISSION CELL  
FOR FIELD PROBE CALIBRATION

by

Stavros Ioannis Mpoukis

December 1979

Thesis Advisor:

O.M. Baycura

Approved for public release; distribution unlimited.

T194267

NAVAL POSTGRADUATE SCHOOL  
Monterey, California 93940

Rear Admiral Tyler F. Dedman  
Superintendent

Jack R. Borsting  
Provost

This work was made possible by using the measurement probes of the BDM Corporation that is resident at the Naval Postgraduate School.



UNCLASSIFIED

SECURITY CLASSIFICATION OF THIS PAGE (When Data Entered)

## REPORT DOCUMENTATION PAGE

READ INSTRUCTIONS  
BEFORE COMPLETING FORM

1. REPORT NUMBER NPS62-79-013		2. GOVT ACCESSION NO.	3. RECIPIENT'S CATALOG NUMBER
4. TITLE (and Subtitle) Design Construction and Evaluation of a TEM Transmission Cell for Field Probe Calibration		5. TYPE OF REPORT & PERIOD COVERED Master's Thesis; December 1979	
7. AUTHOR(s) Stavros Ioannis Mpoukis		6. PERFORMING ORG. REPORT NUMBER	
9. PERFORMING ORGANIZATION NAME AND ADDRESS Naval Postgraduate School Monterey, California 93940		8. CONTRACT OR GRANT NUMBER(s)	
11. CONTROLLING OFFICE NAME AND ADDRESS Naval Postgraduate School Monterey, California 93940		10. PROGRAM ELEMENT, PROJECT, TASK AREA & WORK UNIT NUMBERS	
14. MONITORING AGENCY NAME & ADDRESS (if different from Controlling Office)		12. REPORT DATE December 1979	
		13. NUMBER OF PAGES 116	
		15. SECURITY CLASS. (of this report) Unclassified	
		15a. DECLASSIFICATION/DOWNGRADING SCHEDULE	
16. DISTRIBUTION STATEMENT (of this Report)  Approved for public release; distribution unlimited.			
17. DISTRIBUTION STATEMENT (of the abstract entered in Block 20, if different from Report)			
18. SUPPLEMENTARY NOTES			
19. KEY WORDS (Continue on reverse side if necessary and identify by block number)  TEM cells, expanded bandwidth, absorber loaded, probe calibration			
20. ABSTRACT (Continue on reverse side if necessary and identify by block number)  This paper discusses the design, construction and evaluation of a transverse electromagnetic (TEM) transmission cell for accurate generation of broad-band susceptibility test fields within a shielded environment.  A 0.3 x 0.5 x 1.0 m TEM cell, constructed at the Naval Postgraduate School (NPGS), was designed to operate as a 50-ohm			



#20 - ABSTRACT - CONTINUED

impedance-matched system and was used for calibrating electromagnetic field probes. According to the basic design, uniform and standard TEM fields can be generated inside the cell for frequencies lower than the cutoff frequency of the device. The high frequency multimode effects can be suppressed by loading the cell with radio frequency (RF) absorbing material thus increasing the useful bandwidth. Measurements of characteristic impedance distributed along the cell, voltage standing wave ratio (VSWR) and tests of field uniformity from 1-1000 MHz were taken and described for both empty and absorber loaded cells. The method and the results of calibrating two types of probes are also discussed.



Approved for public release; distribution unlimited.

Design Construction and Evaluation  
of a TEM Transmission Cell  
for Field Probe Calibration

by

Stavros Ioannis Mpoukis  
Lieutenant, Hellenic Navy  
B.S., Naval Postgraduate School, 1979

Submitted in partial fulfillment of the  
requirements for the degree of

MASTER OF SCIENCE IN ELECTRICAL ENGINEERING

from the

NAVAL POSTGRADUATE SCHOOL

December 1979





## ABSTRACT

This paper discusses the design, construction and evaluation of a transverse electromagnetic (TEM) transmission cell for accurate generation of broad-band susceptibility test fields within a shielded environment.

A  $0.3 \times 0.5 \times 1.0$  m TEM cell, constructed at the Naval Postgraduate School (NPGS), was designed to operate as a 50-ohm impedance-matched system and was used for calibrating electromagnetic field probes. According to the basic design, uniform and standard TEM fields can be generated inside the cell for frequencies lower than the cutoff frequency of the device. The high frequency multimode effects can be suppressed by loading the cell with radio frequency (RF) absorbing material thus increasing the useful bandwidth. Measurements of characteristic impedance distributed along the cell, voltage standing wave ratio (VSWR) and tests of field uniformity from 1-1000 MHz were taken and described for both empty and absorber loaded cells. The method and the results of calibrating two types of probes are also discussed.



## TABLE OF CONTENTS

I.	INTRODUCTION -----	13
II.	DESIGN AND CONSTRUCTION OF TEM CELL -----	18
	A. DESIGN THEORY -----	18
	B. CONSTRUCTION -----	20
III.	EVALUATION OF THE ELECTRICAL PERFORMANCE CHARACTERISTICS OF THE EMPTY TEM CELL -----	25
	A. THE CHARACTERISTIC IMPEDANCE OF THE CELL ---	25
	B. VSWR MEASUREMENTS -----	27
	C. MAPPING THE FIELDS INSIDE THE EMPTY CELL ---	32
IV.	EXTENDING THE UPPER USEFUL FREQUENCY RANGE OF THE TEM CELL BY ABSORBER LOADING -----	52
	A. VSWR IMPROVEMENT BY SELECTING ABSORBER LOCATION -----	52
	B. MAPPING THE FIELDS INSIDE THE ABSORBER LOADED CELL -----	59
V.	CALIBRATION OF OMNIDIRECTIONAL FIELD PROBES USING THE ABSORBER LOADED TEM CELL -----	66
	A. SPHERICAL $\vec{H}$ PROBE CALIBRATION -----	67
	B. PYRAMIDAL $\vec{E}$ PROBE CALIBRATION -----	69
VI.	SUMMARY AND CONCLUSIONS -----	76
VII.	RECOMMENDATIONS -----	79
APPENDIX A:	DESIGN DIAGRAM OF THE TWEMES CELL -----	81
APPENDIX B:	CURVES OF MEASURED ELECTRIC FIELD DISTRIBUTION INSIDE EMPTY TEM CELL -----	83
APPENDIX C:	EXAMPLE OF MEASURING THE ELECTRIC FIELD INSIDE THE (EMPTY) TEM CELL -----	92
APPENDIX D:	EXPERIMENTAL PROCEDURE FOR DETERMINING THE BEST TYPE, AMOUNT AND LOCATION OF ABSORBING MATERIAL INSIDE THE TEM CELL --	96



APPENDIX E: CURVES OF MEASURED ELECTRIC FIELD  
DISTRIBUTION INSIDE THE ABSORBER LOADED  
TEM CELL ----- 104

BIBLIOGRAPHY ----- 114

INITIAL DISTRIBUTION LIST ----- 115





## LIST OF FIGURES

1.	Rectangular Coaxial Transmission Line -----	14
2.	Design of Rectangular TEM Transmission Cell -----	16
3.	TEM Transmission Cell. Dimensions as Indicated -----	21
4.	Shielded Strip Line -----	22
5.	Photograph of the Constructed TEM Cell -----	24
6.	Reflection Coefficient Distribution Along the Empty TEM Cell Before Adjusting the 50 Ohm Characteristic Impedance -----	26
7.	Final Curve for Reflection Coefficient as Seen from the Input Port -----	28
8.	Final Curve for Reflection Coefficient as Seen from the Output Port -----	28
9.	Distributed Characteristic Impedance Obtained Along the Empty Cell by Using the TDR -----	29
10.	Block Diagram of VSWR Measurement System for TEM Transmission Cell -----	30
11.	VSWR of Empty Cell Measured at the Input Port (Long Cables Connected) -----	31
12.	VSWR of Empty Cell Measured at the Input Port (Short Cables Connected) -----	33
13.	Distributed Reflection Coefficient Along the Empty Cell from 100 MHz to 1000 MHz (Measured with the Network Analyzer, 10 dB/Div.) -----	34
14.	Picture of Set-Up for Mapping the Fields Inside the Cell -----	35
15.	Block Diagram of Measurement System for Mapping the Fields Inside the Cell -----	36
16.	Cross-Sectional Cut Through Upper Half at Center of Cell -----	38
17.	Probe Locations for Mapping the Fields Inside the Cell for One Level (Same for the Other Two Levels) -	39



18.	Small Dipole Probe (976-4-034) Calibration Curve from 10 MHz to 10 GHz (Courtesy of Sandia Labs) ----	42
19.	Coupling Variations for 778D Dual Directional Coupler -----	43
20.	Relative Electric Field Distribution Inside Empty Cell at Frequency 1 MHz -----	46
21.	Relative Electric Field Distribution Inside Empty Cell at Frequency 10 MHz -----	47
22.	Relative Electric Field Distribution Inside Empty Cell at Frequency 100 MHz -----	48
23.	Relative Electric Field Distribution Inside Empty Cell at Frequency 200 MHz -----	49
24.	Relative Electric Field Distribution Inside Empty Cell at Frequency 400 MHz -----	50
25.	Relative Electric Field Distribution Inside Empty Cell at Frequency 700 MHz -----	51
26.	RF Absorbing Material Used in TEM Cell (from Left to Right: FL-2250, EHP-3 and EHP-5) -----	53
27.	Flat Absorbing Material Placement -----	55
28.	VSWR of Absorber Loaded Cell Measured at Input Port (Short Circuit Measurements at Input of Cell) -	56
29.	Combination of Thin Flat and EHP-3 Absorbing Material Placement -----	57
30.	VSWR of Absorber Loaded Cell Measured at Input Port (Short Circuit Measurements at Output of Cell) -----	58
31.	TDR Trace of Distributed Reflection Coefficient for Absorber Loaded Cell, (a) $\rho/\text{cm} = 0.1$ , (b) $\rho/\text{cm} = 0.02$ -----	60
32.	Relative Electric Field Distribution Inside Absorber Loaded Cell at Frequency 1 MHz -----	62
33.	Relative Electric Field Distribution Inside Absorber Loaded Cell at Frequency 400 MHz -----	63
34.	Relative Electric Field Distribution Inside Absorber Loaded Cell at Frequency 675 MHz -----	64



35.	Relative Electric Field Distribution Inside Absorber Loaded Cell (Access Door Closed) at Frequency 895 MHz -----	65
36.	Orientation Positions for $\bar{H}$ Probe Inside the Cell ---	67
37.	Spherical Omnidirectional $\bar{H}$ Field Probe -----	68
38.	Spherical $\bar{H}$ Probe Calibration Curve (Frequency as a Parameter) -----	70
39.	Spherical $\bar{H}$ Probe Calibration Curves (Incident E Field Strength as a Parameter) -----	71
40.	Pyramidal Omnidirectional $\bar{E}$ Field Probe -----	72
41.	Pyramidal $\bar{E}$ Probe Calibration Curves (Frequency as a Parameter) -----	74
42.	Pyramidal $\bar{E}$ Probe Calibration Curves (Incident E Field Strength as a Parameter) -----	75
A-1.	TWEMES Cell Configuration [7] -----	82
B-1.	Electric Field Distribution Inside Empty Cell at Frequency 1 MHz ( $E_{cal} = 26.04$ [V/m]) -----	84
B-2.	Electric Field Distribution Inside Empty Cell at Frequency 3 MHz ( $E_{cal} = 16.09$ [V/m]) -----	85
B-3.	Electric Field Distribution Inside Empty Cell at Frequency 10 MHz ( $E_{cal} = 4.96$ [V/m]) -----	86
B-4.	Electric Field Distribution Inside Empty Cell at Frequency 30 MHz ( $E_{cal} = 4.96$ [V/m]) -----	87
B-5.	Electric Field Distribution Inside Empty Cell at Frequency 100 MHz ( $E_{cal} = 5.20$ [V/m]) -----	88
B-6.	Electric Field Distribution Inside Empty Cell at Frequency 200 MHz ( $E_{cal} = 5.35$ [V/m]) -----	89
B-7.	Electric Field Distribution Inside Empty Cell at Frequency 400 MHz ( $E_{cal} = 5.50$ [V/m]) -----	90
B-8.	Electric Field Distribution Inside Empty Cell at Frequency 700 MHz ( $E_{cal} = 3.25$ [V/m]) -----	91
C-1.	Tabulated Data for Mapping the Fields Inside the Empty Cell at Frequency 100 MHz by Using the 976-4-034 Dipole Probe -----	93





D-1 through D-7. Curves of VSWR (a) and Reflector Coefficient (b), for the Absorber Loaded TEM Cell Configuration (c) -----	97
E-1. Electric Field Distribution Inside Absorber Loaded Cell at Frequency 1 MHz ( $E_{cal} = 23.0$ [V/m]) -	105
E-2. Electric Field Distribution Inside Absorber Loaded Cell at Frequency 3 MHz ( $E_{cal} = 16.28$ [V/m]) -	106
E-3. Electric Field Distribution Inside Absorber Loaded Cell at Frequency 260 MHz ( $E_{cal} = 5.31$ [V/m]) -----	107
E-4. Electric Field Distribution Inside Absorber Loaded Cell at Frequency 400 MHz ( $E_{cal} = 5.46$ [V/m]) -----	108
E-5. Electric Field Distribution Inside Absorber Loaded Cell at Frequency 500 MHz ( $E_{cal} = 5.36$ [V/m]) -----	109
E-6. Electric Field Distribution Inside Absorber Loaded Cell at Frequency 675 MHz ( $E_{cal} = 2.78$ [V/m]) -----	110
E-7. Electric Field Distribution Inside Absorber Loaded Cell at Frequency 675 MHz ( $E_{cal} = 8.4$ [V/m]) -----	111
E-8. Electric Field Distribution Inside Absorber Loaded Cell at Frequency 895 MHz ( $E_{cal} = 7.08$ [V/m], Access Door Open) -----	112
E-9. Electric Field Distribution Inside Absorber Loaded Cell at Frequency 895 MHz ( $E_{cal} = 7.08$ [V/m], Access Door Closed) -----	113



## TABLE OF ABBREVIATIONS

TEM	Transverse Electromagnetic
NPGS	Naval Postgraduate School
RF	Radio Frequency
VSWR	Voltage Standing Wave Ratio
EMI	Electromagnetic Interference
EMC	Electromagnetic Susceptibility
NBS	National Bureau of Standards
CW	Continuous Wave
EUT	Equipment Under Test
TDR	Time Domain Reflectometer
EMES	Electromagnetic Environments Simulator
TWEMES	1/20 <sup>th</sup> EMES
EMR	Electromagnetic Radiation
EMP	Electromagnetic Pulse
E	Electric
TE <sub>10</sub>	First Order Transverse Electric Mode
EHP	Extra High Performance
H	Magnetic



## ACKNOWLEDGMENTS

The author is indebted to those who have contributed their assistance, encouragement and patience during the preparation of this thesis. First and foremost to Professor O.M. Baycura, my thesis advisor, I want to express my appreciation and thanks for his patient guidance, sense of humor, and his unfailing support throughout this work.

I owe a debt of gratitude to Dr. Richard W. Adler for providing from National Bureau of Standards papers from previous works related to mine, an identical TEM cell, two calibrated small dipole probes with their calibrating curves and also two uncalibrated omnidirectional probes constructed at the Naval Postgraduate School for my thesis work by his assistant Mark Hubbard who I would like also to thank. Without his assistance and experience this work would not have been accomplished.

I wish to express my appreciation to the staff of the Microwave Lab. Jose N. Velasquez and Victor McCullough and also to the staff of the Aeronautical Department facilities of the NPGS Glenn Middleton and Ronald Ramaker for their cooperation.

Finally, I would like to thank my wife, Mary, for her continuing support and understanding throughout graduate school.





## I. INTRODUCTION

For many years several techniques were used in generating uniform and standard electromagnetic fields for performing electromagnetic interference (EMI) and electromagnetic susceptibility (EMC) tests. For example standard gain horns, parallel plate and parallel wire transmission lines have been widely used.

All the above techniques have the disadvantage of radiating energy into the surrounding space which may be hazardous to the operator, interfere with the measurements, or interfere with other experiments performed within the same transmission range. Although shielded enclosures can be used, they may introduce serious measurement problems resulting in errors as large as  $\pm 40$  dB [3]. Because of the high conductivity and reflectivity of the enclosure walls, standing waves are produced which interfere with the signal being measured.

In recent years TEM cells have been developed. An extensive effort has been undertaken by the National Bureau of Standards (NBS) in designing, constructing, testing and improving these cells [1] to [6].

The TEM cell is a two port device in the form of an expanded rectangular coaxial transmission line (Figure 1) with tapered ends. Standard coaxial connectors couple the RF energy to the line from a transmitter connected to the cell input port. The TEM cells of which a typical design is



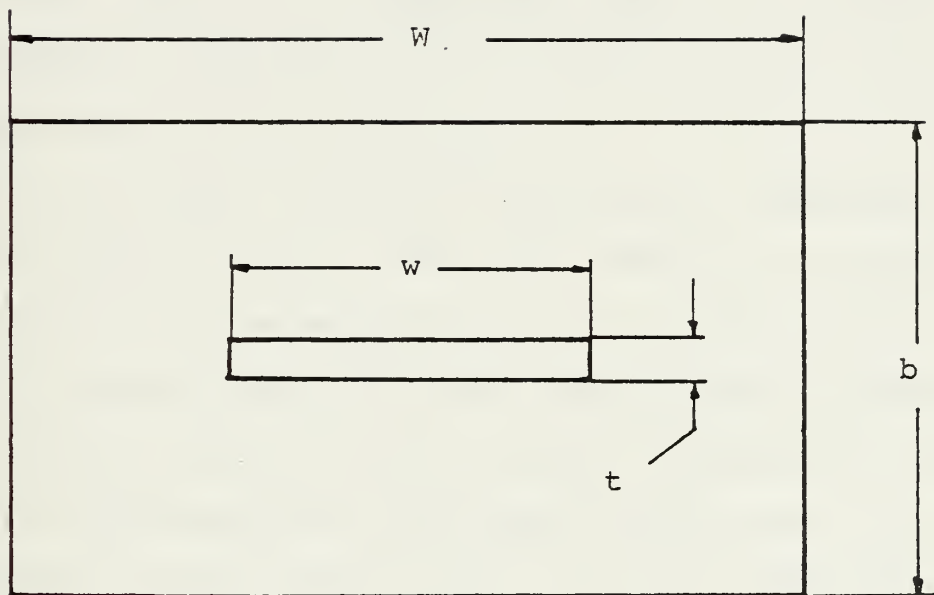


Figure 1. Rectangular Coaxial Transmission Line



shown in Figure 2, are extremely broadband, having linear phase and amplitude response from dc to the cell's cutoff frequency. This characteristic allows continuous-wave (CW) or swept frequency, as well as impulsive and modulated signal testing [6]. They either simulate a free-space radiated field for susceptibility testing of equipment under test (EUT), or couple to the RF energy radiated from EUT for emission testing [4]. The cell is especially useful for calibrating electromagnetic radiation hazard monitors and for special low-level sensor calibrations [2].

All the problems discussed above are not completely eliminated by the use of a TEM cell. There is a significant improvement in the whole situation; for example limited success in solving these problems was achieved at frequencies down to 200 MHz by using special hooded antennas and absorbing material, but measurement techniques from 20 MHz to 200 MHz still suffer serious problems [3]. Using the TEM cell as described in this paper, measurements from 1 MHz up to 1000 MHz have been obtained without significant errors. The primary limitation of the TEM cell is that the upper useful frequency which can be achieved is a function of the dimensions of the cell together with the shape of the transitions and the tapered ends. At frequencies above the cell's waveguide cutoff or resonant frequency, multimoding phenomena occur within the cell resulting in distortion of the uniform characteristics of the cell's TEM mode.



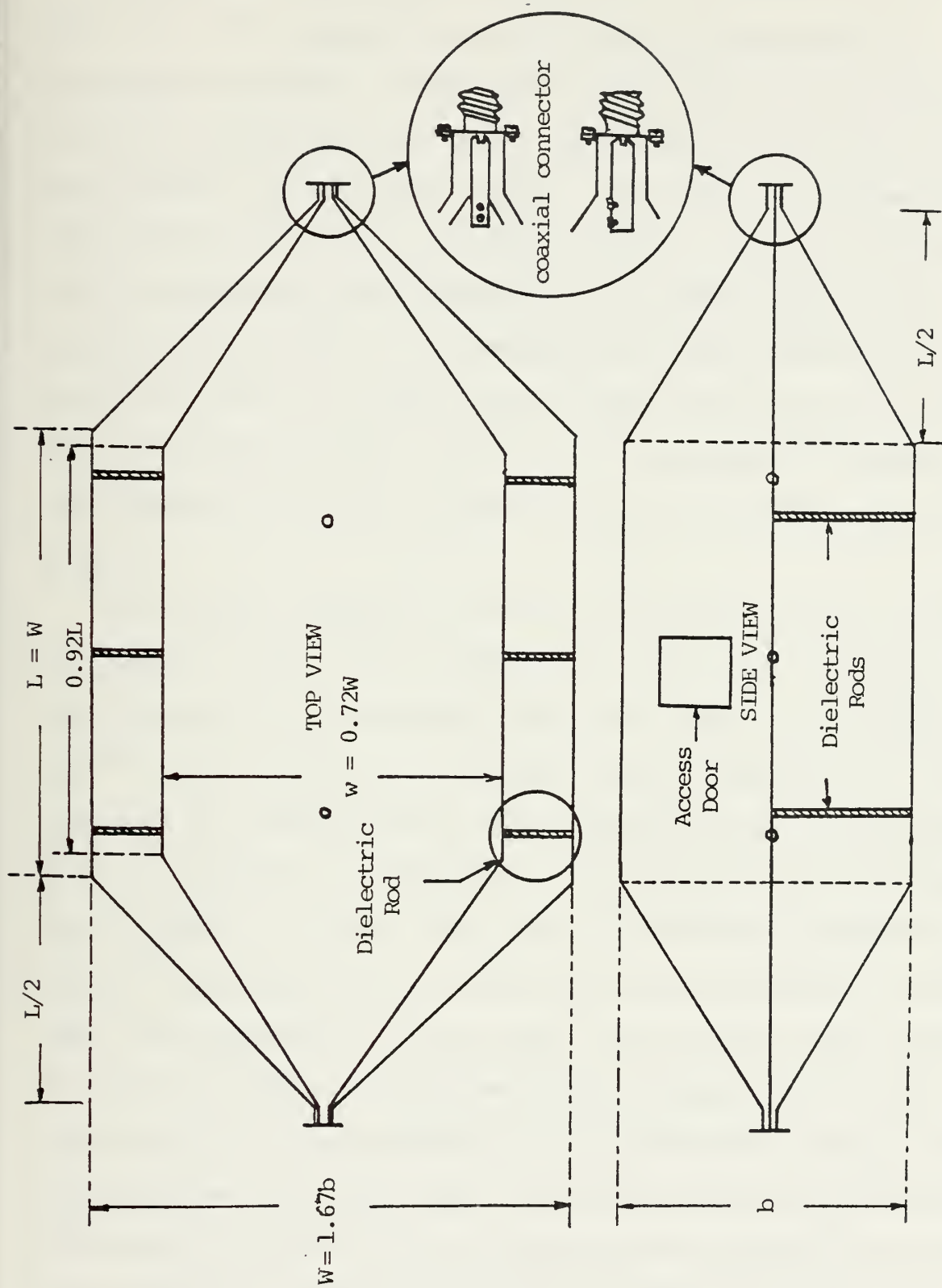


Figure 2. Design of Rectangular TEM Transmission Cell





This paper describes the design of a  $0.3 \times 0.5 \times 1.0$  m TEM cell, the construction of the walls, plates and the transition sections. Measurements were taken of the characteristic impedance distributed along the cell by using the Time Domain Reflectometer (TDR). The VSWR for frequencies from 100-1000 MHz was obtained by using a Vector Voltmeter and a Network Analyzer system, for the empty and for the absorber loaded cell. The strength and the uniformity of the field inside the cell was measured and verified by testing with calibrated probes. Finally two uncalibrated probes (one spherical  $\bar{H}$  field and one pyramidal  $\bar{E}$  field) were calibrated .

During the testing of the cell, construction of a different form of a TEM cell was started. This cell called an Electromagnetic Environments Simulator (EMES) is actually a  $1/20^{\text{th}}$  scale (TWEMES) of the EMES facility (about  $8 \times 20 \times 33$  m) designed and constructed in Sandia Laboratories. This TWEMES, shown in Appendix A, Figure A-1, is designed for frequencies from 100 MHz to 10 GHz. The full size EMES was designed to provide the capability of performing electromagnetic radiation (EMR), electromagnetic pulse (EMP) and lightning near stroke testing of systems, subsystems and components in a single facility [7]. The combination of the frequency ranges achieved with the TEM and TWEMES cell and careful testing techniques provides the possibility of establishing standard and uniform electromagnetic fields at frequency ranges from dc up to 10 GHz.



## II. DESIGN AND CONSTRUCTION OF TEM CELL

### A. DESIGN THEORY

The design of the TEM cell was based on NBS reports [1] to [6]. Major design considerations were to:

1. maximize the usable test cross section area,
2. maximize the upper useful frequency limit,
3. minimize cell impedance mismatch,
4. minimize the VSWR over the range of frequencies from 100 MHz up to 1000 MHz,
5. maximize the uniformity of the electromagnetic field pattern characteristic of the cell.

The characteristic impedance of the cell was chosen to be 50 ohms in order to match the 50 ohm nominal characteristic impedance of available RF generators and detection equipments. The approximate equation for the characteristic impedance,  $Z_0$ , of shielded strip line (Figure 2) was used for determining the characteristic impedance of the cell [1], [2], [3].

$$Z_0 \approx \frac{94.15}{\sqrt{\epsilon_r} \left[ \frac{w}{b(1-t/b)} + \frac{C_f'}{0.0885 \epsilon_r} \right]} \quad [\Omega] \quad (1)$$

where:

$\epsilon_r$  = relative dielectric constant of the medium between the conductors (here, air)



- w = the width of the center conductor called the septum, in cm
- b = the height of the cell in cm
- t = the thickness of the septum in cm
- $C'_f$  = fringing capacitance in pF/cm.

The capacitance  $C'_f$  has already been determined, [1], having a value of 0.053 pF/cm. This was done previously by evaluating a small scale model of the cell, using a TDR.  $C'_f$  was used in transforming the shielded strip line into a "rectangular coaxial" line. The height of the cell was chosen such that the length of the probe used for mapping the electric (E) field inside the cell did not exceed  $1/3 \times b/2$ , in order to meet the design considerations 1, 3, 4 and 5 [2], [3]. The factor of  $1/3$  assures minimum perturbation of the 50 ohm characteristic impedance when the probe is inserted inside the test area of the cell. The thickness  $t$  for the septum was selected for mechanical rigidity. The width of the septum was calculated from equation (1) knowing the values for  $\epsilon_r$  (for the air  $\epsilon_r = 1.0006$ ),  $C'_f$ ,  $b$ ,  $t$  and assuming a value for  $Z_0$  equal to 51 ohms. The 51 ohm value was selected to compensate for reduction of the characteristic impedance of the cell which occurs when the probe or EUT is inserted into the cell or when the cell is loaded with absorbing material.

The first order transverse electric mode ( $TE_{10}$ ) cutoff frequency is given by the following equation:



$$(f_c)_{10} = \frac{c}{2W} \quad (2)$$

where:

$c$  = velocity of propagation of light ( $\approx 3.0 \times 10^8$  m/s)

$W$  = width of the cell as shown in figure 2

The cutoff frequency for any higher order mode in general is given by:

$$(f_c)_{m,n} = \frac{c(b^2 m^2 + W^2 n^2)^{1/2}}{2bW} \quad (3)$$

where:

$c, W$  as in (2)

$b$  = the height of the cell as shown in figure 2

$m, n$  = integers related to the half sine variations of the cell in the vertical and transverse directions.

Other useful expressions for characterizing the TEM cells are given in [6].

## B. CONSTRUCTION

The  $0.3 \times 0.5 \times 1.0$  m TEM cell was constructed at the facilities of the Aeronautical Department of the NPGS. Its dimensions are shown in Figure 3. This cell is identical to the NBS one which was loaned to NPGS to obtain construction details. The cell is fabricated from 0.080 inch (2.032 mm)





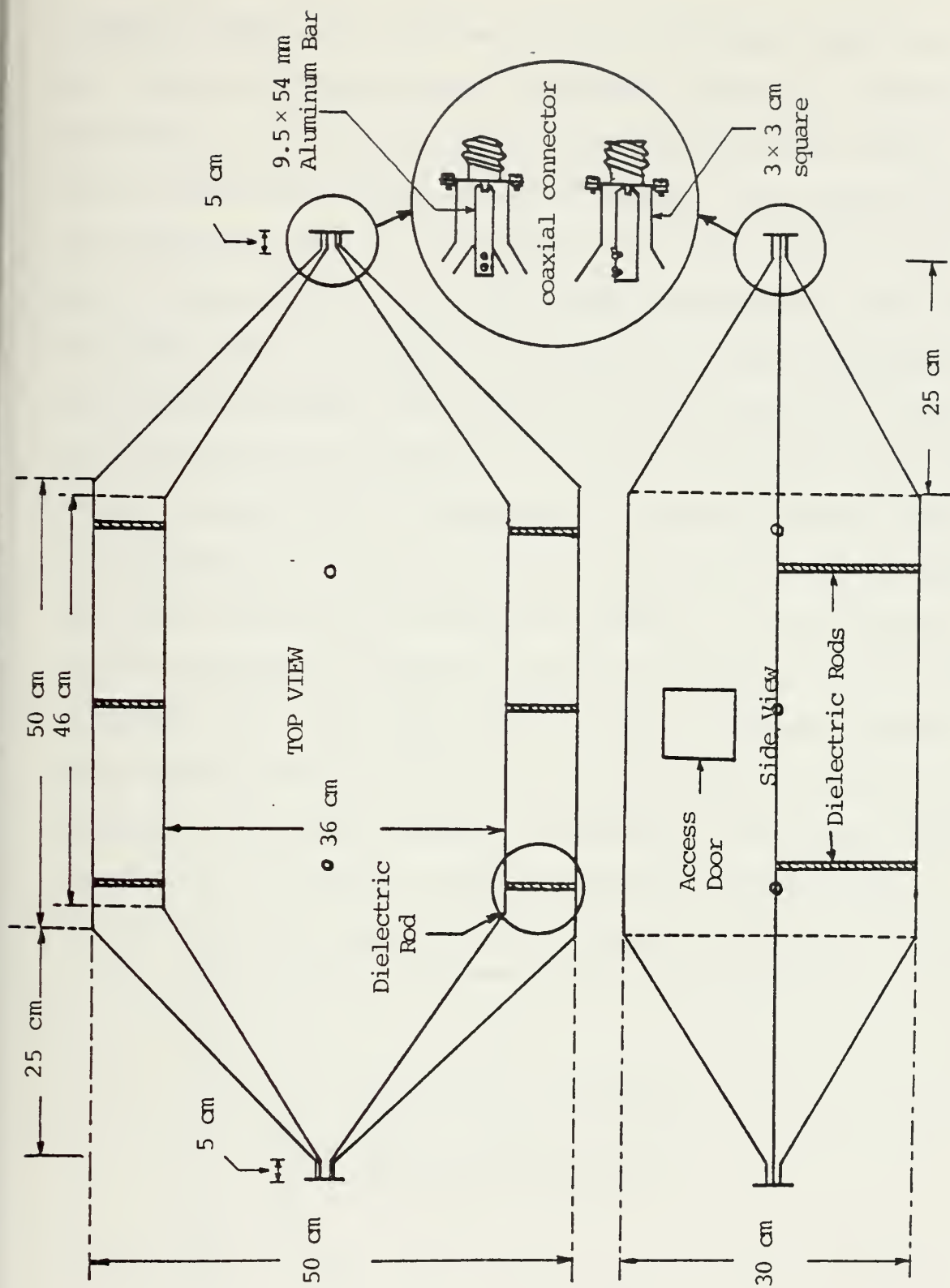


Figure 3. TEM Transmission Cell. Dimensions as Indicated



aluminum sheet and is welded around the edges except for the top wall, including the transition sections. The top is connected to sides by screws. This construction forms a continuous outer conductor and RF shield. The center plate, or septum, is made of 0.185 inch (4.699 mm) aluminum sheet and is supported by dielectric rods connected to both lower and side walls. The rods are threaded so that the septum can be straightened and aligned with the long axis of the cell maintaining a parallel orientation with the four outer walls. At each end of the septum one small aluminum bar of dimensions  $3/8 \times 2\frac{1}{4}$  inch ( $9.525 \times 53.975$  mm) is connected by screws, as shown in detail in figure 3. This type of septum termination together with the transition of the outer walls down to a  $1\frac{3}{16} \times 1\frac{3}{16}$  inch ( $30.162 \times 30.162$  mm) square cross section was converted the strip line transmission line (Figure 4) to square coaxial transmission line with type N connectors. An access door of dimensions  $4\frac{1}{2} \times 4\frac{1}{2}$  inch ( $114.3 \times 114.3$  mm) was cut into one side of the cell at the

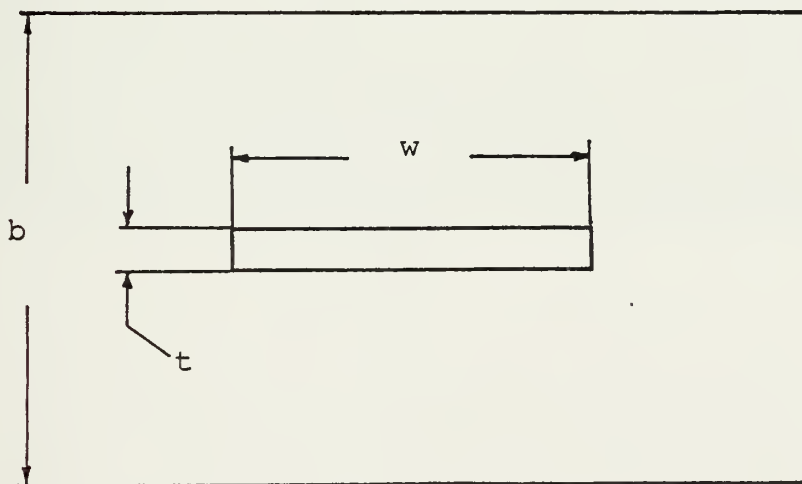


Figure 4. Shielded Strip Line



middle of the space between the septum and the upper wall for inserting the calibrating probes. Finally the crack at the upper wall was sealed with conductive copper tape to provide both uniform conductivity and RF shielding. Figure 5 shows a photograph of the constructed TEM cell.





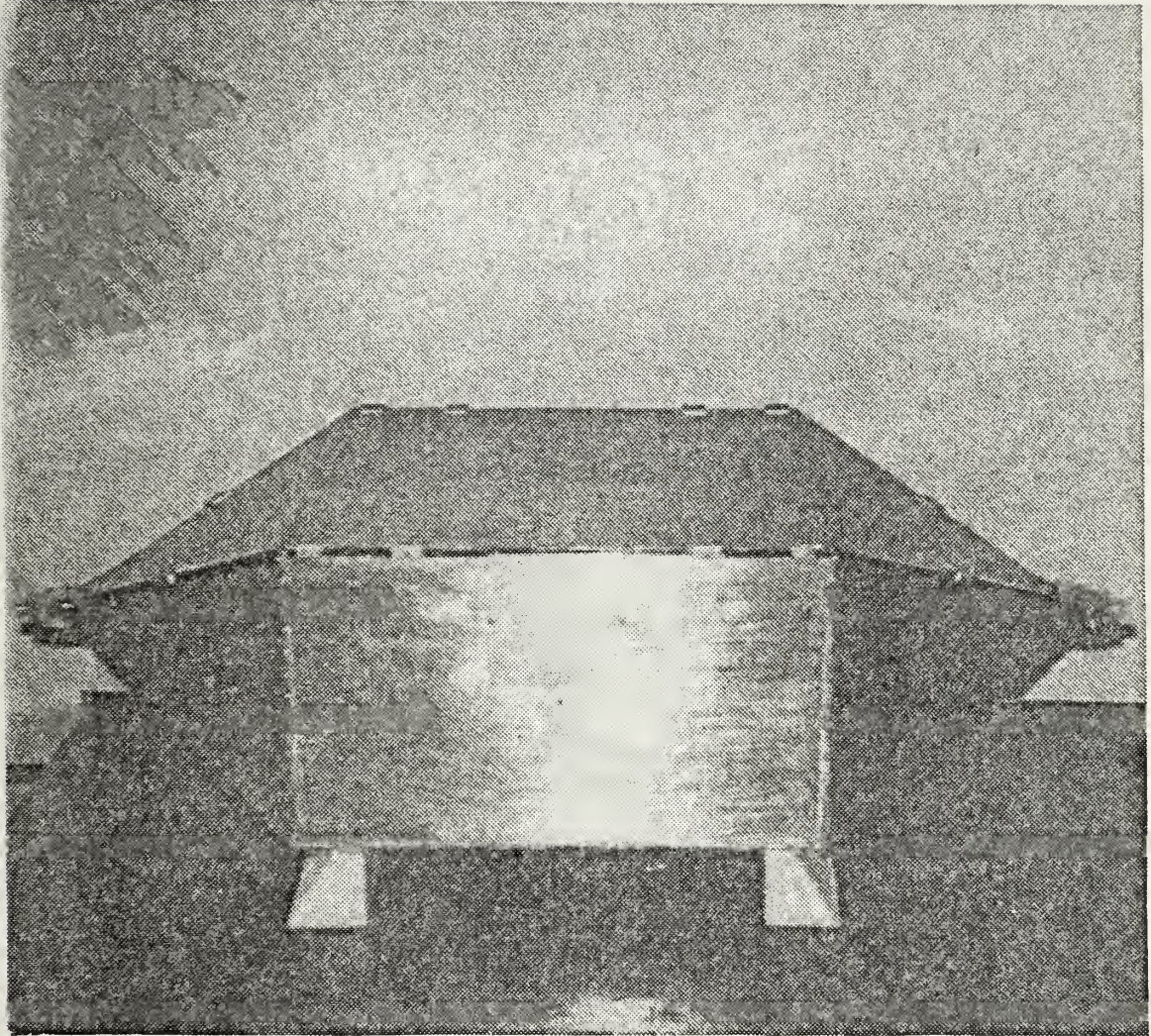


Figure 5. Photograph of the Constructed TEM Cell





### III. EVALUATION OF THE ELECTRICAL PERFORMANCE CHARACTERISTICS OF THE EMPTY TEM CELL

The evaluation of the electrical performance of the empty cell (no absorber) is discussed in this section. The methods used and the results obtained for establishing a 50 ohm distributed characteristic impedance along the cell, a low VSWR from 100 MHz to 1 GHz and a standard and uniform E field inside the cell, are also shown. The initial evaluation provided familiarization in working with such a complicated and unknown device. The data obtained proved useful when evaluating the absorber loaded cell and provided a basis for comparison for the final configuration of the device.

#### A. THE CHARACTERISTIC IMPEDANCE OF THE CELL

The characteristic impedance distributed along the entire length of the cell was measured using the TDR (a H.P.181A oscilloscope and 1815A TDR/sampler). Since the magnitude of the characteristic impedance is linearly related to the magnitude of the reflection coefficient,  $\rho$ , the shape of the curves obtained for  $\rho$  should be analogous to that of the characteristic impedance. The TDR was used for measuring the distribution of  $\rho$  along the cell when a matched 50 ohm termination was connected to the cell's output port. The magnitude of the impedance was obtained from a special calculator provided by the manufacturer of the TDR. The reflection coefficient along the cell as viewed from the input port is



shown in Figure 6 (scale,  $\rho/\text{cm} = 0.1$ ) and was obtained just after the cell was constructed.

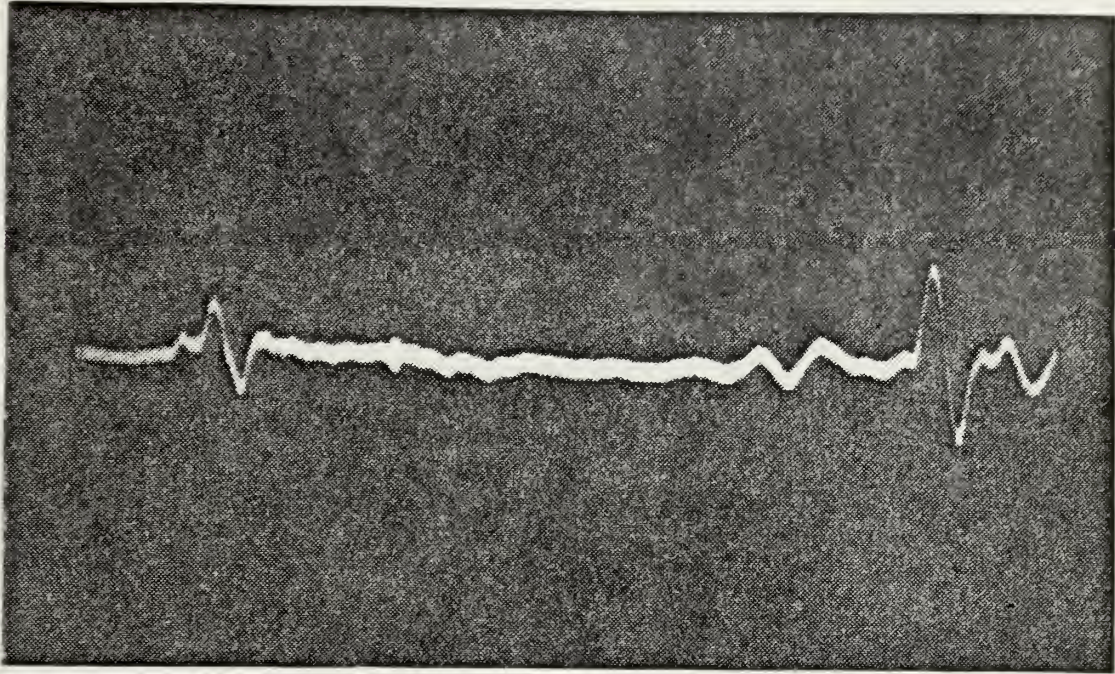


Figure 6. Reflection Coefficient Distribution Along the Empty TEM Cell Before Adjusting the 50 Ohm Characteristic Impedance

Even though the characteristic impedance was about 50 ohms throughout most of the length of the cell, two large spikes at the input and output ports (impedance variations of 40 to 55 ohms and 40 to 60 ohms respectively) suggested mismatch problems. An extensive effort was made to reduce or eliminate the spikes without affecting the approximately 50 ohm impedance at the other portions of the cell. These refinements were made by trimming the width of the septum and by using conductive copper tape for changing the cross-section





and the shape of the small aluminum bars at the ends of the center conductor, until the proper characteristic impedance was obtained.

The curves for the final reflection coefficient are shown in Figures 7 and 8 for the input and output ports (since the cell is symmetric the words "INPUT" and "OUTPUT" are written on the cell and are used here for descriptive purposes).

Although both ports, when they were used as inputs, were tuned to about 50 ohms, they appeared to have an impedance variation between 43 and 60 ohms when used as outputs. Additional efforts to improve this undesirable situation were fruitless. Figure 9 shows the TDR trace of distributed characteristic impedance obtained for the empty cell (the distributed impedance due to the length of the circular coaxial connectors is not shown in this figure).

## B. VSWR MEASUREMENTS

The VSWR for the empty cell was obtained by using a Vector Voltmeter. The set up for these measurements is shown in Figure 10. It consists of the 8405A, H.P., Vector Voltmeter, the 612A (for VHF) or 637-07171 (for VHF) signal generator (set in CW mode), the 778D Dual Directional Coupler and the cell with a matched 50 ohm load at the output port. The obtained data were plotted on log-log scale paper and the curve of VSWR versus frequency from 100 MHz up to 1 GHz is shown in Figure 11. The abrupt changes of VSWR appearing in this plot were due to the contribution of small resonance



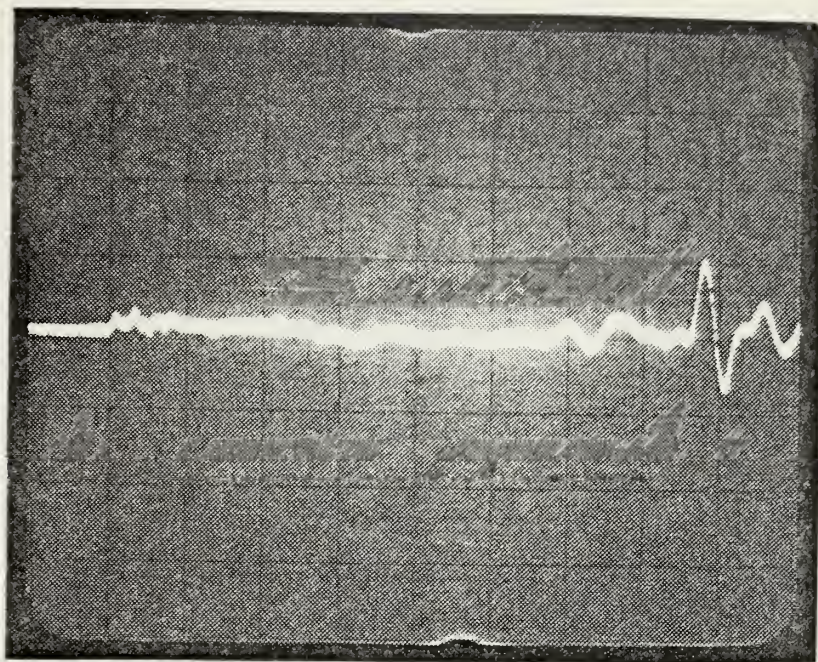


Figure 7. Final Curve for Reflection Coefficient as Seen from the Input Port

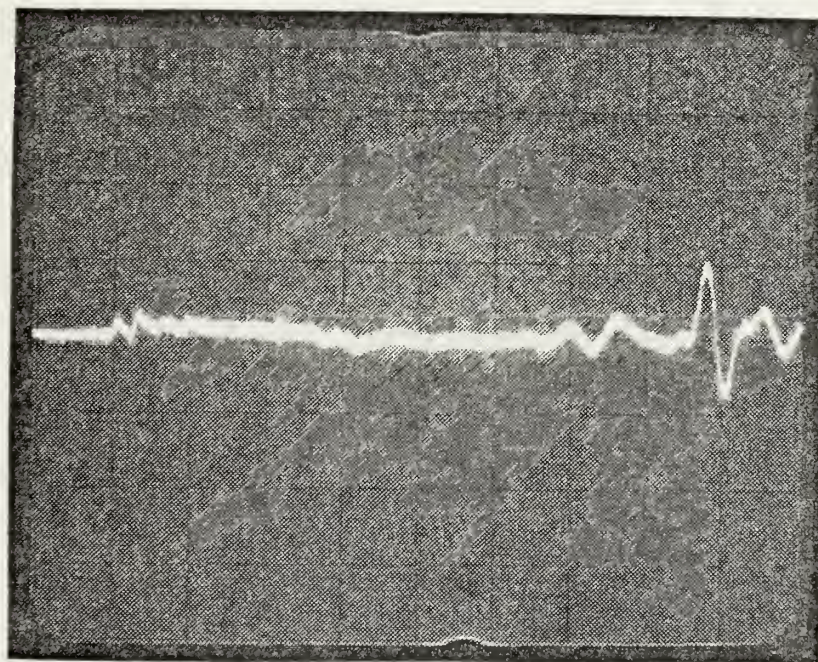


Figure 8. Final Curve for Reflection Coefficient as Seen from the Output Port







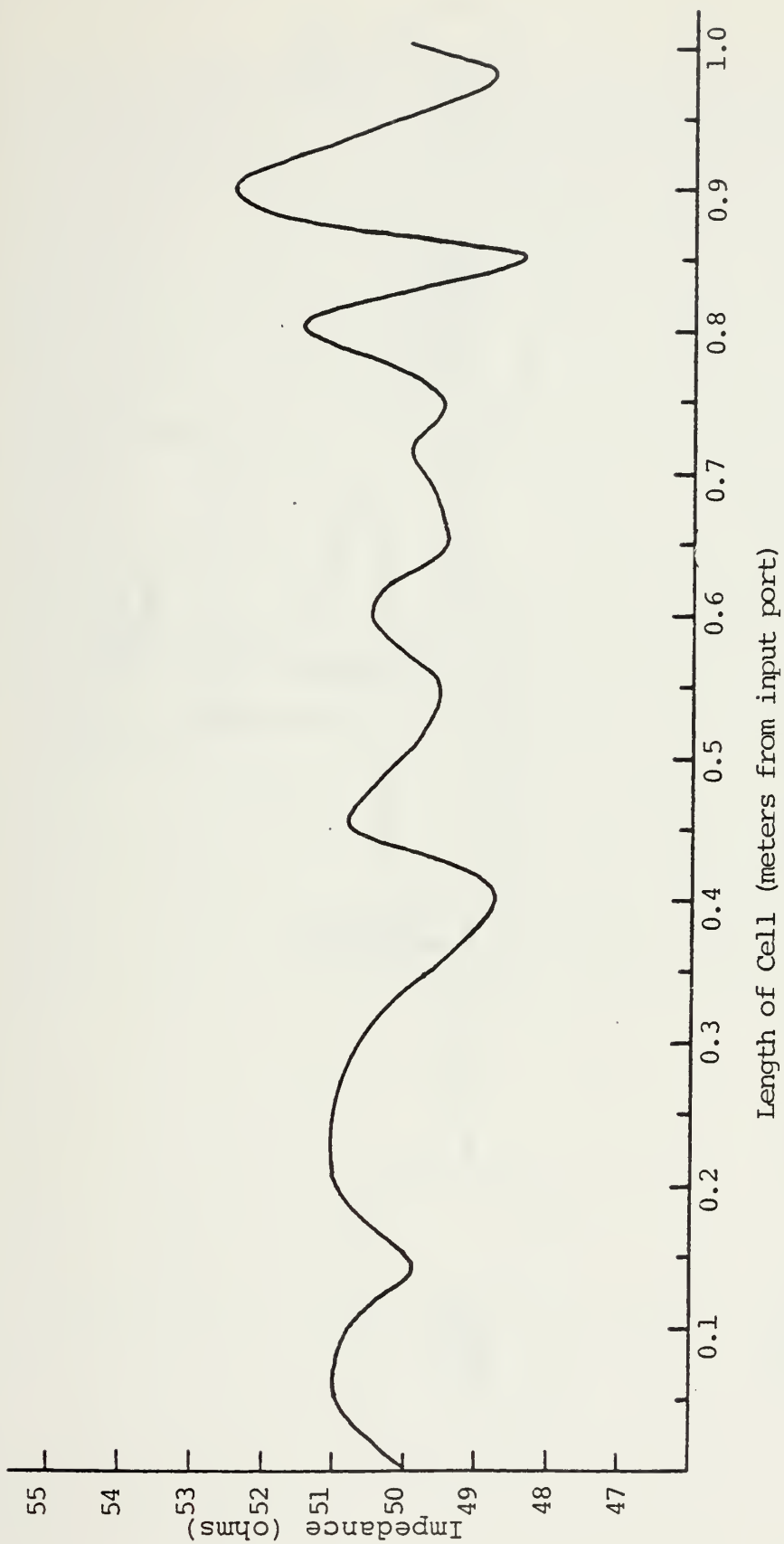


Figure 9. Distributed Characteristic Impedance Obtained Along the Empty Cell by Using the TDR



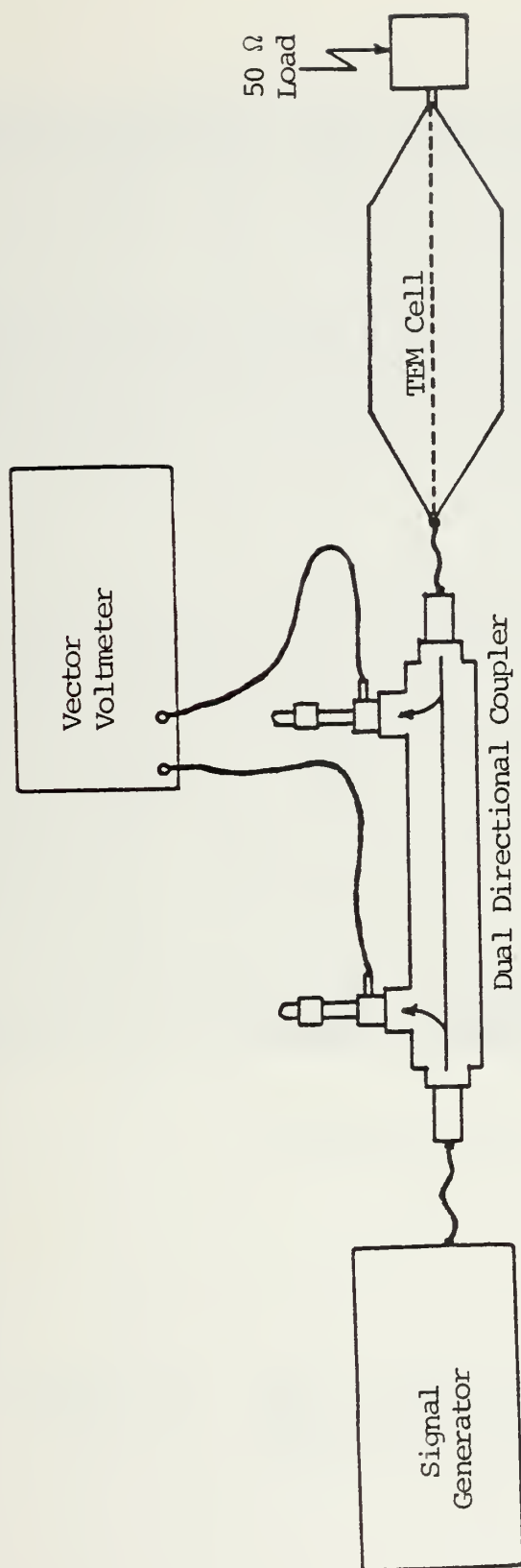


Figure 10. Block Diagram of VSWR Measurement System for TEM Transmission Cell



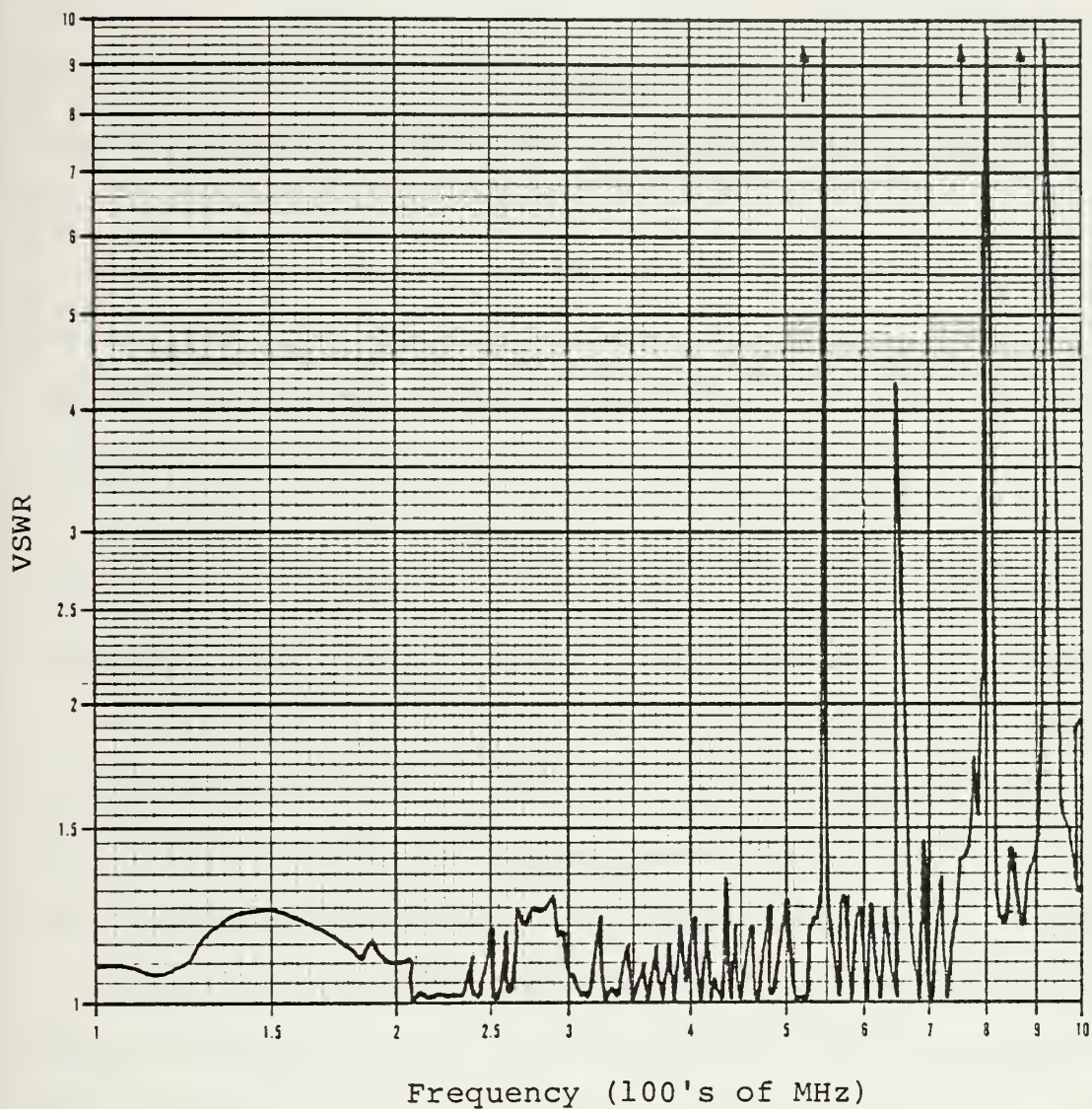


Figure 11. VSWR of Empty Cell Measured at the Input Port (Long cables connected)



phenomena occurring in the long cables used. The final VSWR is shown in Figure 12, where the cables were replaced with minimum length ones. The smoothness of the curve and the lower average value of VSWR demonstrate the necessity for short instrumentation cabling.

Due to the symmetry of the empty cell, the  $TE_{10}$  mode is not excited [1]. However, as shown in figures 11 and 12, the  $TE_{11}$  and/or  $TM_{11}$  mode can exist contributing to resonances inside the cell's cavity as evidenced by the high VSWR spikes.

The VSWR for the empty cell was less than 1.12 for frequencies from 100 MHz up to 535 MHz, giving an initial indication of "flat" performance for this range of frequencies.

It was anticipated that better results could be obtained if the Dual Directional Coupler was connected directly (without cables) between the signal generator and the cell's input. This was done without any significant improvement in VSWR.

Finally the VSWR of the empty cell was measured using the Network Analyzer system. The curve for the reflection coefficient from 100 MHz to 1000 MHz is shown in Figure 13. These results agree with previous measurements.

### C. MAPPING THE FIELDS INSIDE THE EMPTY CELL

The measurement system of Figures 14 and 15 was used for mapping the fields inside the empty cell. The system consists of the signal generator as in Section III(B) (or the 8690B, H.P. sweep oscillator), the 778D Dual Directional Coupler; the 432A, H.P. power meter with the 478A, H.P.,





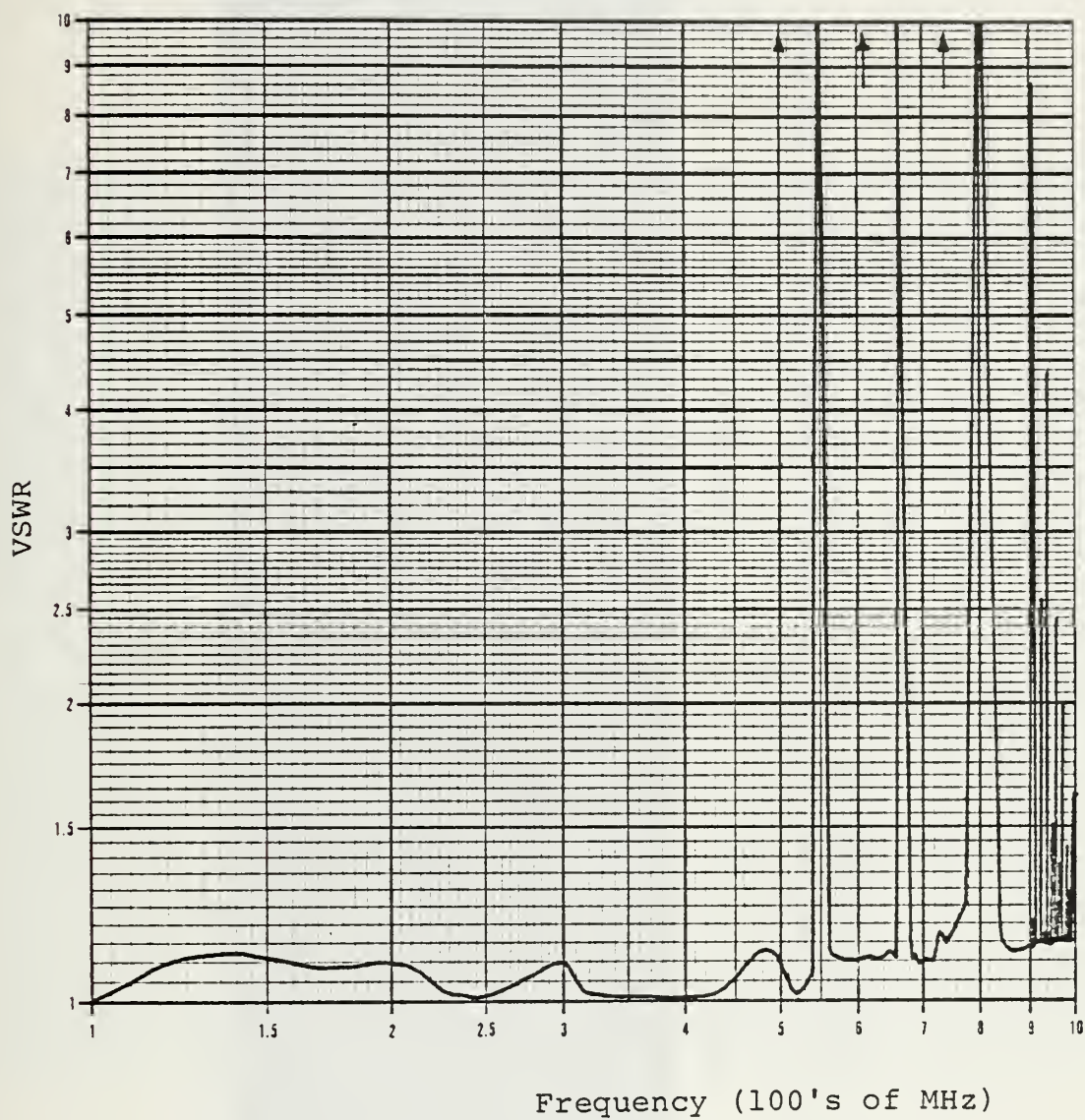


Figure 12. VSWR of Empty Cell Measured at the Input Port (Short Cables Connected)



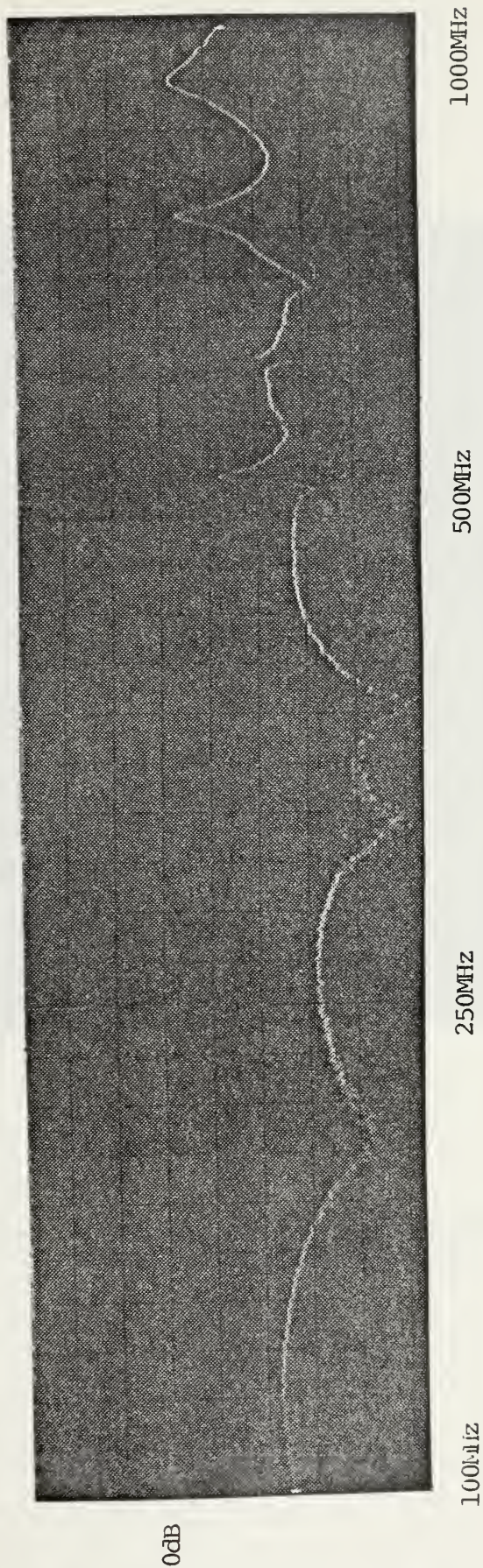


Figure 13. Distributed Reflection Coefficient Along the Empty Cell from 100 MHz to 1000 MHz (Measured with the Network Analyzer, 10 dB/Div.)





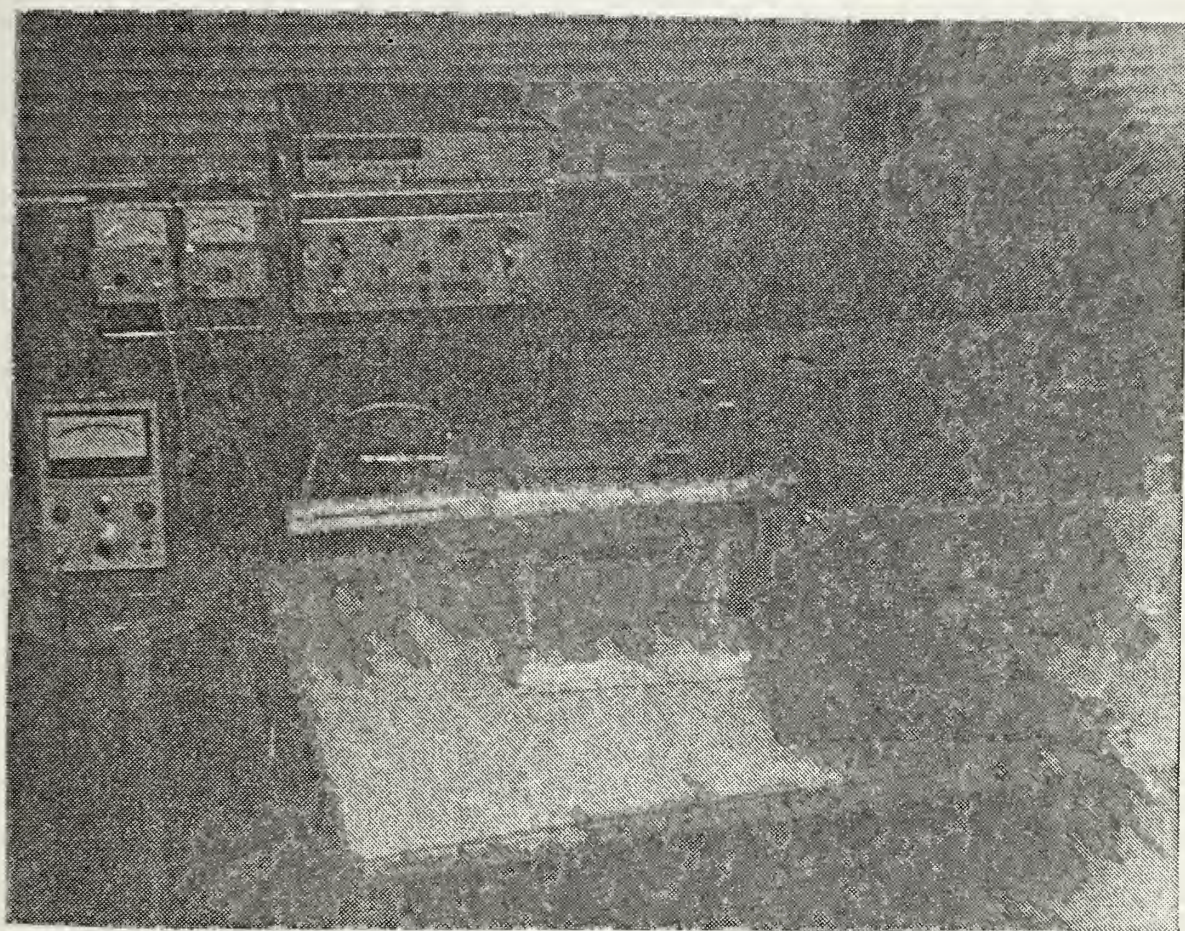


Figure 14. Picture of Set-Up for Mapping the Fields Inside the Cell



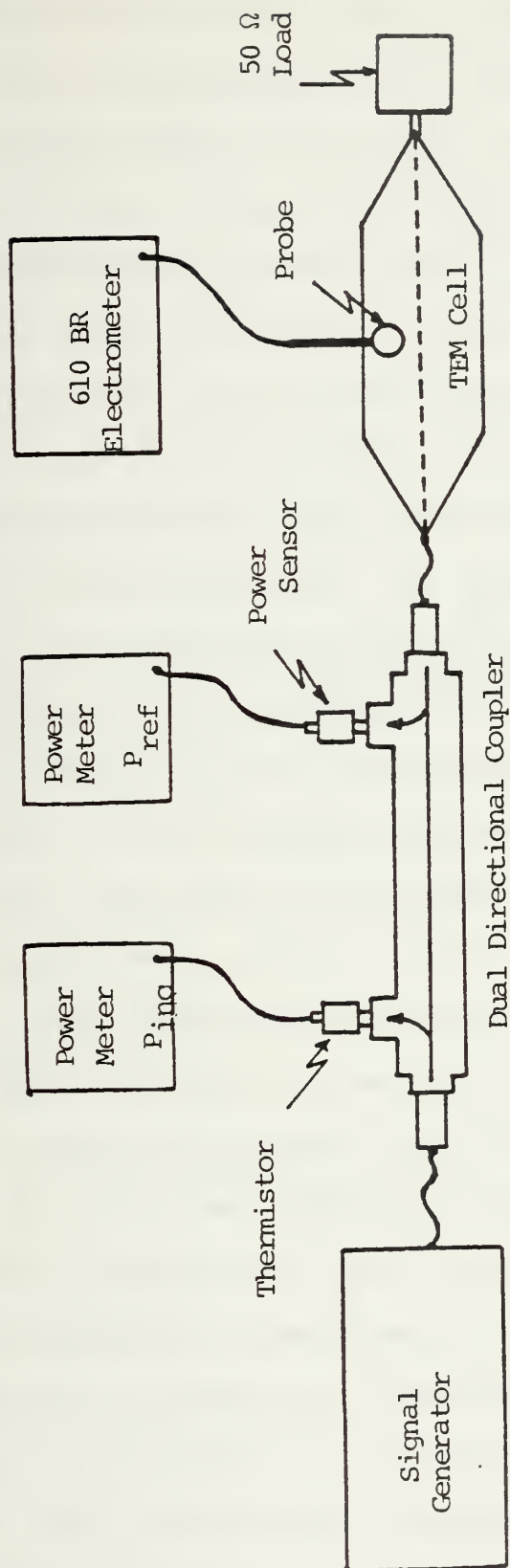


Figure 15. Block Diagram of Measurement System for Mapping the Fields Inside the Cell





thermistor for measuring the incident power, the 435A, H.P. power meter with the 848A, H.P. power sensor for measuring the reflected power, the 610 BR electrometer for measuring the probe output voltage, the TEM cell with a matched 50 ohm load connected at the output port and the calibrated 976-4-034 short dipole for probing the E fields inside the cell. The dipole probe was on loan from Sandia Labs.

The variations of E field versus position were measured by moving the probe in the longitudinal, transverse and vertical directions within the upper half area of the cell. The test area was determined as the volume of an imaginary  $4\frac{1}{2}$  in  $\times$   $4\frac{1}{2}$  in  $\times$   $\frac{b}{2}$  parallelepiped centered along the vertical axis of the cell at the space between the septum and the upper wall. This was done because the E field is essentially vertically polarized in the region near the center of the cell and gradually becomes horizontally polarized as one moves in the horizontal direction toward the gap at the side [1]. The measurements were taken at three equidistant horizontal levels at distances from the upper wall of  $\frac{3}{8}b$ ,  $\frac{1}{4}b$ , and  $\frac{1}{8}b$  for the lower, middle and upper level respectively as shown in Figure 16. The probe was mounted on a dielectric bar of polystyrene foam material (dielectric constant 1.05). A supporting platform was constructed and used outside of the door (see figure 14), to establish the three different levels. The probe output voltage was measured at the positions determined by a  $4\frac{1}{2} \times 4\frac{1}{2}$  inch matrix, as shown in Figure 17, which had been sketched on the bar's supporting platform.



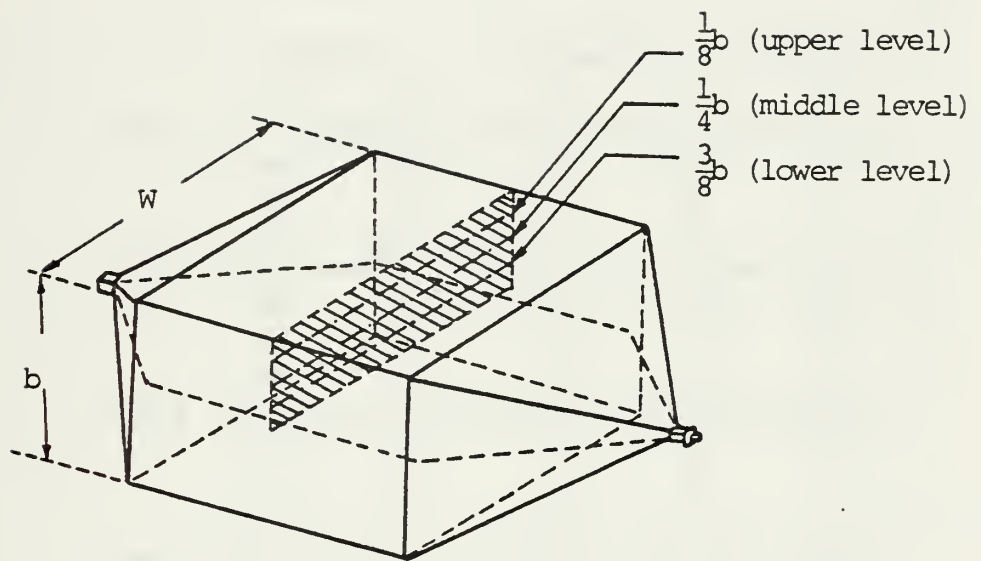


Figure 16. Cross Sectional Cut Through Upper Half at Center of Cell



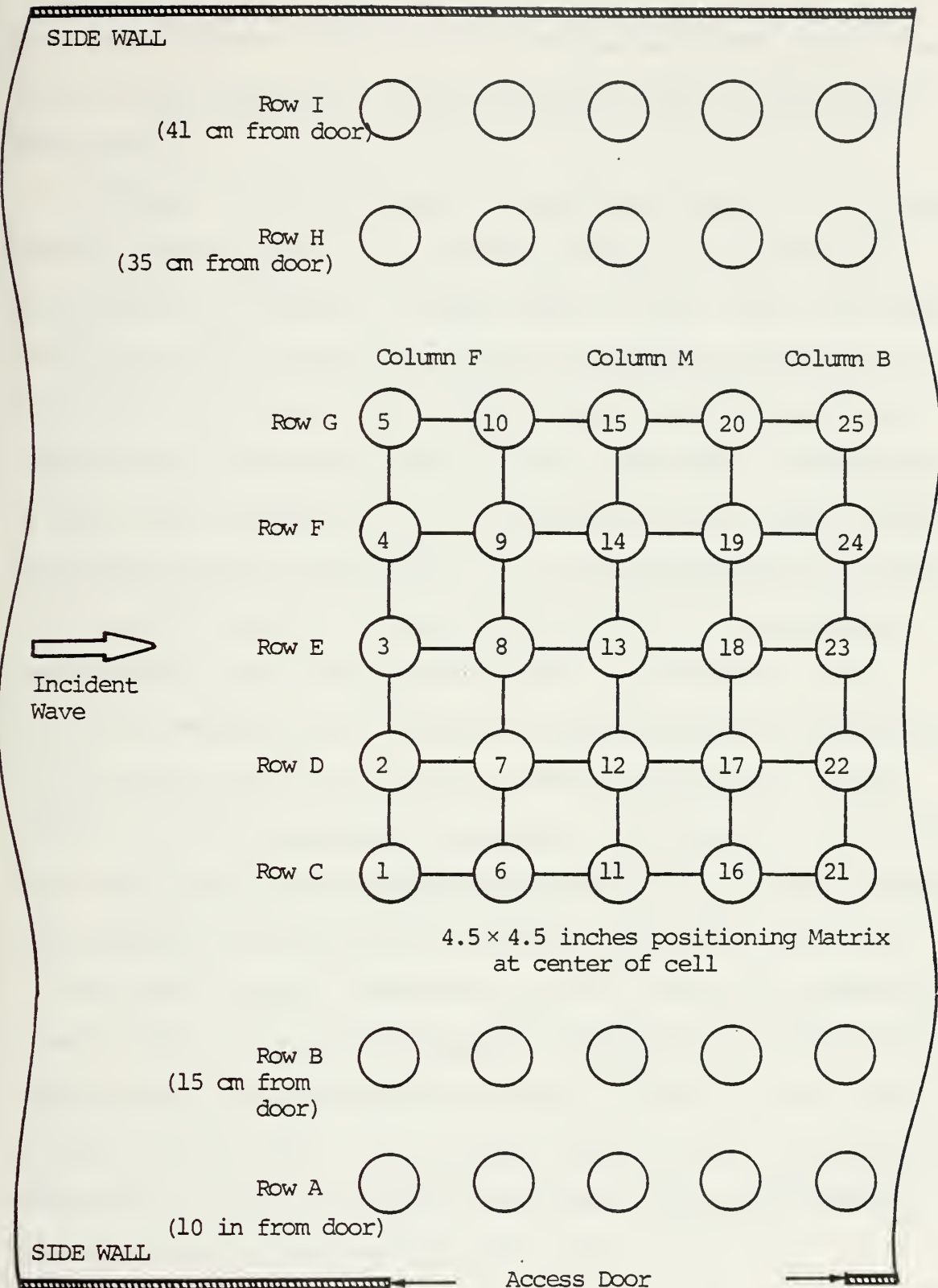


Figure 17. Probe Locations for Mapping the Fields Inside the Cell for One Level (Some for the Other Two Levels)



Data were obtained for 25 points of the matrix at each level and for each frequency, maintaining the same incident power throughout.

Although the test volume as determined above is of interest for field strength and field uniformity measurements, data were also obtained at each level in the space extending beyond the  $4\frac{1}{2} \times 4\frac{1}{2}$  inch area in the transverse direction up to 0.2 W (10 cm) and 0.8 W (40 cm) from the door opening. This was done in order to get a better feel for the fringing of the fields, especially at the areas near the gaps between the septum and the side walls. In the longitudinal direction the available space is bounded by the door's dimensions so measurements toward the ports of the cell were not taken. During the measurements the small dipole probe was maintained in a vertical position, but its output voltage was always checked in the horizontal orientation. The leads of the probe were always maintained perpendicular to E field, the position for minimum lead interaction with the test field [1], [2].

Only the vertical component of the E field was measured at each point since the horizontal component was found to be insignificant, contributing less than 0.1 V/m to the total E field in all cases. If both the vertical and the horizontal components of the E field are measured, the total electric field is given by the equation [1], [2],

$$E = (E_V^2 + E_H^2)^{1/2} \quad (4)$$





when the vertical component  $E_v$  and the horizontal component  $E_H$  are in phase. The probe calibration curve, provided by Sandia Labs, is shown in Figure 18 as a function of  $V_{\text{probe}}/E_{\text{inc}}^2$  versus frequency from 10 MHz to 10 GHz. The coupling variation in dB with frequency in GHz for the Dual Directional Coupler are shown in Figure 19.

The procedure for measuring the electric field strength inside the cell from 1 MHz to 1 GHz was as follows: The generator output was adjusted until a desired probe output voltage was obtained. The test field was then calculated from the equation given by [1], [2], [3], [5].

$$E_{\text{cal}} = \frac{(P_n R_c)^{1/2}}{d} \quad (5)$$

where:

$P_n$  = net power flowing through the cell

$R_c$  = measured characteristic impedance of the cell at the test location (here ~50 ohm from figure 9)

$d$  = separation distance between the upper wall and the septum ( $d = 0.1425$  m).

Substituting in equation (5) the known values for  $R_c$  and  $d$  and also setting the net power in milliwatts, the following equation for the calculated E field is obtained.

$$E_{\text{cal}} = 1.569 (P_n [\text{mW}])^{1/2} [\text{V/m}] \quad (6)$$



LEAST SQUARES POLYNOMIALS FOR DEVICE 4034  
 # OF DATA POINTS = 28 . DEGREE = 7

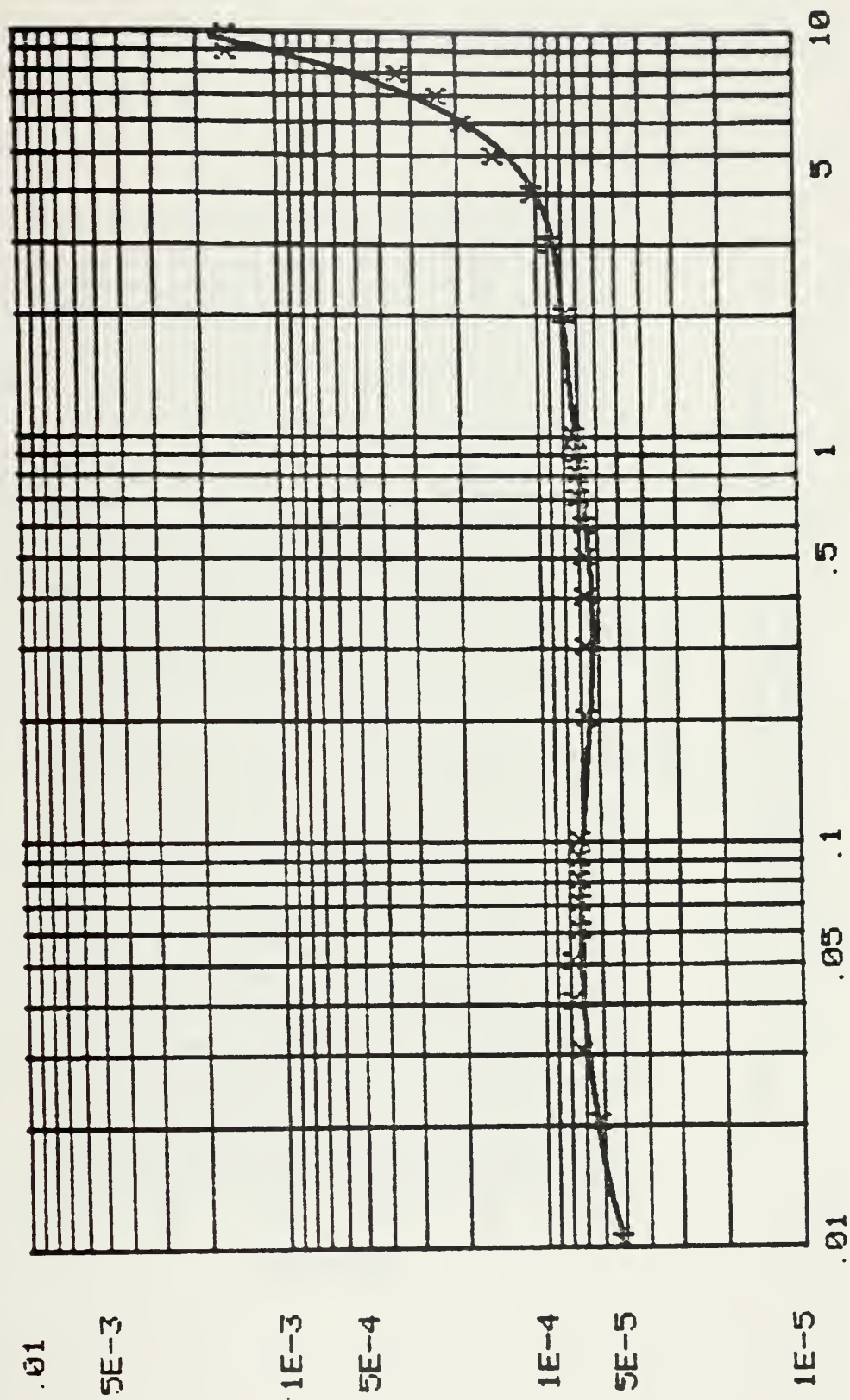


Figure 18. Small Dipole Probe (976-4-034) Calibration Curve from 10 MHz to 10 GHz (Courtesy of Sandia Labs)



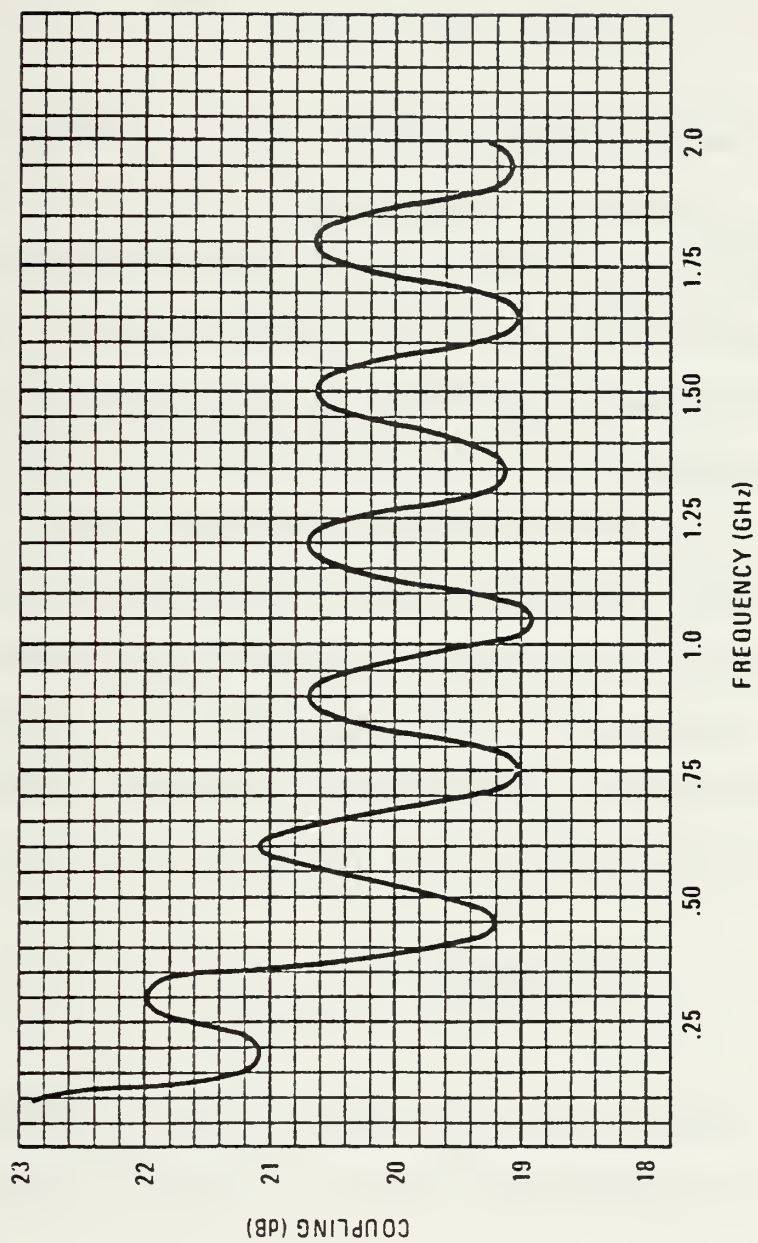


Figure 19. Coupling Variations for 778D Dual Directional Coupler





$P_n$  was determined from the power meter readings on the sidearms of the Dual Directional Coupler using the following equation.

$$P_n = CR_f \cdot P_{inc} - CR_R \cdot P_{ref} \quad (7)$$

where,  $CR_f$  and  $CR_R$  are the forward and reverse coupling ratios of the bi-directional coupler and  $P_{inc}$  and  $P_{ref}$  are the indicated incident and reflected coupler sidearm power meter readings.  $P_n$  is invariant with position along the length of the cell since the cell is essentially lossless [1]. The probe output voltage was measured at each of the three levels inside the cell at all positions marked with circles in figure 17 for several frequencies between 1 MHz and 1 GHz. The measured E field was then calculated by using the value of the ratio  $(V_{probe}/E_{inc}^2) = K$  from figure 18, corresponding to the frequency where the probe output voltage was obtained. The measured E field inside the cell is given by the equation,

$$E_{meas} = \left( \frac{V_{probe}}{K} \right)^{1/2} \quad (8)$$

For frequencies below 10 MHz, where the K factor can not be obtained from figure 18, it was calculated by the formula,

$$K = \frac{V_{probe}}{E_{cal}^2} \quad (9)$$



and then was averaged over all measured points of three levels. The variation of the E field inside the cell was plotted separately for each level as relative electric field strength versus the distance of the probe from the door opening. This was done by averaging the 5 values of E field along each row from A to I as indicated in figure 17. The relative electric field strength was calculated by forming the ratio  $E_{\text{meas}}/E_{\text{cal}}$ .

Results obtained from mapping the fields inside the empty cell are shown in Figures 20 through 25. The same plots together with several others for different frequencies, but for the actual measured (not relative) electric field strength are shown in Appendix B. An example of how the E field was determined inside the cell is given in Appendix C.

Finally, it was observed that when measurements of E were taken inside the empty cell at frequencies near resonance (i.e., at the points where large VSWR spike occurred), there was a considerable effect due to the open door. Similar results occurred when the copper tape was removed from the joints of the upper wall (i.e., with open door and copper tape removed  $V_{\text{probe}_{\text{OUT}}} = 2.5 \text{ mV}$ , with door closed and copper tape in place  $V_{\text{probe}_{\text{OUT}}} = 10 \text{ mV}$ ). This did not happen for frequencies removed from resonance. Also with the door closed and the copper tape in place, at frequencies near resonance, the reflected power decreased by 3 dBm.



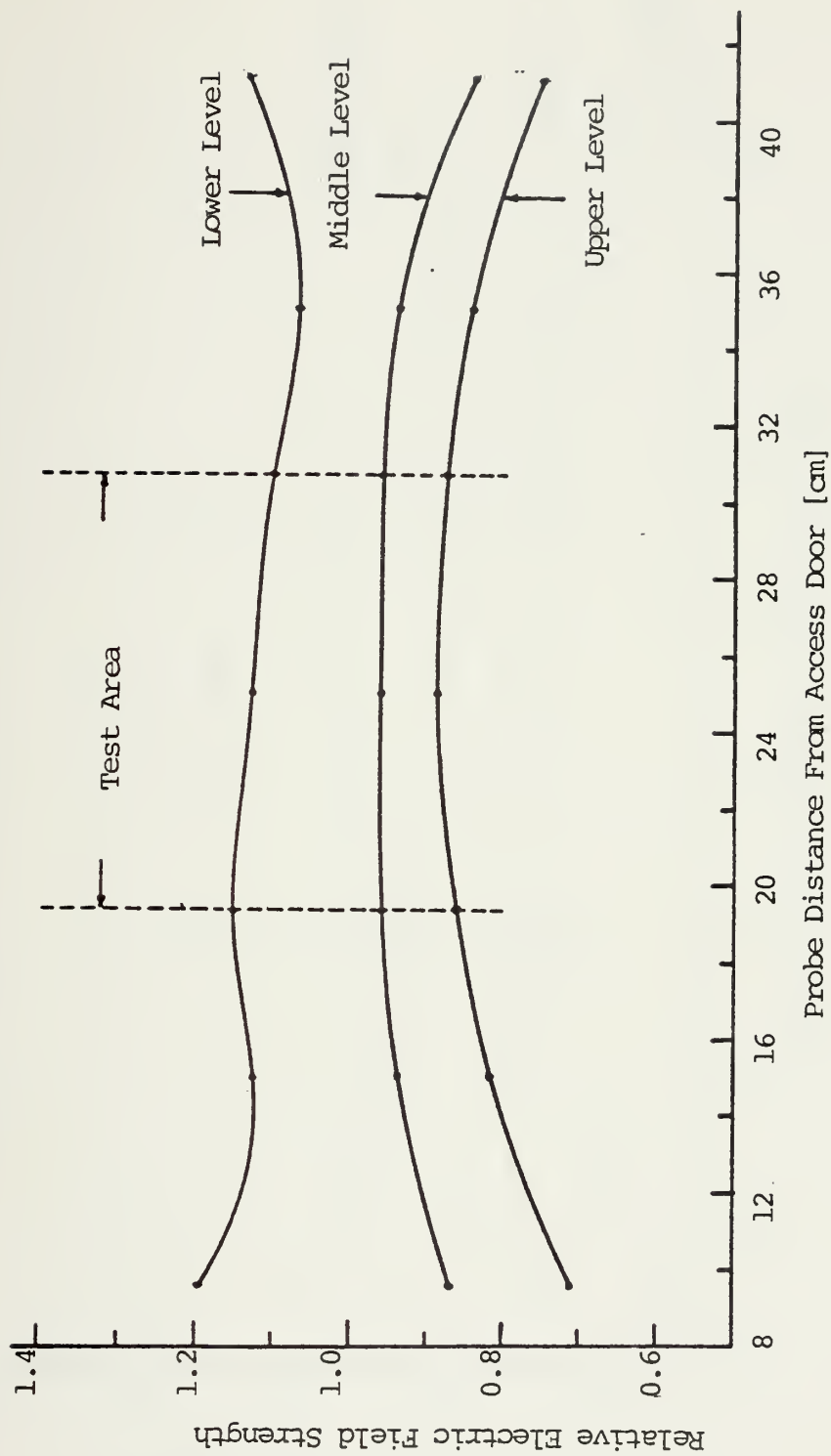


Figure 20. Relative Electric Field Distribution Inside Empty Cell at Frequency 1 MHz



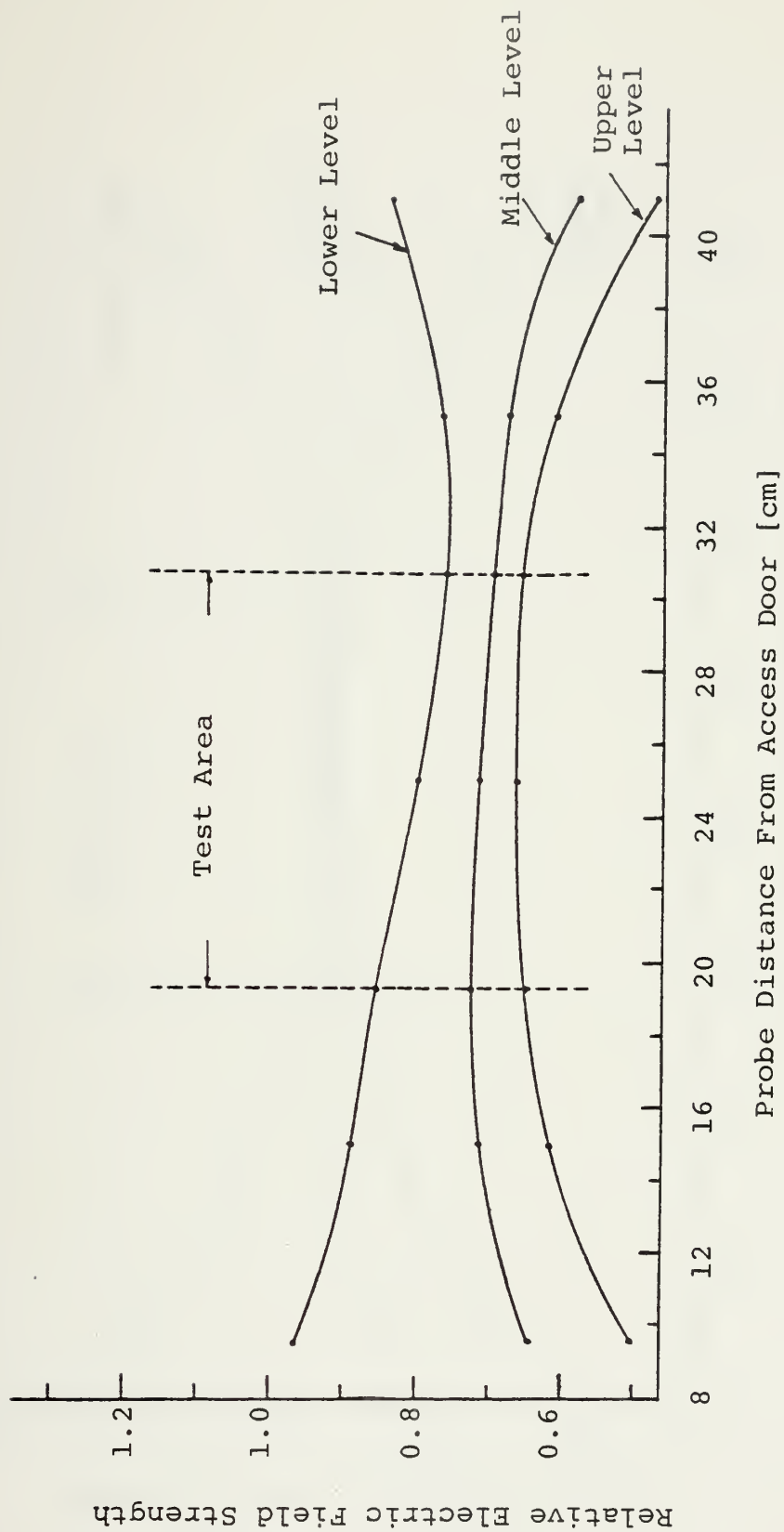


Figure 21. Relative Electric Field Strength Distribution Inside Empty Cell at Frequency 10 MHz





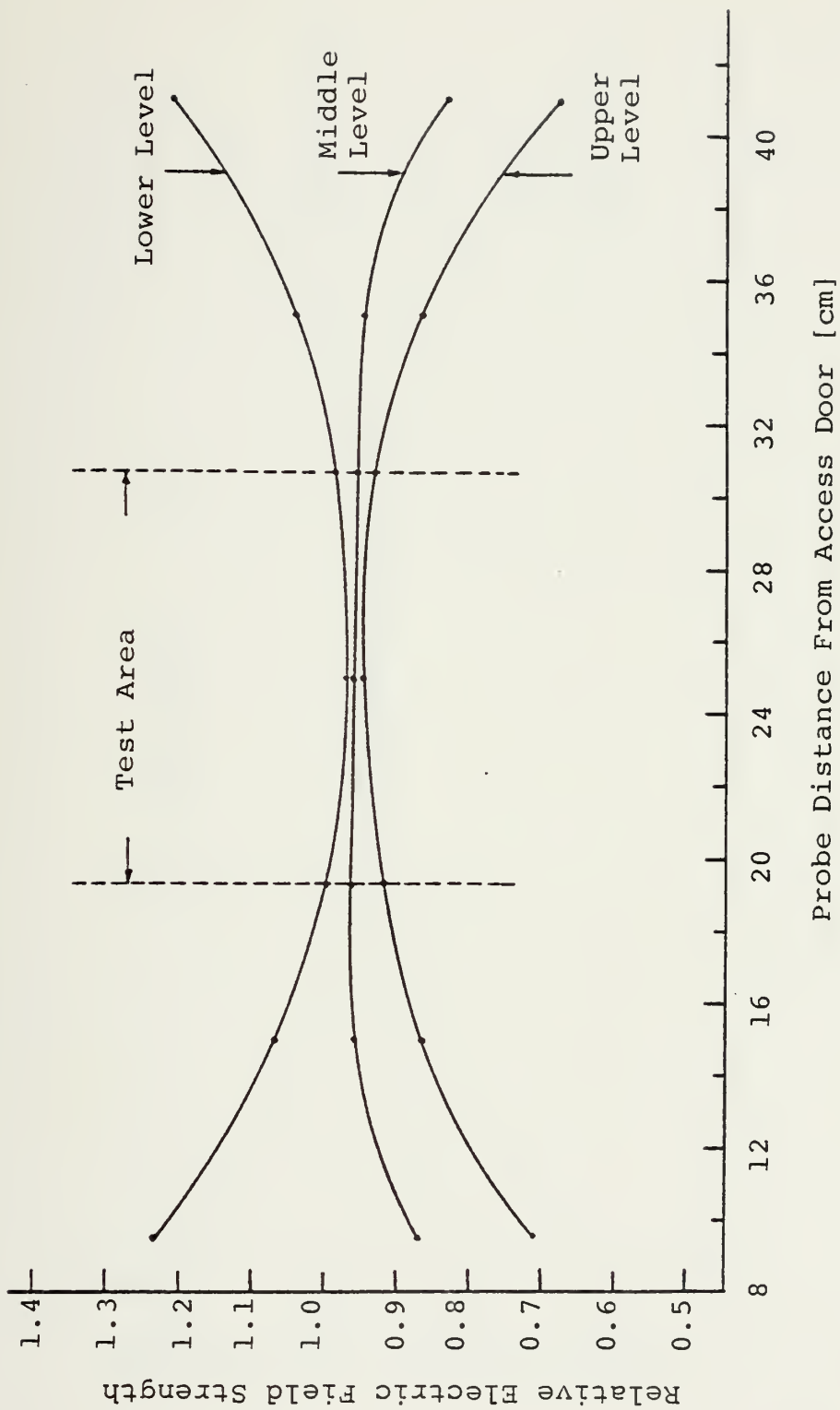


Figure 22. Relative Electric Field Distribution Inside Empty Cell at Frequency 100 MHz



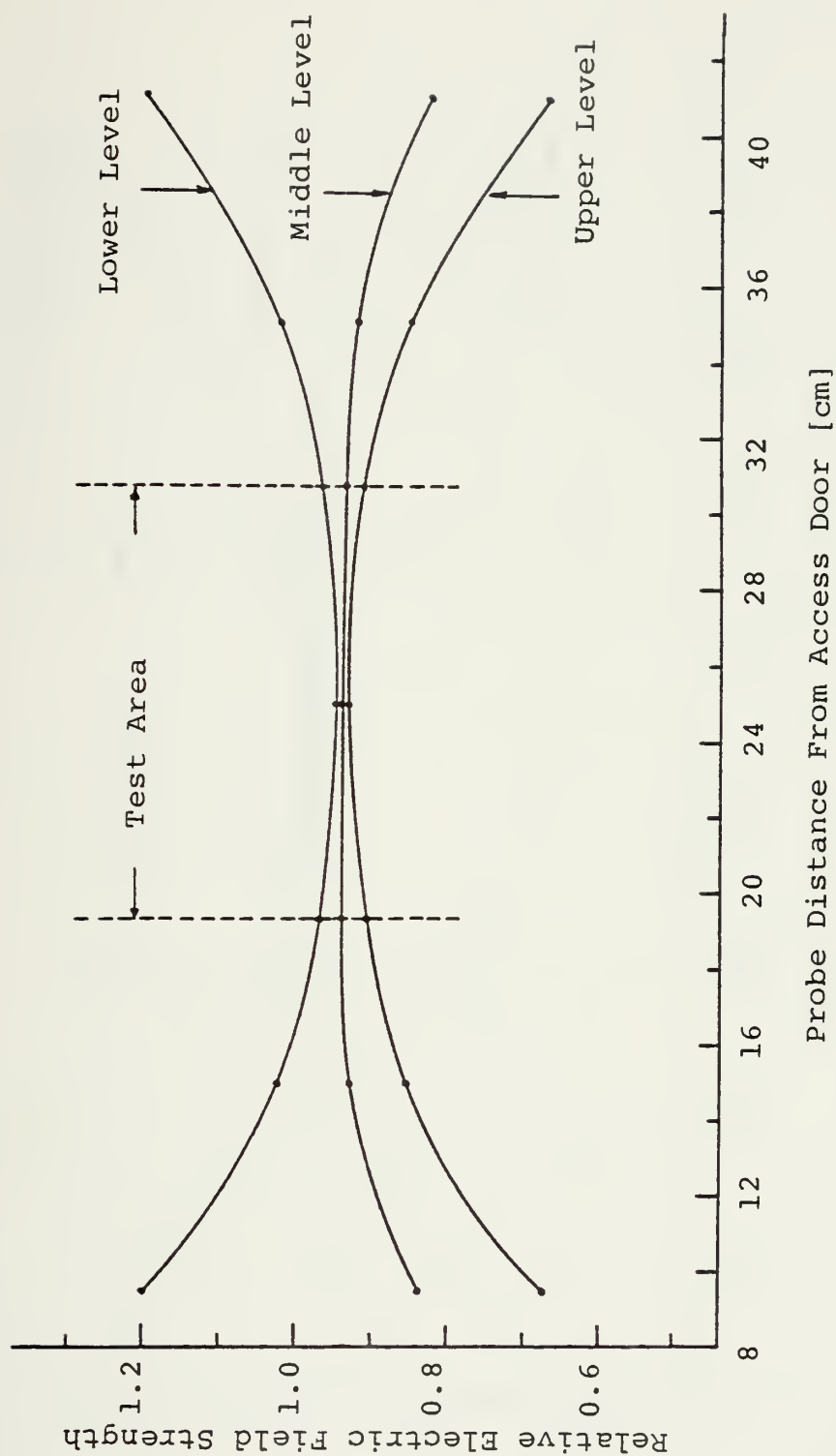


Figure 23. Relative Electric Field Distribution Inside Empty Cell at Frequency 200 MHz



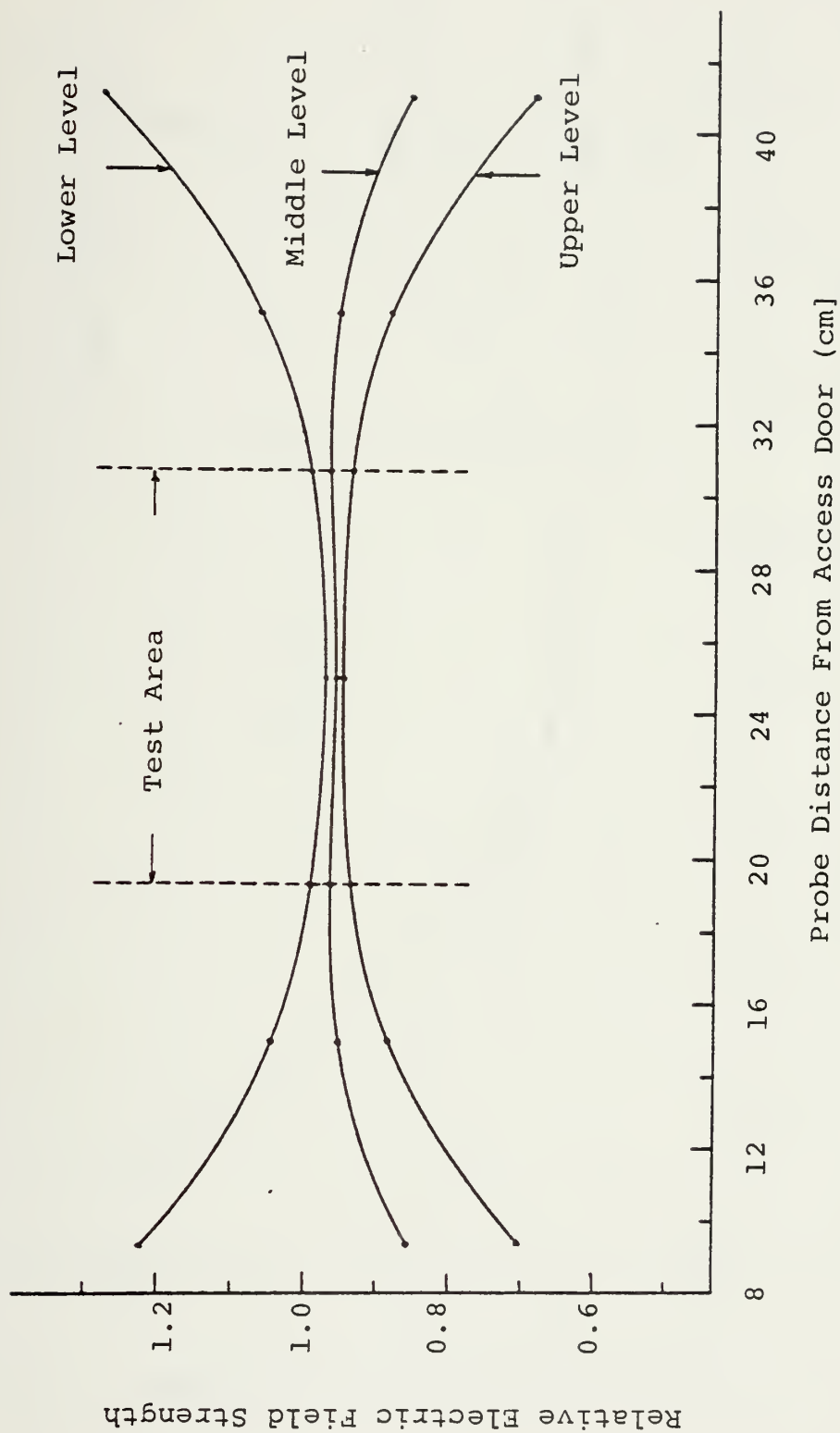


Figure 24. Relative Electric Field Distribution Inside Empty Cell at Frequency 400 MHz





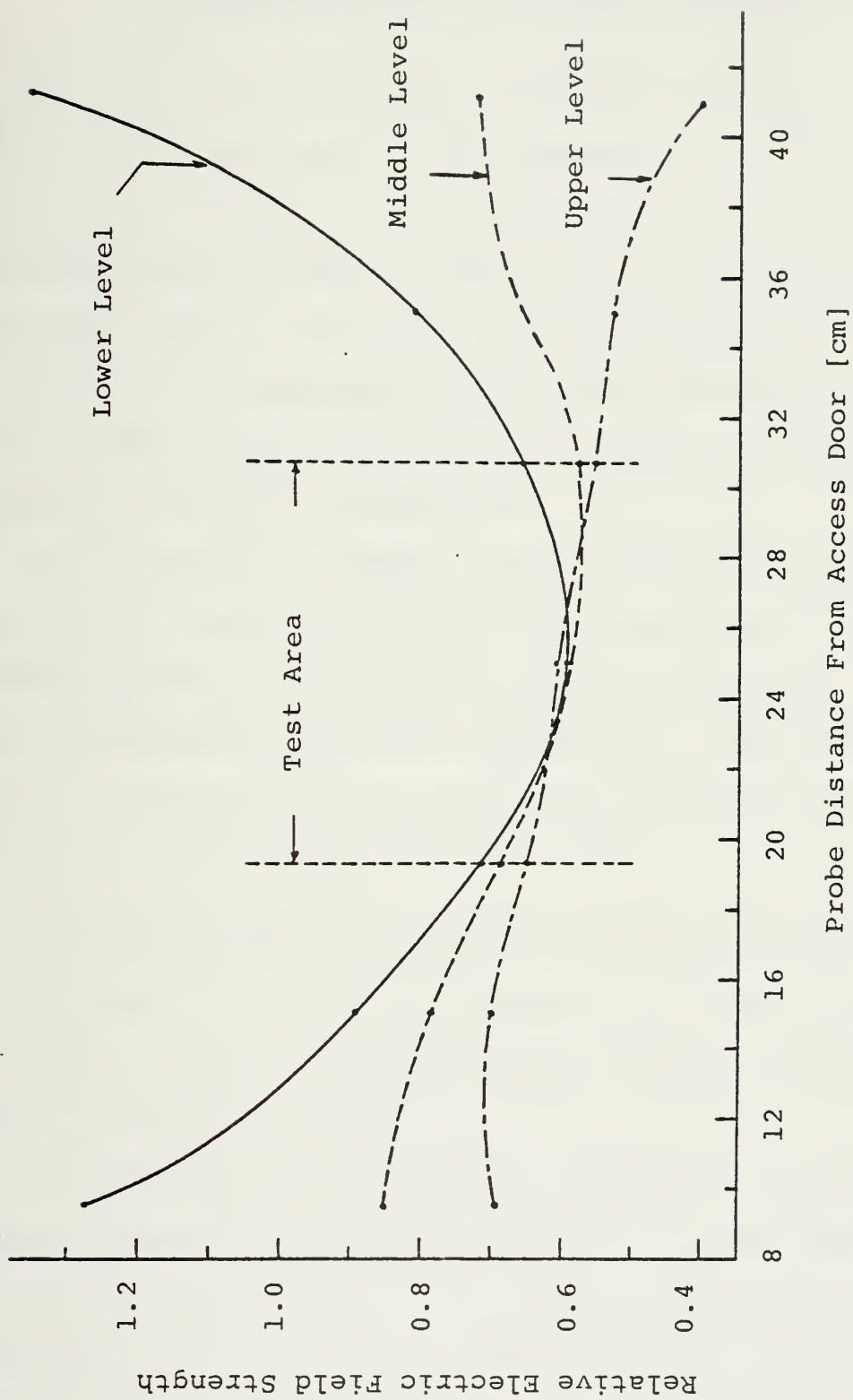


Figure 25. Relative Electric Field Distribution Inside Empty Cell at Frequency 700 MHz



#### IV. EXTENDING THE UPPER USEFUL FREQUENCY RANGE OF THE TEM CELL BY ABSORBER LOADING

The cell can be used at frequencies as low as desired since the TEM mode has no low frequency cut-off, limited only by the cell's magnetic shielding effectiveness, which is determined by the material from which it is made [5]. As mentioned earlier the upper useful frequency of the cell is limited by the distortion of the signal caused by resonances and multimodes that occur within the cell at frequencies related to the cell's dimensions.

The technique of loading the cell with RF absorbing material for suppressing the multimoding effects at high frequencies are discussed in this section and the results for the characteristic impedance obtained, the VSWR measured and the evaluation of the electrical performance characteristics of the absorber loaded cell shown.

##### A. VSWR IMPROVEMENT BY SELECTING ABSORBER LOCATION

The same set-up as for the empty cell shown in figure 10, was used to measure the VSWR for the absorber loaded cell from 100 MHz up to 1 GHz.

The objective was to determine experimentally the optimum amount and location of the absorber to minimize VSWR. Three types of absorbing material, as shown in Figure 26 were tested together with several combinations of them. The first type was the "Rontec" FL-2250 (thickness 2.250 inches) which is a





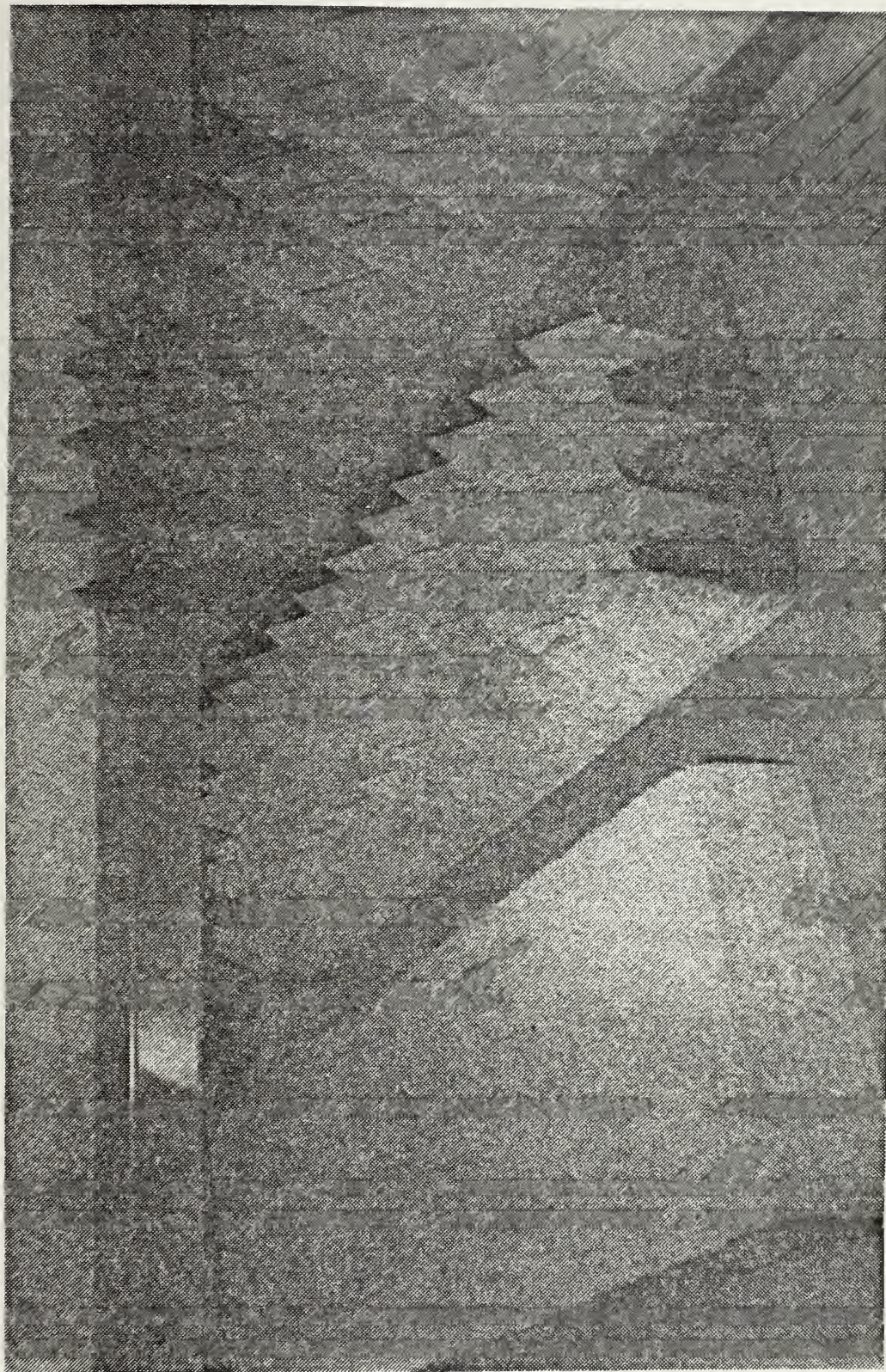


Figure 26. RF Absorbing Material used in TEM Cell (from Left to Right: FL-2250, EHP-3 and EHP-5)





broadband graded dielectric, flat laminate absorber with three electrically different layers having uniform thickness. The other two types were the "Rontec" EHP-3 (Extra High Performance) and EHP-5 absorber, which is a broadband material fabricated from low density flexible polyurethane foam and is cut into a pyramidal configuration. The EHP-3 has an overall height of 3 inches and the EHP-5 5 inches.

The flat absorber was first tested and was placed according to the configuration of Figure 27. No significant improvement was obtained in the VSWR. The same situation was encountered when many other absorber locations were tried using this absorbing material. It was observed that the best results were obtained in cases where some pieces were oriented vertically to the long axis of the cell with the larger dimension facing the input and output ports. This was believed due to wave impedance matching characteristics of the absorber and its alignment in the cell relative to the fields traveling through the cell (i.e., maximum absorption occurs at normal incidence of the field to the absorber) [4]. By using the EHP-3 and EHP-5 absorbing material better results were obtained and the VSWR spikes at frequencies 500 MHz to 1 GHz were reduced significantly to values of less than 2:1. The best VSWR was achieved by using the EHP-3 absorber. The VSWR curve for 100 MHz to 1 GHz is shown in Figure 28 corresponding to the absorber location shown in Figure 29. Figure 30 shows the VSWR trace for the same absorber location, but when the short





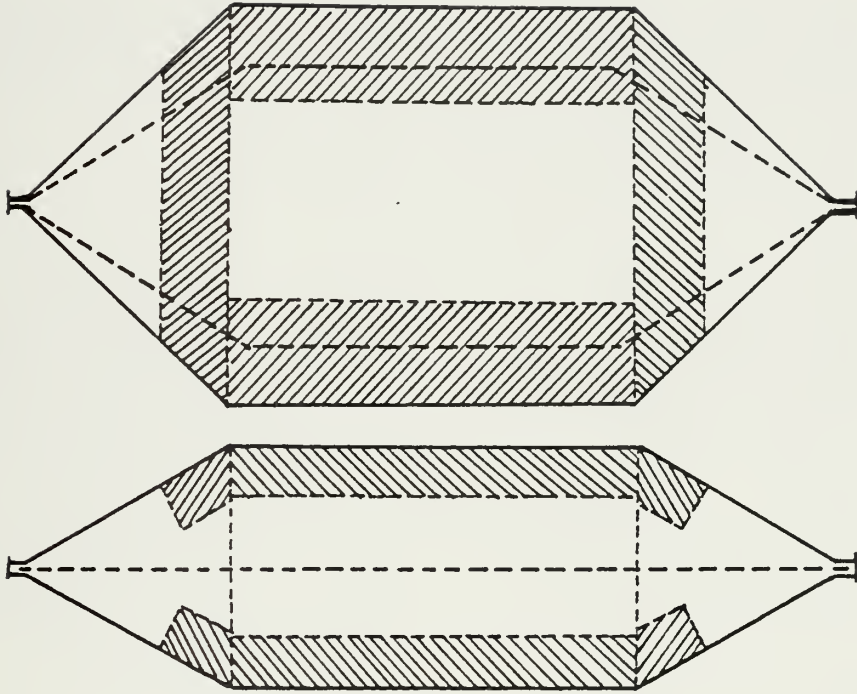


Figure 27. Flat Absorbing Material Placement



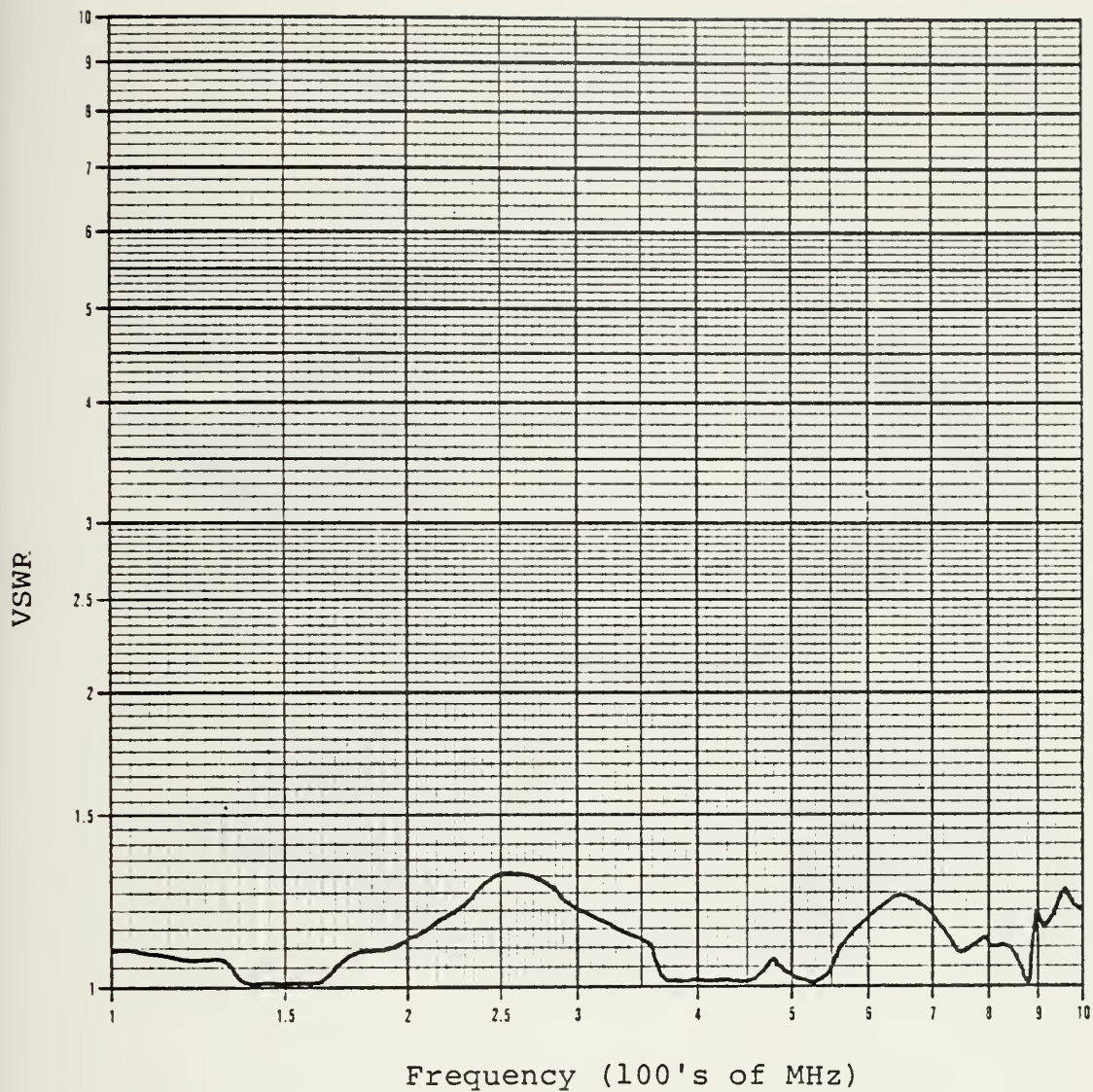


Figure 28. VSWR of Absorber Loaded Cell Measured at Input Port (Short Circuit Measurement at Input of Cell)



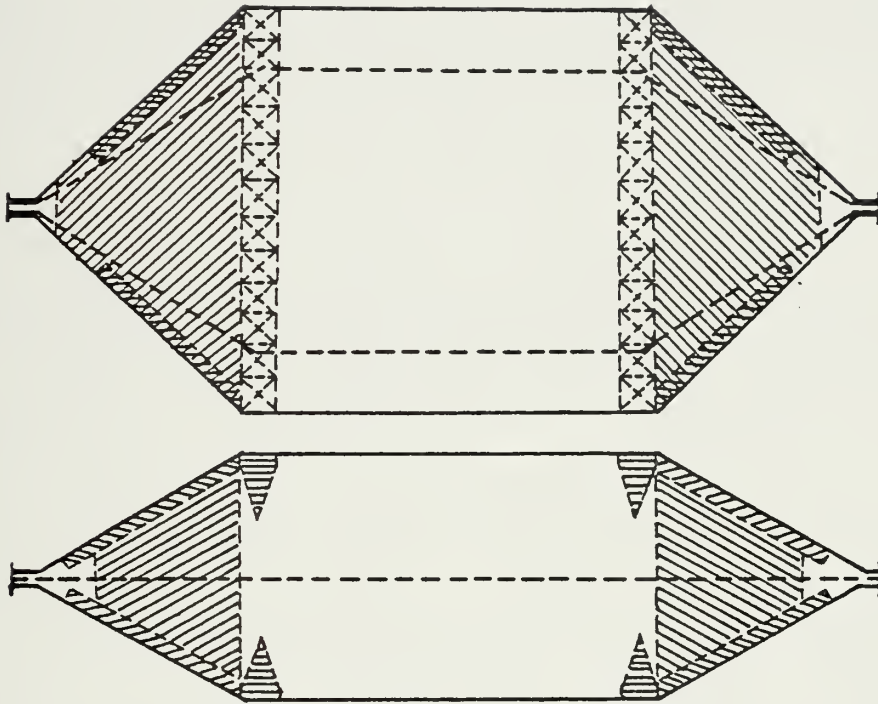


Figure 29. Combination of Thin Flat and EHP-3 Absorbing Material Placement





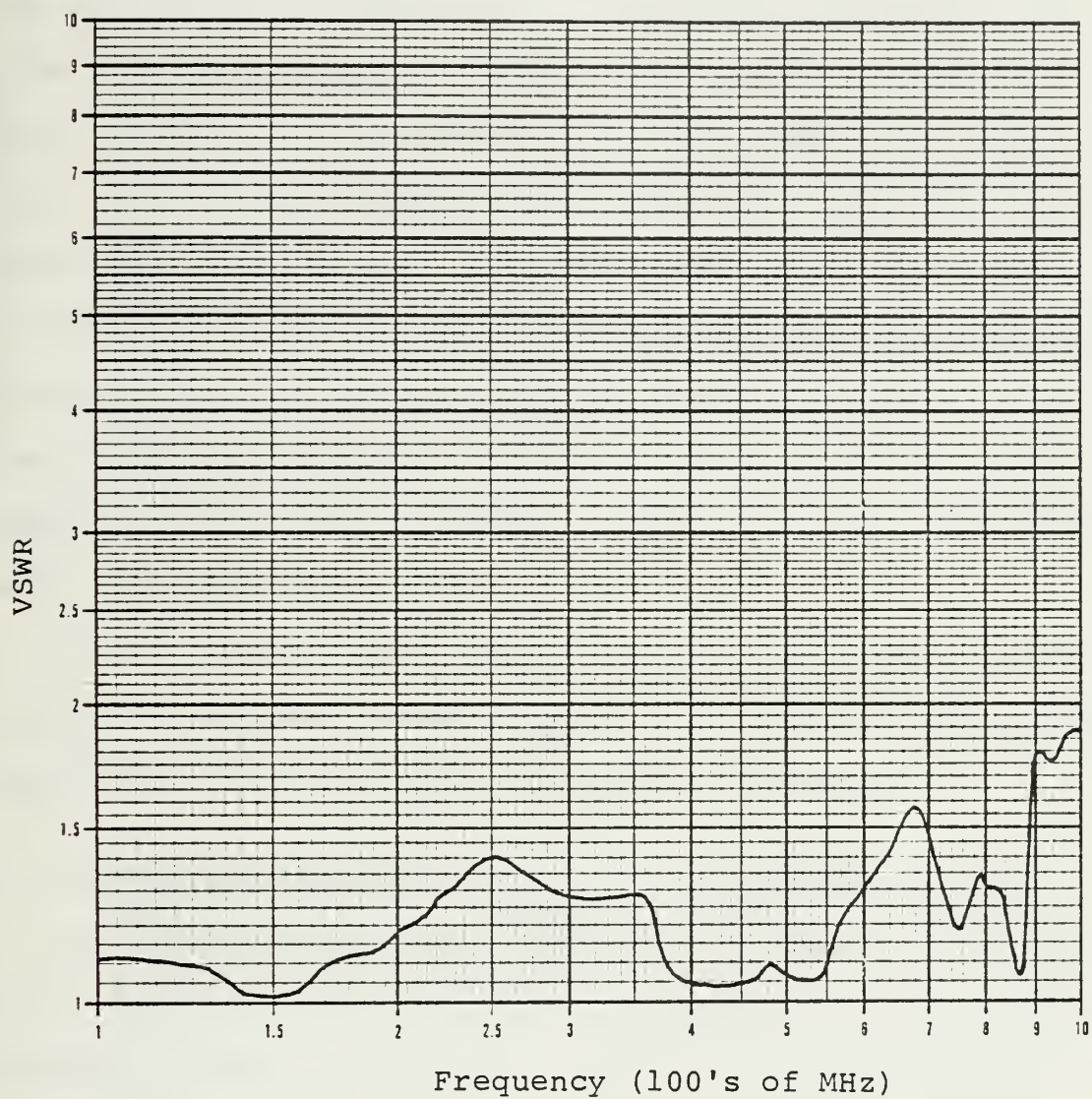


Figure 30. VSWR of Absorber Loaded Cell  
Measured at Input Port (Short  
Circuit Measurements at Output  
of Cell)



circuit measurements are made at the output of the cell and not at the cable connecting to the input of the cell (see measurements procedure in the Vector Voltmeter manual).

From figure 28 it was observed that the VSWR has a value lower than 1.3 for all frequencies of interest. Comparing with the empty cell (figure 12), there is a VSWR increase from 200 to 350 MHz. This was proven to be an unavoidable consequence of obtaining low VSWR for frequencies of 500 MHz to 1 GHz. The distribution of the reflection coefficient along the absorber loaded cell is shown in Figure 31 for  $\rho/\text{cm} = 0.1$  and  $\rho/\text{cm} = 0.02$ .

Finally seven other complete representations involving absorber locations, VSWR curves and pictures of the reflection coefficient distributions are shown in Appendix D.

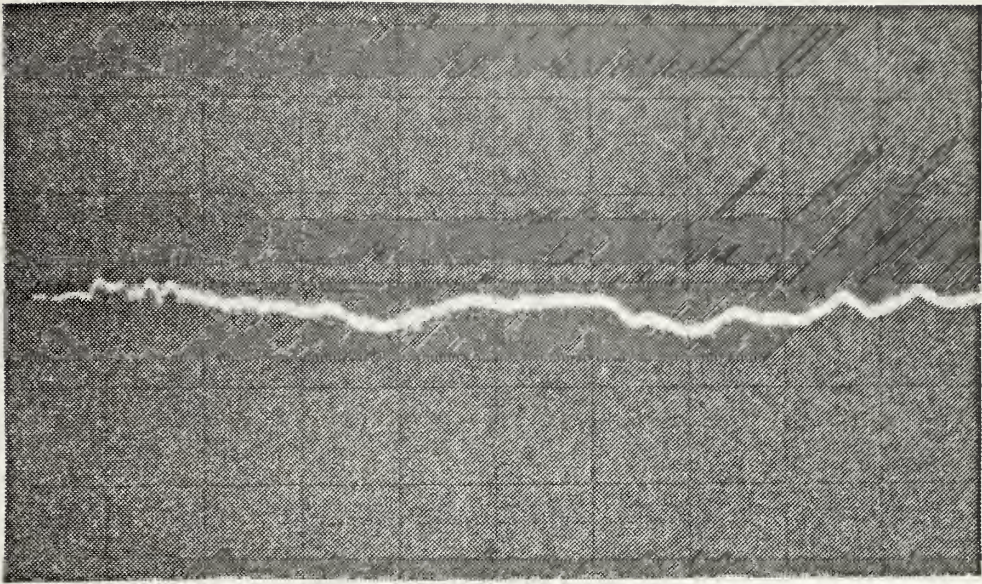
#### B. MAPPING THE FIELDS INSIDE THE ABSORBER LOADED CELL

The measurement system described in Section III(C) and shown in figure 15 was used for mapping the fields inside the absorber loaded cell. The procedure was the same as in the empty cell case. The only differences were in the values of the characteristic impedance and the net power substituted in equation (5). The measured value of  $R_c$  was found to be 48 ohms in the test area of the cell as shown in figure 31. The power flowing through the same area was calculated by the formula

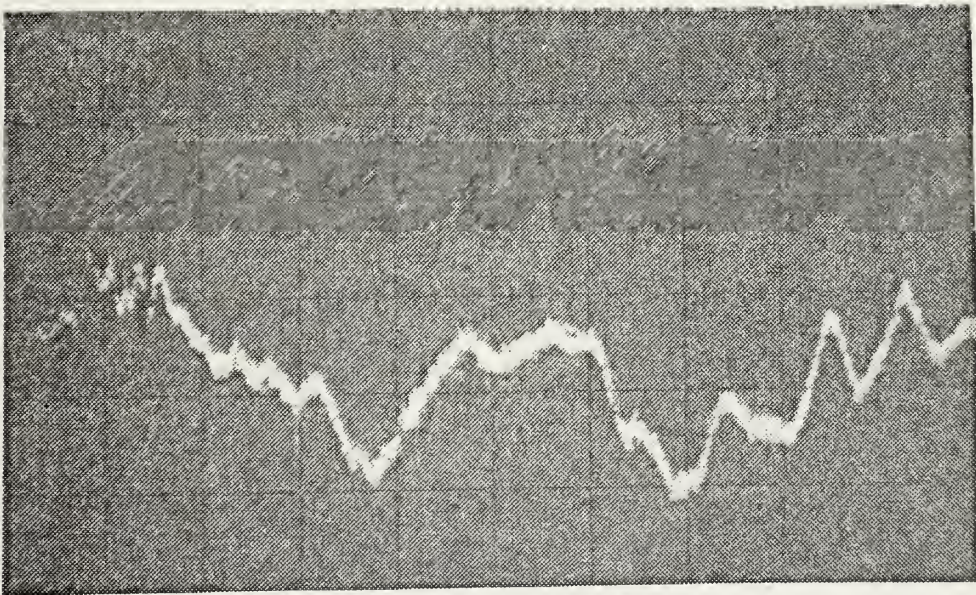
$$P_{\text{center}} = \frac{P_{\text{in}} + P_{\text{out}}}{2} \quad (10)$$







(a)



(b)

Figure 31. TDR Trace of Distributed Reflection Coefficient  
for Absorber Loaded Cell (a)  $\rho/\text{cm} = 0.1$ ,  
(b)  $\rho/\text{cm} = 0.02$



since the cell is not lossless due to the effect of the absorbing material.

Data are plotted and shown in Figures 32 through 35 as a function of the relative electric field strength versus distance of the probe from the access door, for frequencies of 1 MHz, 400 MHz and 895 MHz.

The above plots together with many others obtained for different frequencies are shown in Appendix E as a function of the measured electric field strength versus probe distance from the door.





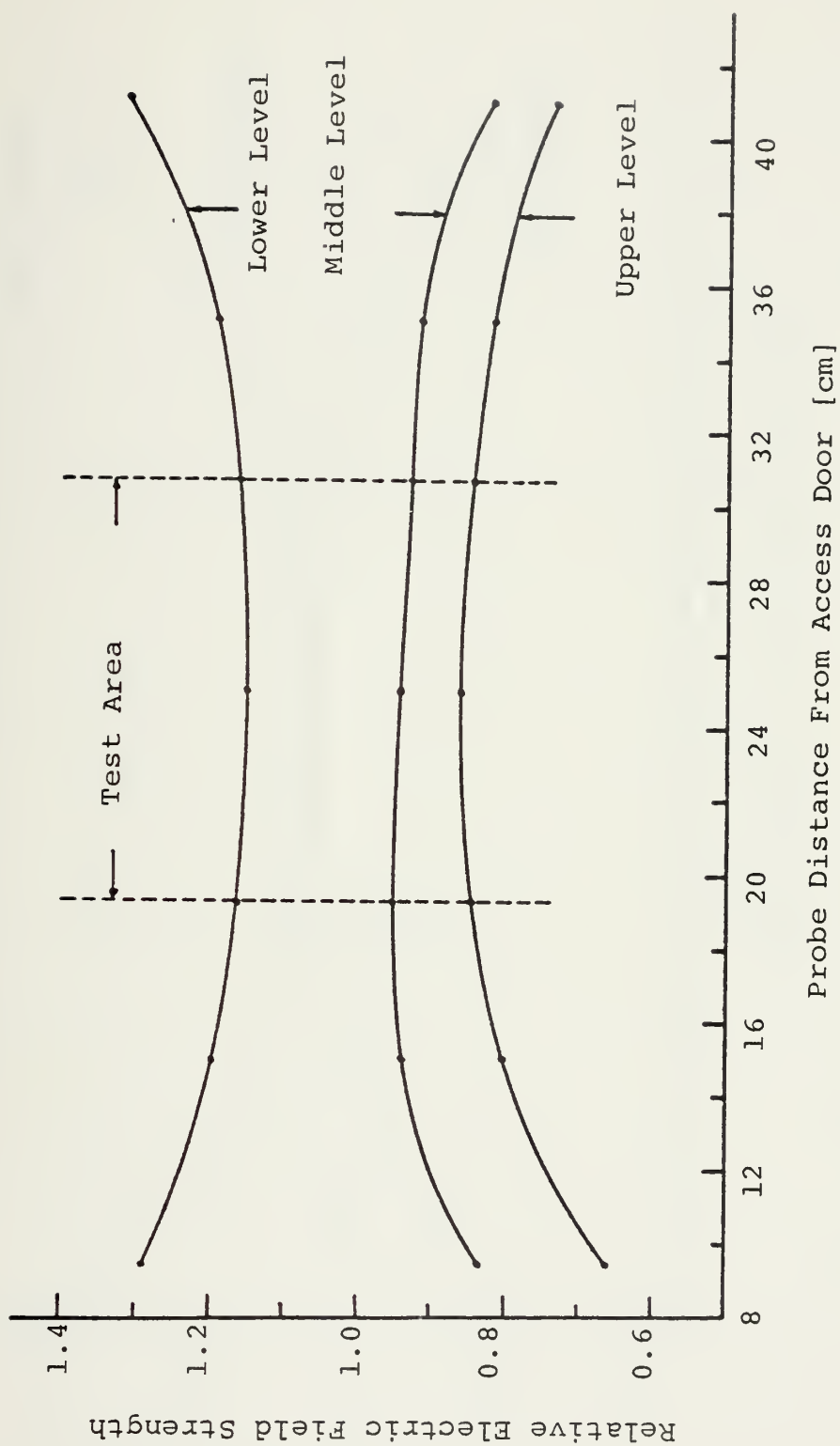


Figure 32. Relative Electric Field Distribution Inside Absorber Loaded Cell at Frequency 1 MHz



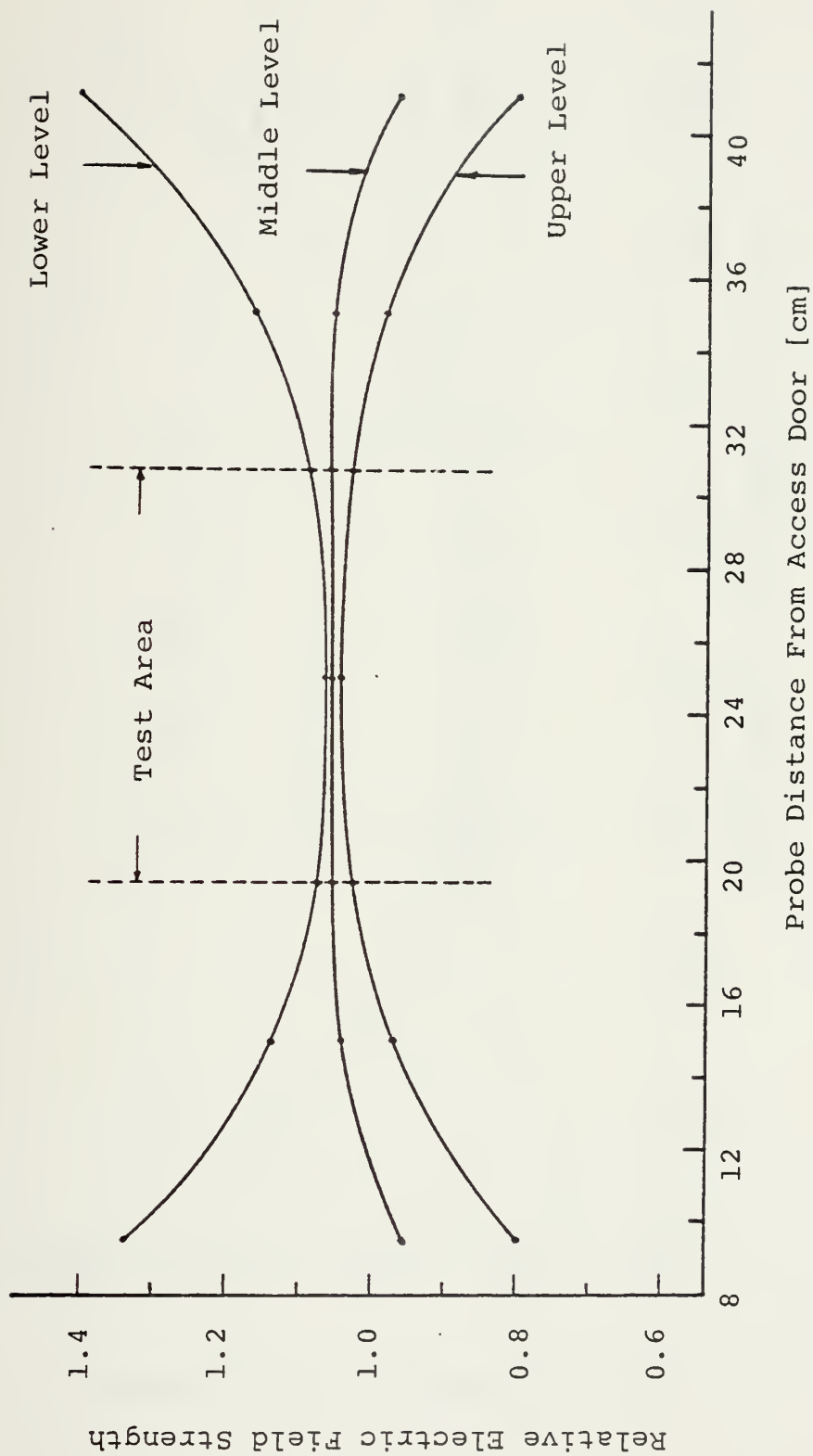


Figure 33. Relative Electric Field Distribution Inside Absorber Loaded Cell at Frequency 400 MHz



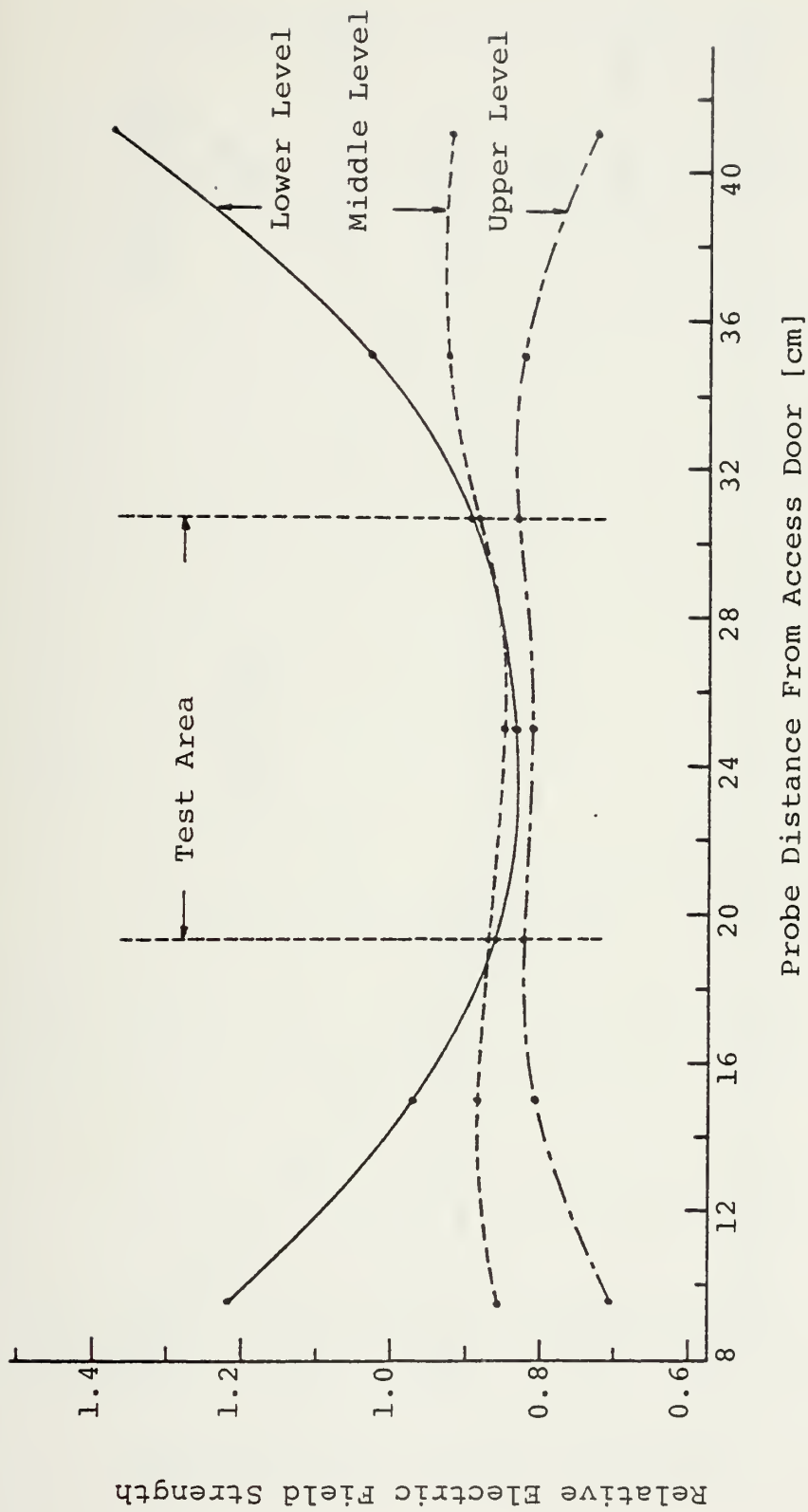


Figure 34. Relative Electric Field Distribution Inside Absorber Loaded Cell at Frequency 675 MHz





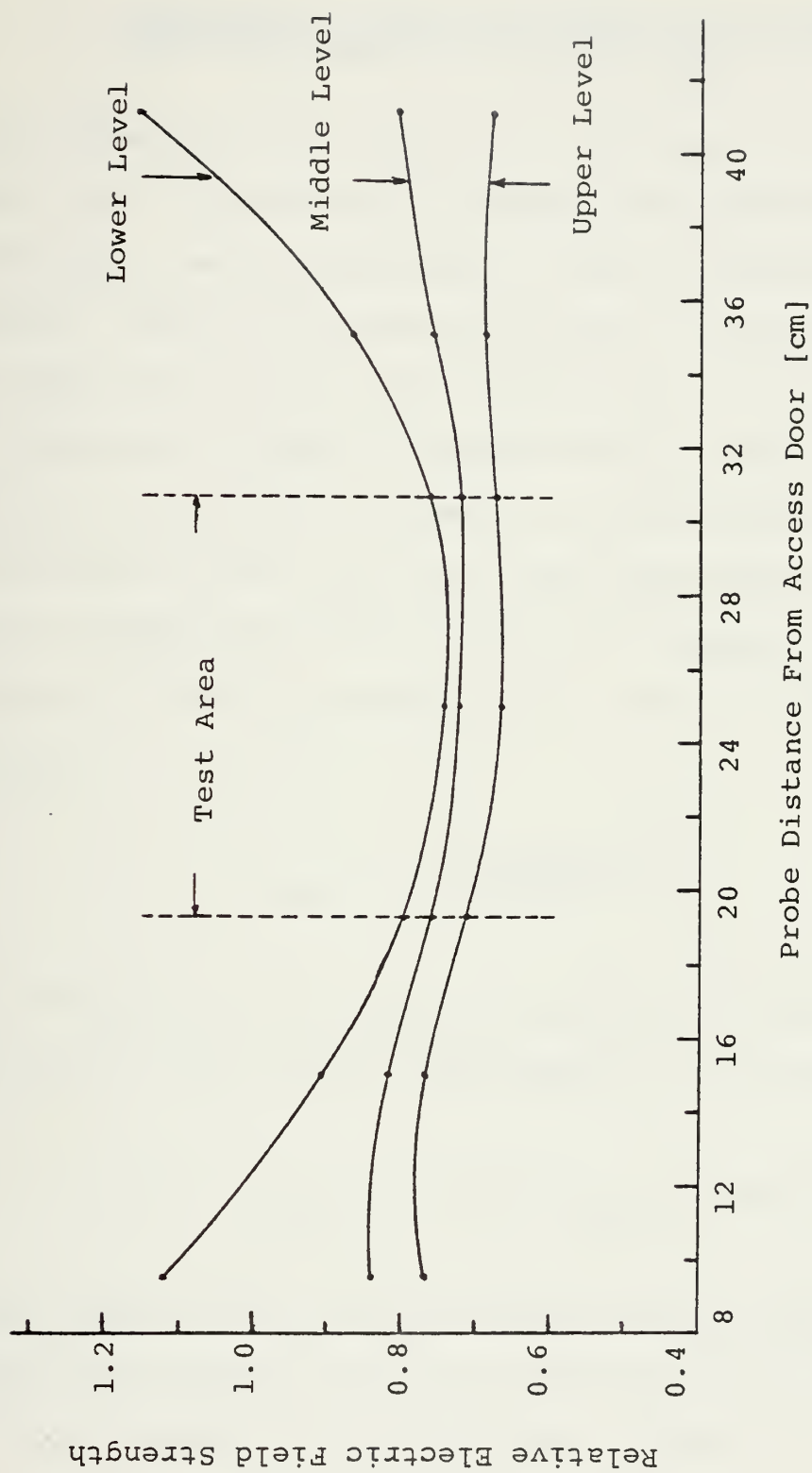


Figure 35. Relative Electric Field Distribution Inside Absorber Loaded Cell at Frequency 895 MHz (Access Door Closed)



V. CALIBRATION OF OMNIDIRECTIONAL FIELD PROBES  
USING THE ABSORBER LOADED TEM CELL

The completed cell was used to calibrate two isotropic probes. An  $\bar{H}$  field spherical shaped and a pyramidal shaped  $\bar{E}$  field probe were constructed at NPGS and provided by Dr. Richard W. Adler of the BDM corporation for calibration. Each probe was inserted into the test area of the cell and data obtained for output voltage readings. The E field was calculated for several frequencies between 100 KHz and 1 GHz. At the center of the cell  $\bar{E}$  was determined from the power flowing through this area by using the equation (10), cell impedance  $R_c$  and plate separation  $d$ , using the following equation,

$$E_{cal} = \frac{(P_{center} R_c)^{1/2}}{d} \quad (11)$$

Substituting the value of  $R_c = 48$  ohms  $d = 0.1425$  m and setting the  $P_{center}$  in milliwatts, the equation (11) becomes:

$$E_{cal} = 1.537 (P_{center} \text{ [mW]})^{1/2} \quad (12)$$

The directionality of the probes was also determined by measuring the output voltage at different probe orientations for every frequency and for all power levels.



#### A. SPHERICAL $\bar{H}$ PROBE CALIBRATION

In the vertical plane the 4 inch sphere, Figure 36, was rotated through  $360^\circ$ , with 4 points of measurement being established at each octant. Orthogonal to the vertical plane, the sphere was rotated through  $360^\circ$  again, establishing

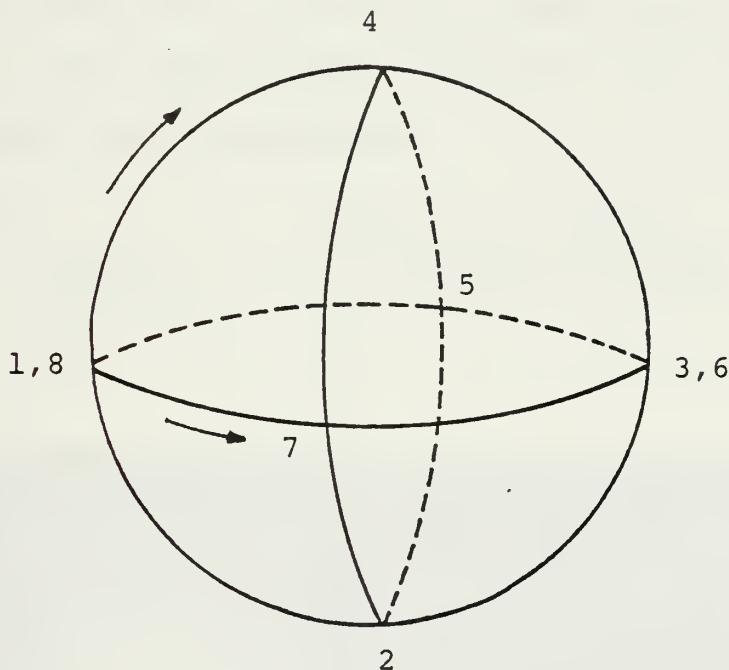


Figure 36. Orientation Positions for  $\bar{H}$  Probe Inside the Cell

4 more octant points. (Note that only one point is completely "common," the other at the opposite side being reversed in direction.) A picture of the spherical probe is shown in Figure 37.

The set-up of figure 15 minus the reflectometer was used. The sweep oscillator was used for frequencies above 100 MHz and the "Wavetek" generator below.





The calibration procedure was as follows: The probe was placed at the center of the testing area inside the cell on a polystyrene foam base. The RF signal source was set in CW mode and the desired frequency was selected. The highest possible output power was obtained and measurements were made using appropriate attenuators. The probe output voltage was monitored for each one on the seven predetermined probe orientations. The probe output voltage at each power level was calculated using the relation

$$V_{\text{probe}_{\text{OUT}}} = \frac{V_{\text{probe}_{\text{MIN}}} + V_{\text{probe}_{\text{MAX}}}}{2} \quad (13)$$

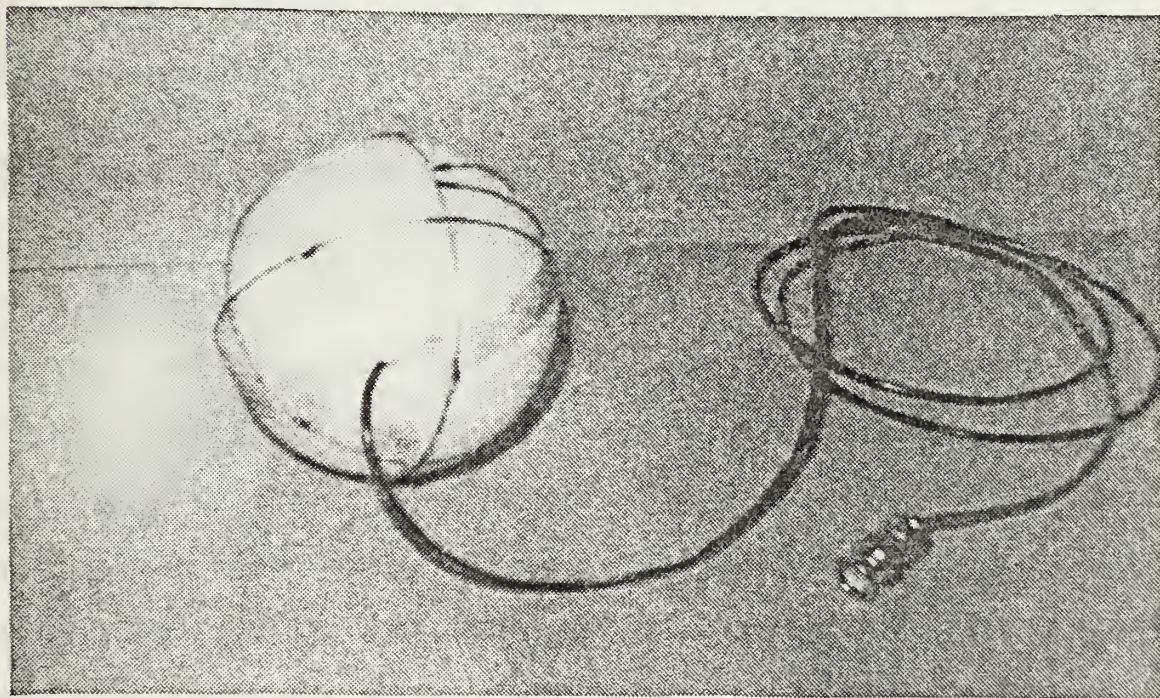


Figure 37. Spherical Omnidirectional  $\bar{H}$  Field Probe





The generator output power was then reduced by 5 dBm and the same procedure was repeated down to the minimum possible generator output power coincident with probe output voltages above the noise level of the electrometer. Finally the E field at each power level was calculated by using the equation (12).

Figure 38 shows the variations of the probe output voltage versus calculated incident E field for frequencies 0.1, 1, 10, 100, 500 and 1000 MHz. Figure 39 shows the variations of the probe output voltage versus frequency for several values of calculated incident E field.

The directionality of the spherical probe was also determined and the #5 orientation position was found to have the closest values to the probe output voltages calculated by the equation (12).

#### B. PYRAMIDAL $\bar{E}$ PROBE CALIBRATION

The set-up and the measurements procedure for calibrating the  $3\frac{1}{2}$  inch pyramidal  $\bar{E}$  probe, shown in Figure 40, were exactly the same as for the spherical one. The pyramid was placed inside the cell on its polystyrene foam base. The pyramid's orientation was determined by the axis coincident with its leads. Measurements were obtained for 6 points as it was rotated around the vertical axis and for 3 points when the axis was oriented in a horizontal position.

The probe output voltage versus calculated incident E field for frequencies 0.1, 1, 10, 100, 500, 1000 MHz are



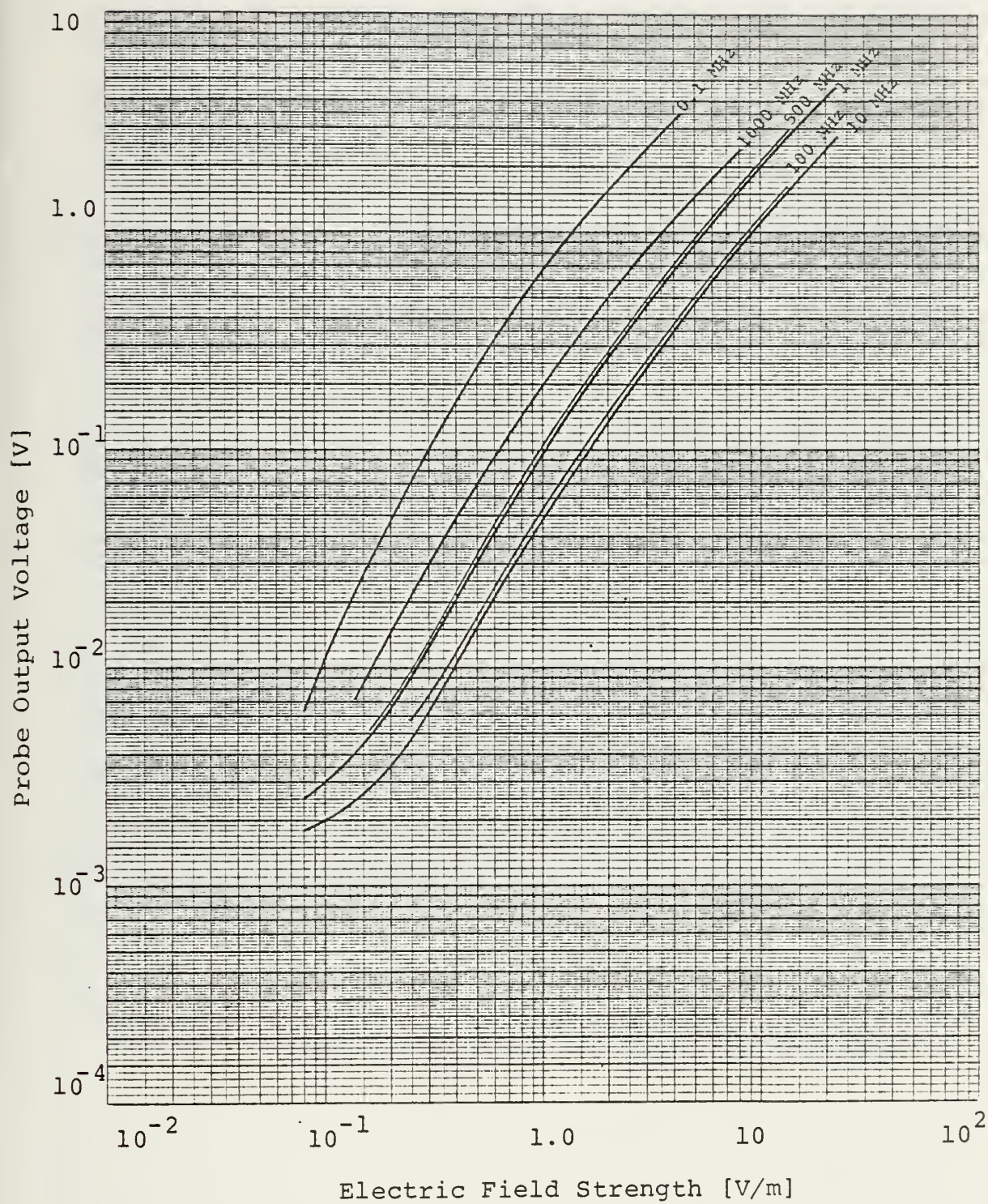


Figure 38. Spherical  $\bar{H}$  Probe Calibration Curves  
(Frequency as Parameter)





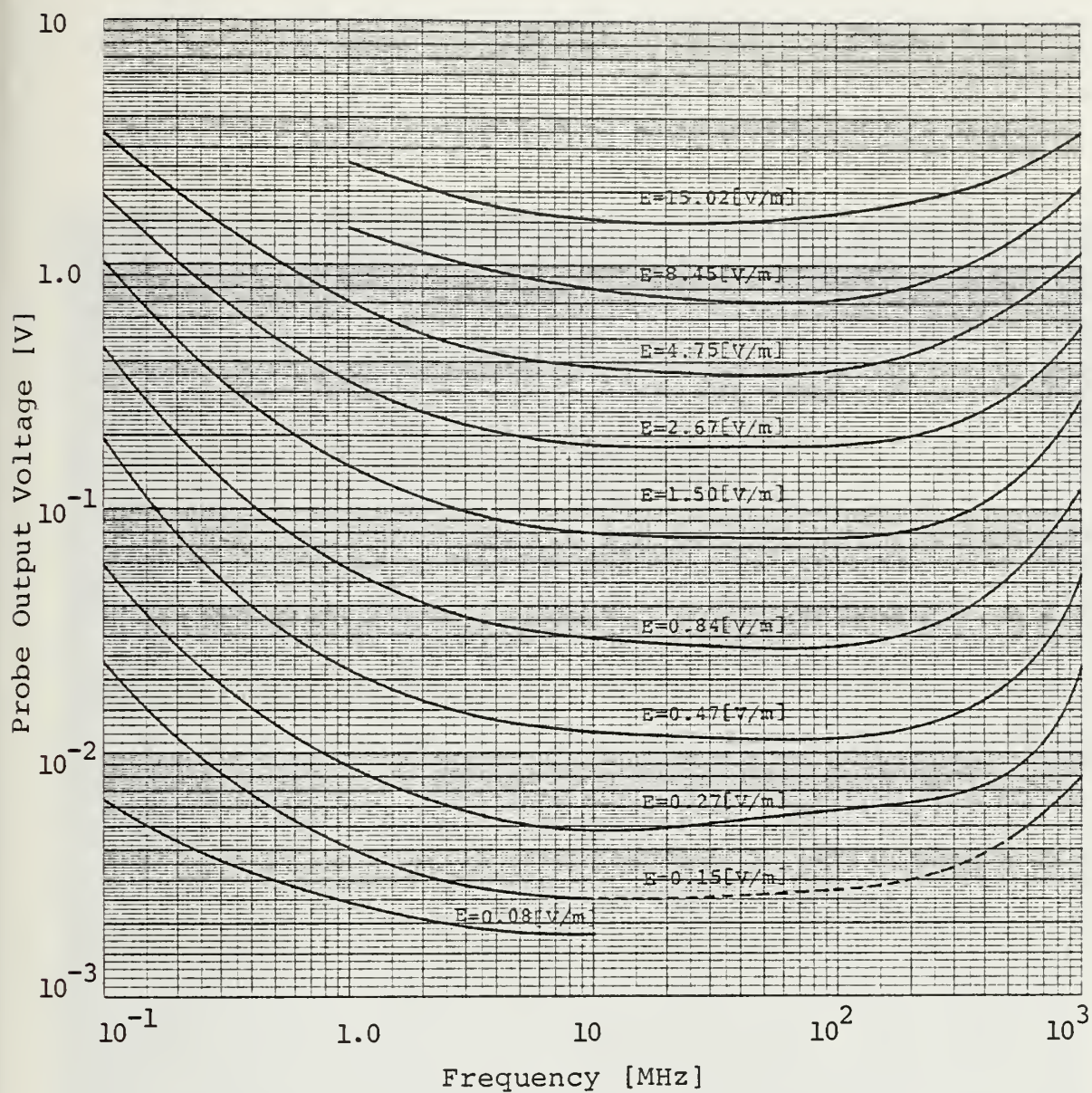


Figure 39. Spherical  $\bar{H}$  Probe Calibration Curves  
(Incident E Field Strength As Parameter)





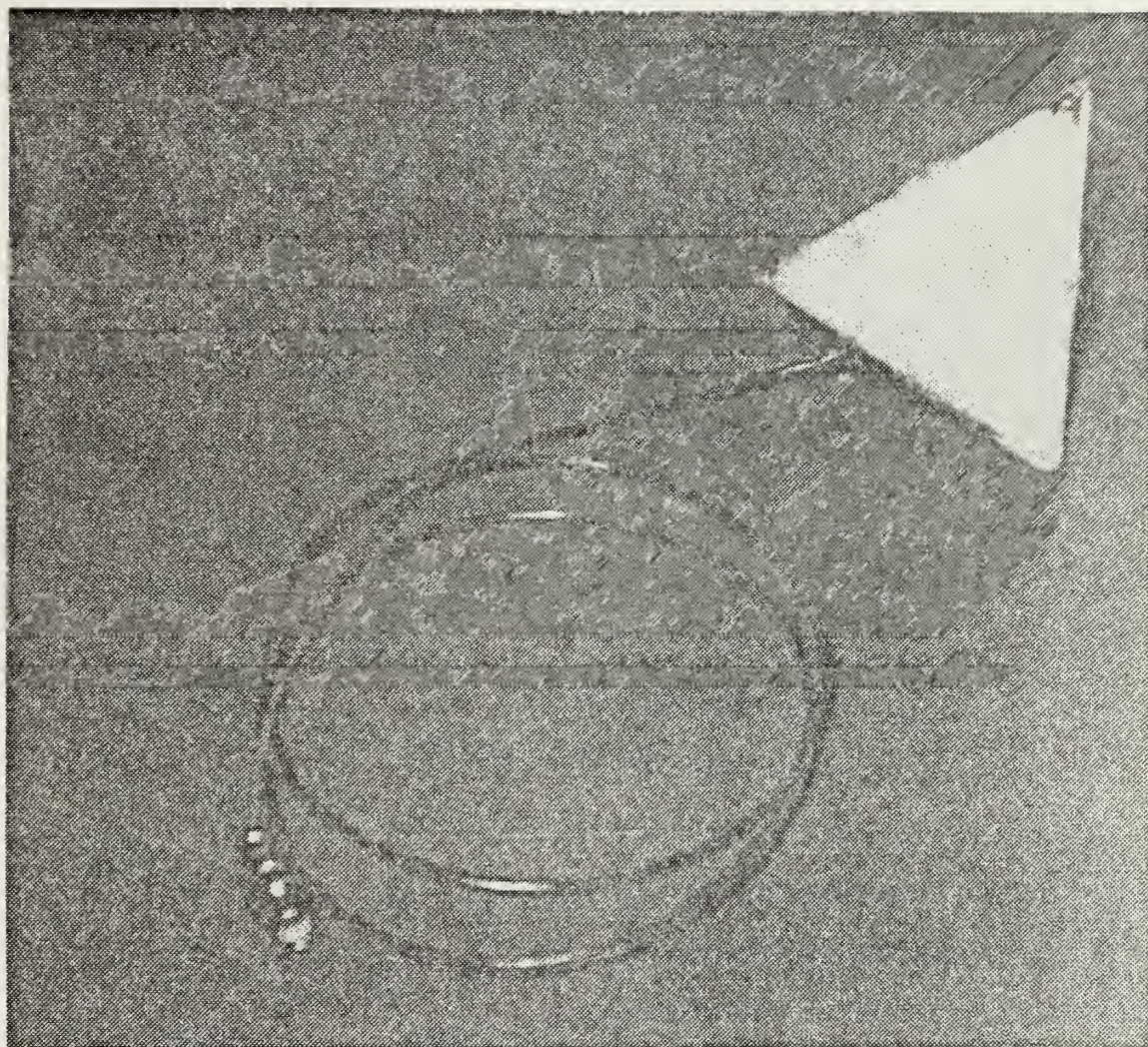


Figure 40. Pyramidal  $\bar{E}$  Field Probe



shown in Figure 41. Also the probe output voltage versus frequency, for several values of the calculated incident E field, are shown in Figure 42.





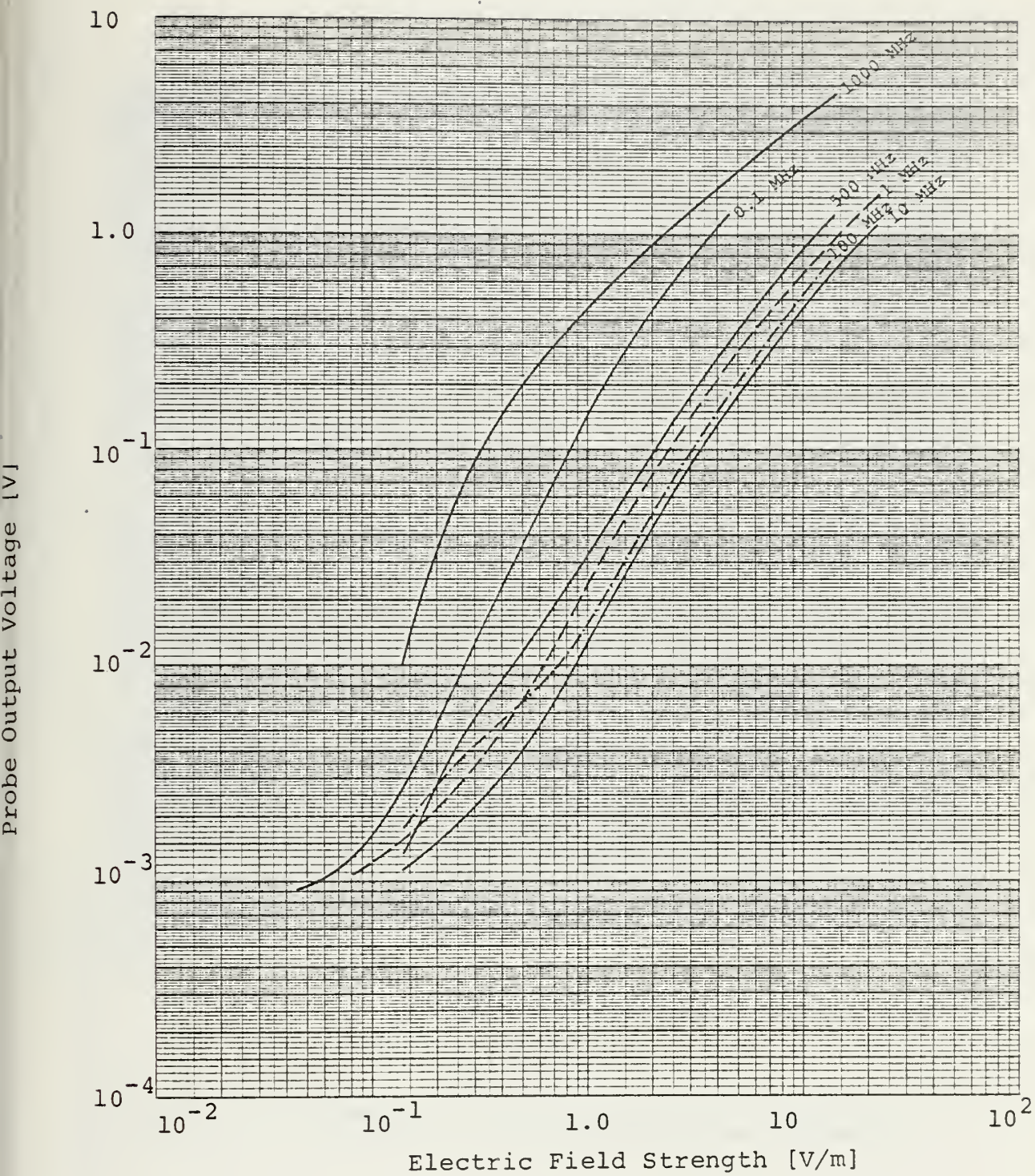


Figure 41. Pyramidal  $\bar{E}$  Probe Calibration Curves  
(Frequency as Parameter)





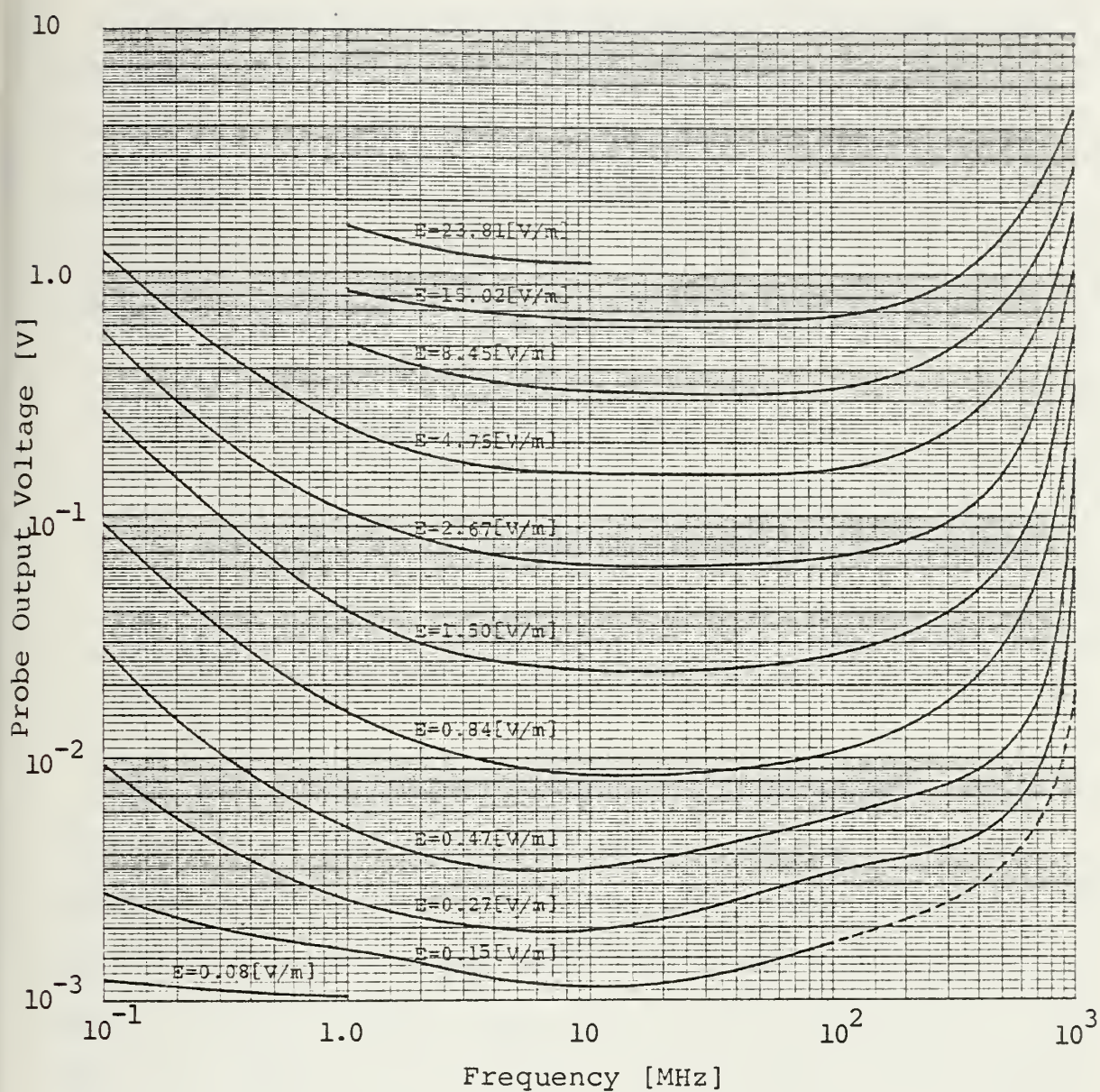


Figure 42. Pyramidal  $\bar{E}$  Probe Calibration Curves  
(Incident  $E$  Field Strength as Parameter)





## VI. SUMMARY AND CONCLUSIONS

The objective of the work described in this paper was the application of a new technique involving the TEM cell for calibrating field probes. Standard electromagnetic environments were simulated inside the cell by generating known RF fields for frequencies from 100 KHz up to 1 GHz. The entire work was divided into four major parts.

1. The design of the cell
2. The construction of the cell
3. The evaluation of the electrical performance characteristics of the empty and of the absorber loaded cell
4. The calibration of two field probes constructed at NPGS.

The cell was designed after those made at NBS. It was constructed at NPGS facilities using 0.08 and 0.185 inch aluminum sheet for the side walls and the septum respectively. Type N coaxial connectors were used at the input and output ports with the tapered output port being terminated in a 50 ohm load. The cell was found to have a characteristic impedance very close to 50 ohms, a VSWR of less than 1.3 and improved E field uniformity via carefully located absorbing material.

Finally the achievement of the overall objective was confirmed from the calibration results of the spherical and pyramidal omnidirectional field probes.



The conclusions from this study can be summarized as follows: The cost of the cell is reasonable and no unique equipment is needed to make the measurements, especially for field probe calibration. The operation and the data acquisition provide no significant difficulty except that careful attention is required when data are obtained at low power levels.

The greatest advantage of using the cell for susceptibility (or emission) measurements is that the background noise does not interfere with the measurements. Problems encountered with shielded or anechoic enclosures are not present when the TEM cell technique is used. The available space for the simulation of electromagnetic environments is completely bounded by the cell's walls, so that uniform and standard fields can be produced, while the operator is well protected. Also a significant factor of repeatability is maintained.

Although the cell is considered to have a wide-band frequency response, the main restriction of using the device is due to multimoding phenomena starting with frequencies higher than the cutoff frequency. An extension of the upper useful frequency can be achieved by loading the cell with absorbing material, with the main disadvantage of size limitations. By using small cells, higher useful frequencies can be obtained, but only small objects can be tested inside the cell due to the design criterion that the EUT must not exceed the  $\frac{1}{3} \times \frac{b}{2}$  dimensions. On the other hand larger objects can



be calibrated inside larger cells, but with lower upper useful frequencies.





## VII. RECOMMENDATIONS

A few recommendations may be useful, especially for future work.

Since the placement of absorbing material is considered necessary and it is believed that better results for field uniformity can be obtained in all cases, the characteristic impedance of the empty cell must be set at about 52 ohms in order to compensate for absorber loading and EUT effects. This turns out to be practical if absorbing pyramids of 3 inches height are used, as in this experiment. Also the use of thin flat absorber is helpful in fine tuning the impedance by a TDR. Another point of interest is in solving the impedance matching problem. The process of adjusting the characteristic impedance of the empty cell and finding the best absorber location, must be done simultaneously.

Further experimental and/or analytical work is needed to eliminate the large transition mismatch of the distributed characteristic impedance at the output port of the cell. Constructing special connectors at this position is considered worthwhile since the mismatch occurs exactly at this point. It is believed that additional theoretical work is needed for solving the size limitation problems, for analyzing the transition sections and for determining the optimum amount and placement of the absorbing material.



As a final comment, a cell with removable and adjustable side walls and septum, especially near the beginning of the output transition, may be useful.



## APPENDIX A

### Design Diagram of the TWEMES Cell

Figure A-1 shows the top view and side views of the design diagram for the TWEMES cell discussed in Section (I).





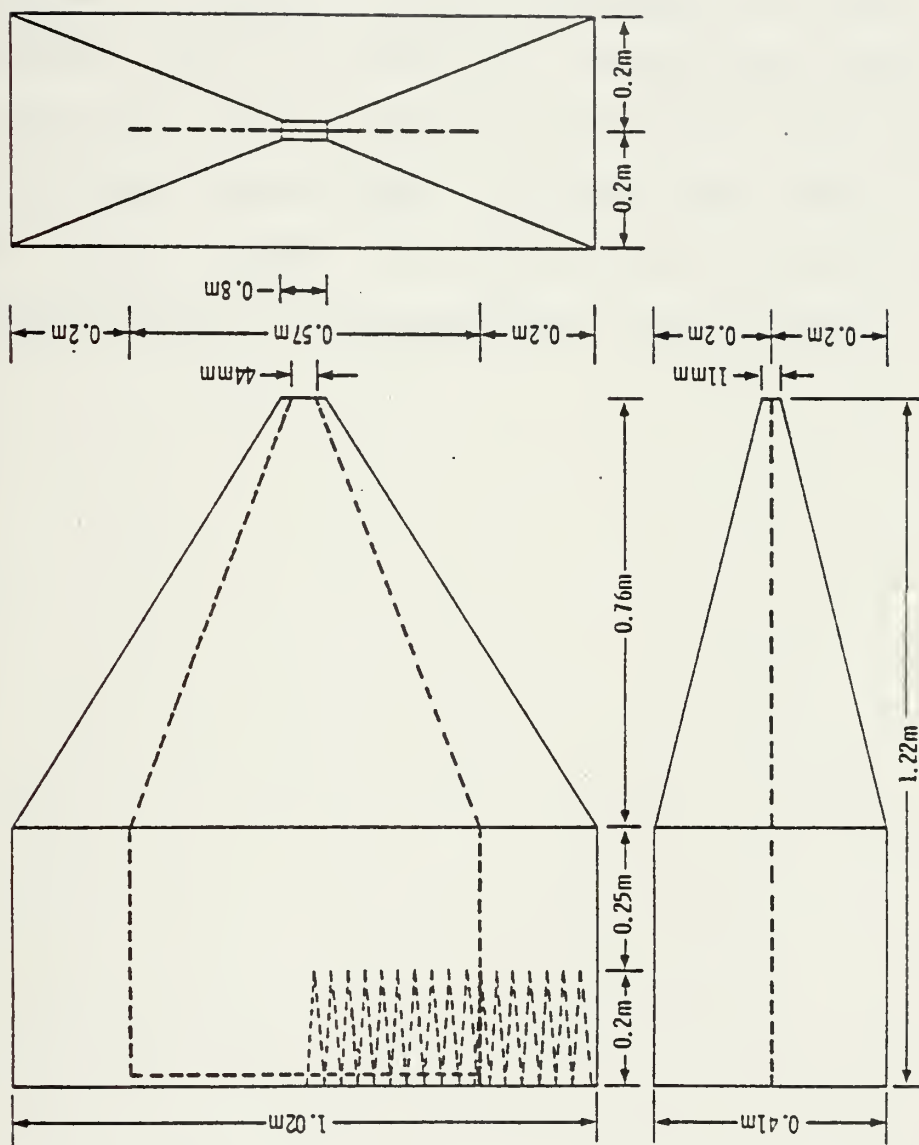


Figure A-1. TWEMES Cell Configuration [7]



## APPENDIX B

### Curves of Measured Electric Field Distribution Inside Empty Cell

Figures B-1 through B-8 show the measured E field distribution inside the empty cell versus probe distance from the access door, for the lower level at  $\frac{3}{8}b$ , middle level at  $\frac{1}{4}b$  and upper level at  $\frac{1}{8}b$ , for frequencies 1 MHz, 3 MHz, 10 MHz, 30 MHz, 100 MHz, 200 MHz, 400 MHz and 700 MHz, using the Sandia 976-4-034 calibrated small dipole probe.



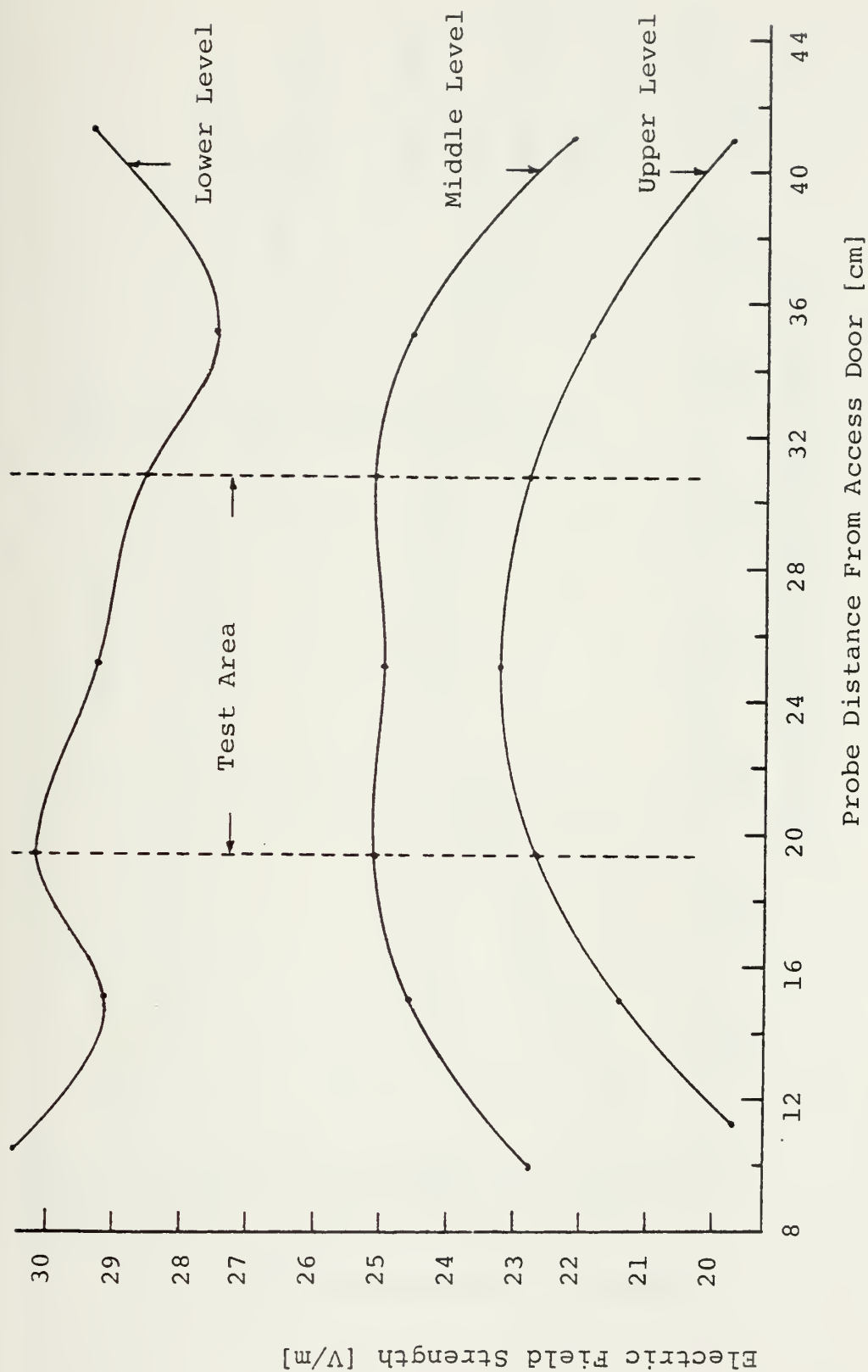


Figure B-1. Electric Field Distribution Inside Empty Cell  
at Frequency 1 MHz ( $E_{cal} = 26.04$  [V/m])





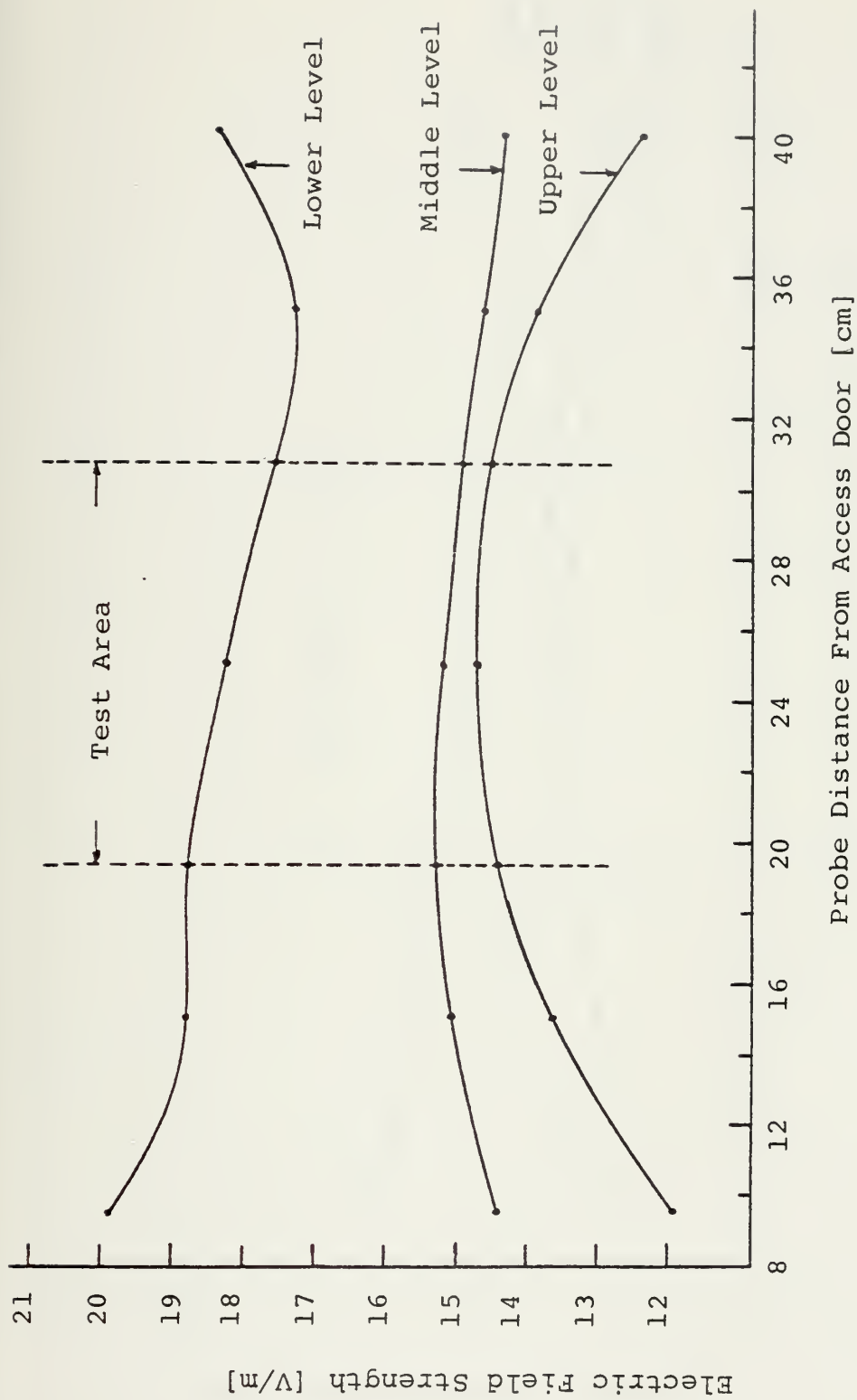


Figure B-2. Electric Field Distribution Inside Empty Cell  
at Frequency 3 MHz ( $E_{cal} = 16.09$  [V/m])



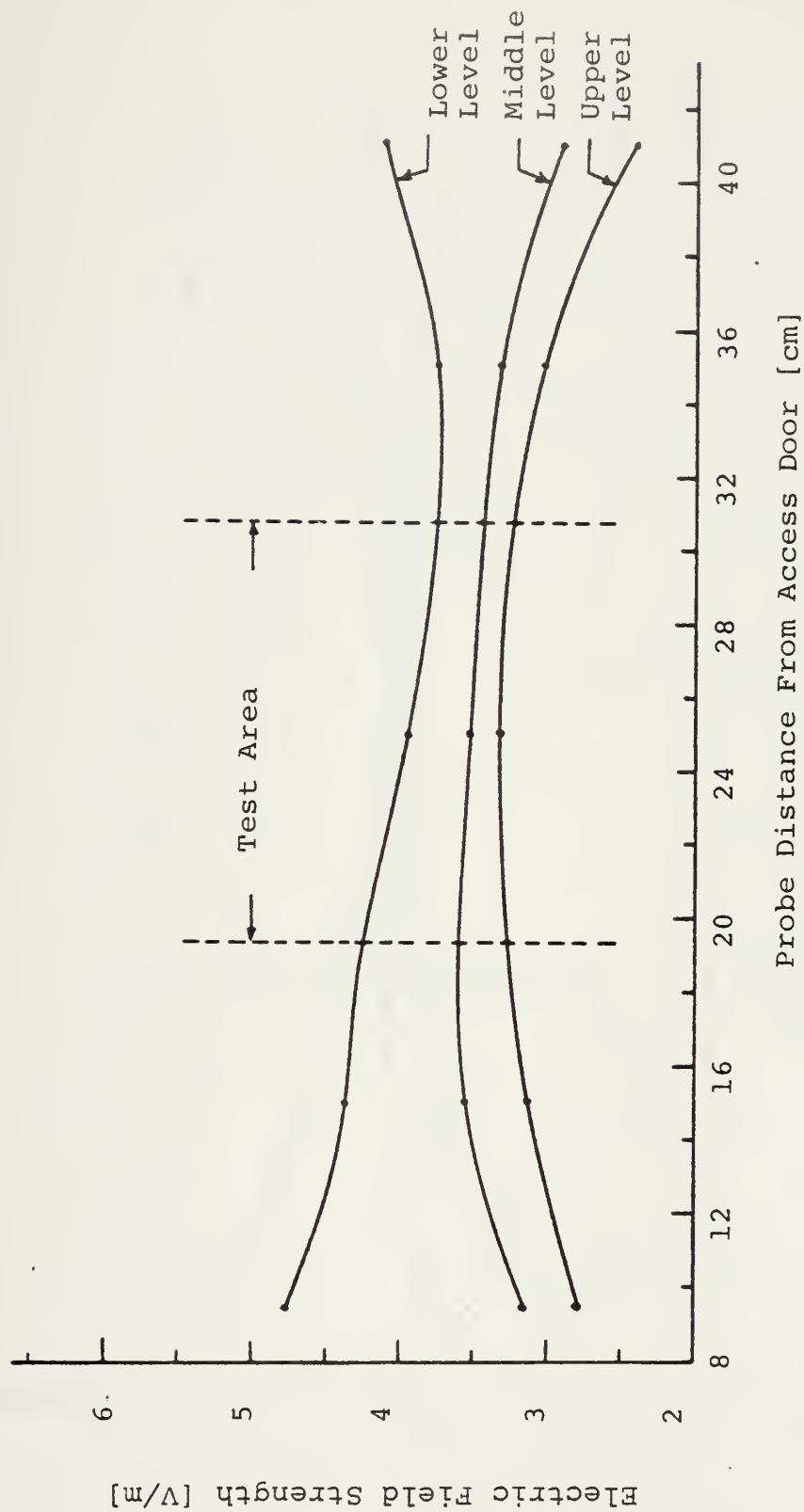


Figure B-3. Electric Field Distribution Inside Empty Cell at Frequency 10 MHz ( $E_{cal} = 4.96$  [V/m])



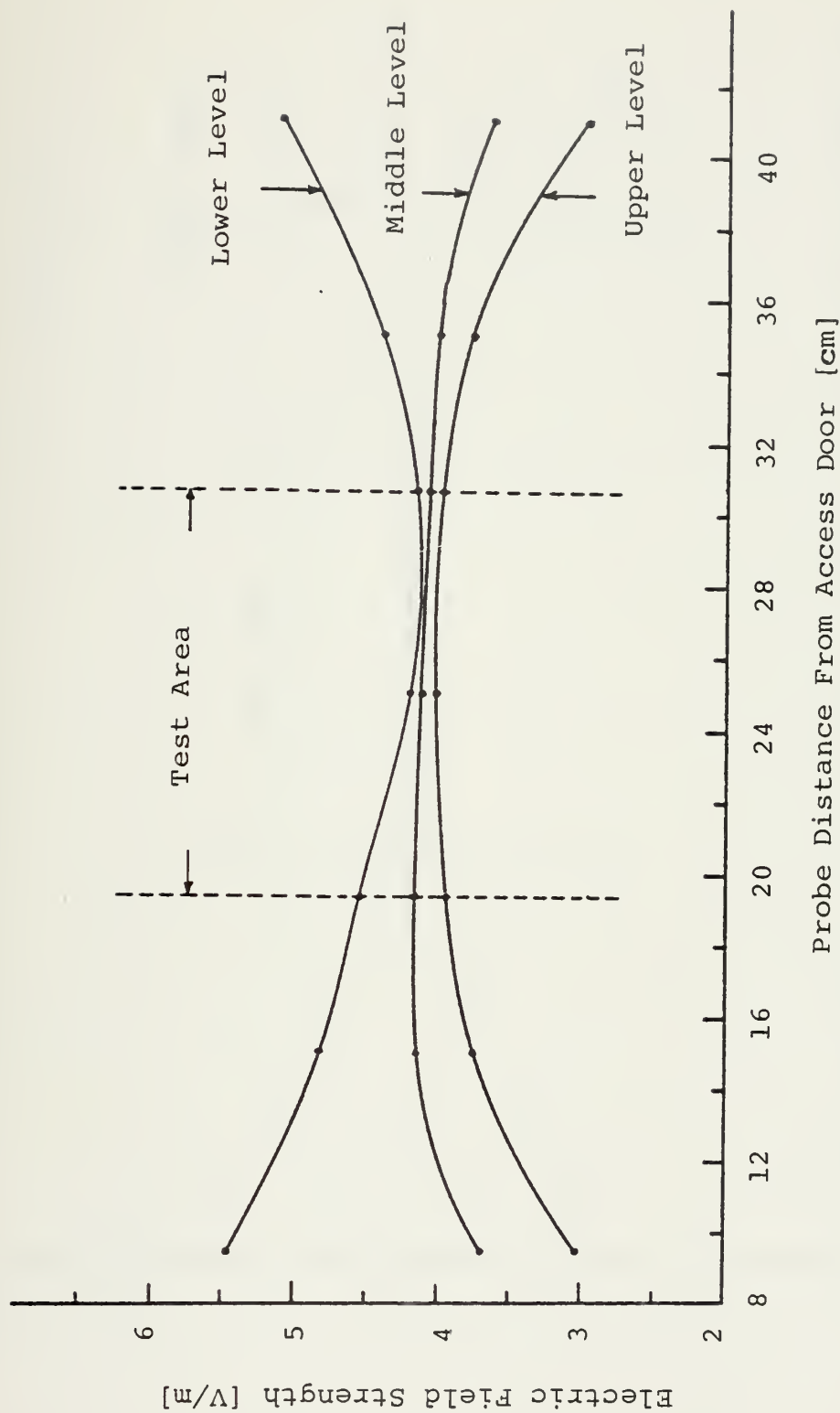


Figure B-4. Electric Field Distribution Inside Empty Cell at Frequency 30 MHz ( $E_{cal} = 4.96$  [V/m])



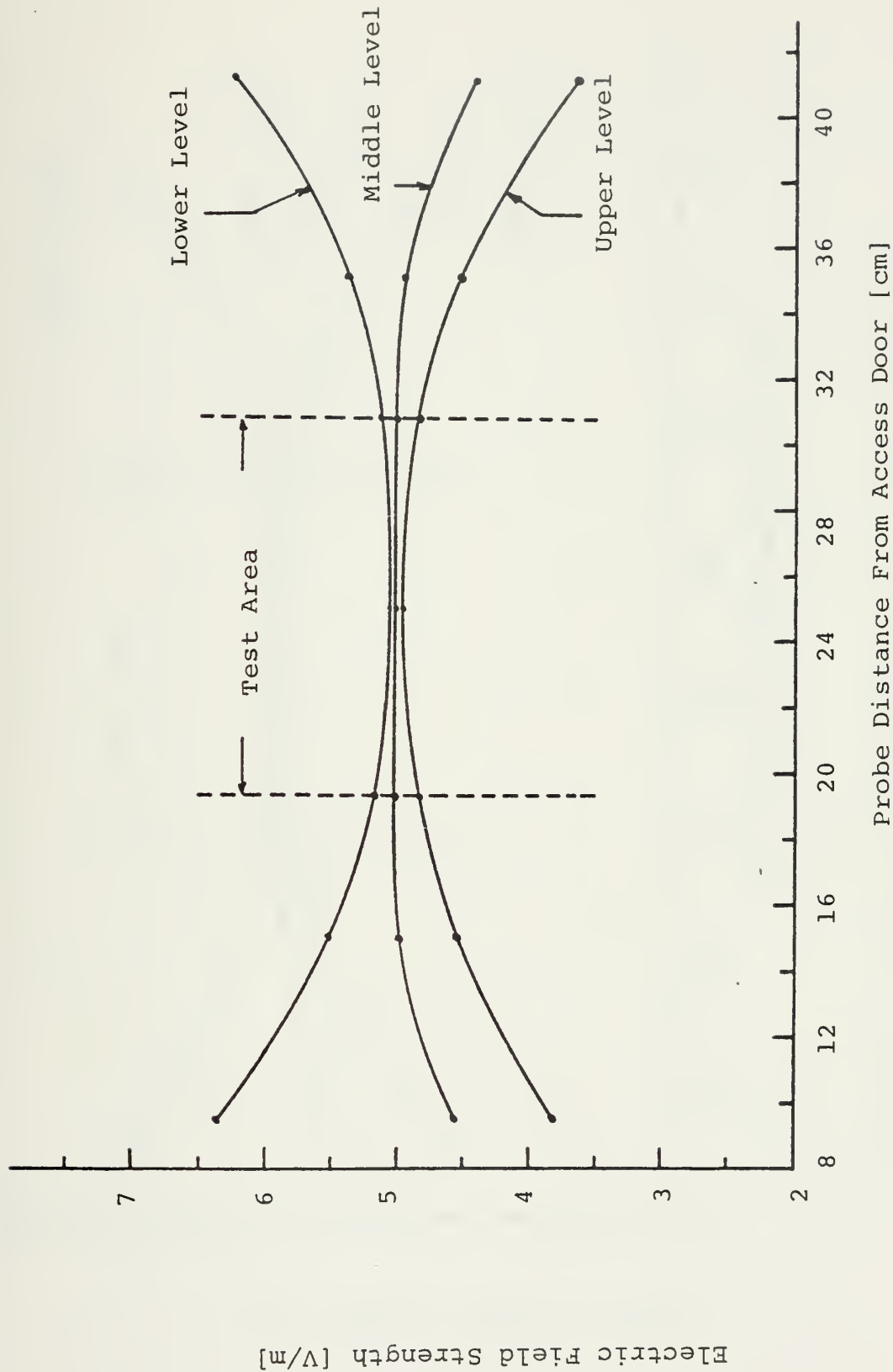


Figure B-5. Electric Field Distribution Inside Empty Cell at Frequency 100 MHz ( $E_{cal} = 5.20$  [V/m])





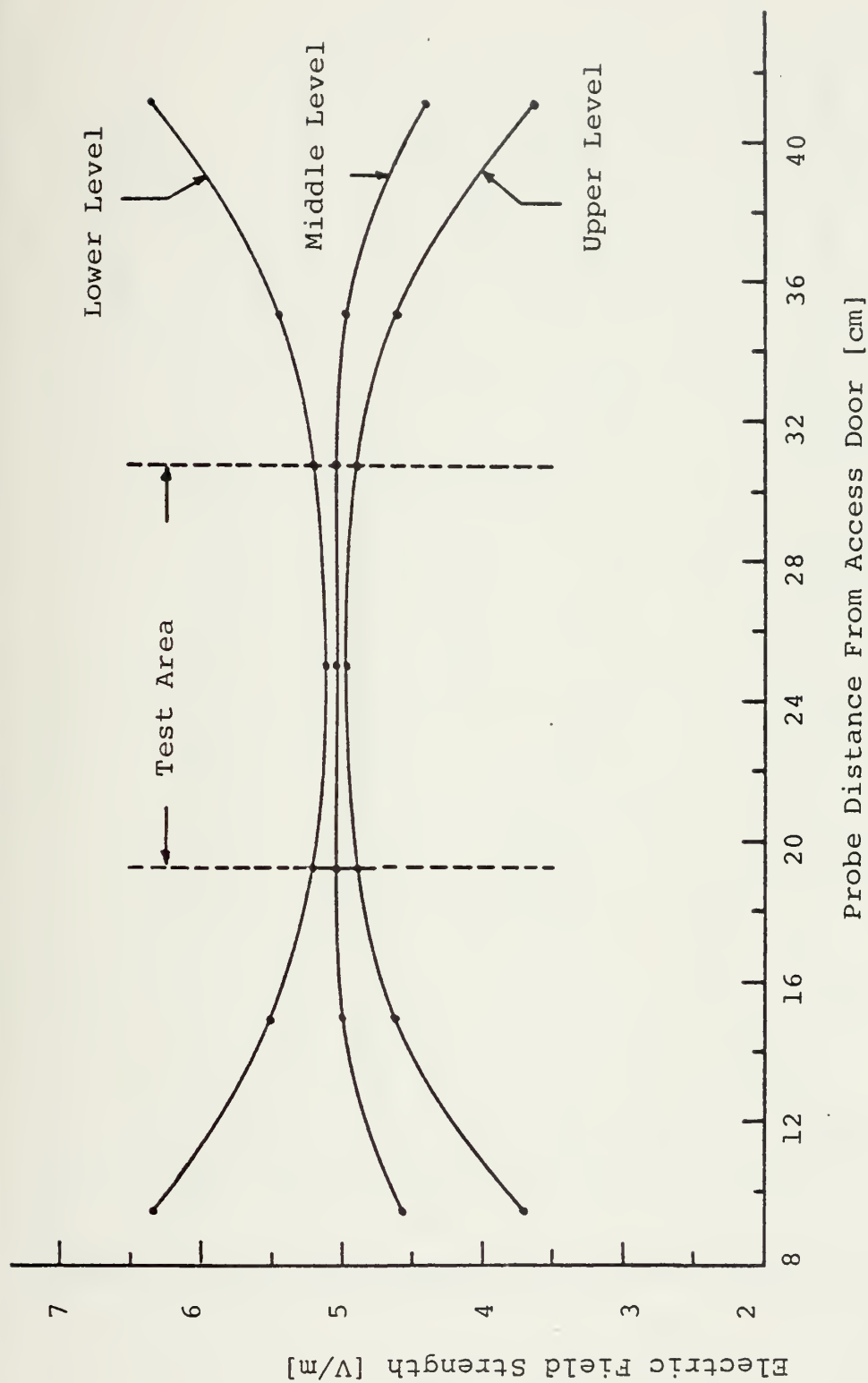


Figure B-6. Electric Field Distribution Inside Empty Cell at Frequency 200 MHz ( $E_{cal} = 5.35$  [V/m])



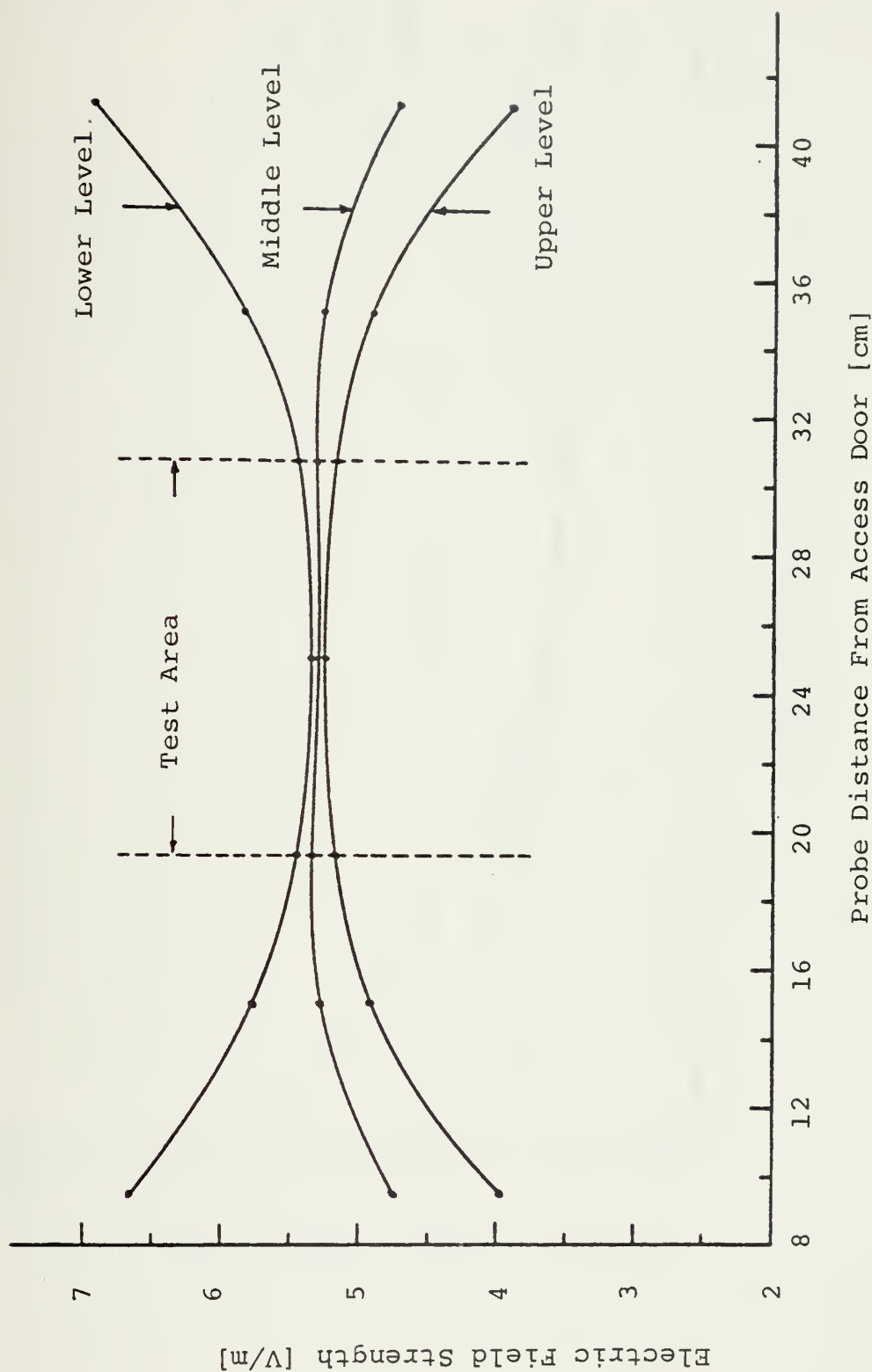


Figure B-7. Electric Field Distribution Inside Empty Cell at Frequency 400 MHz ( $E_{cal} = 5.50$  [V/m])



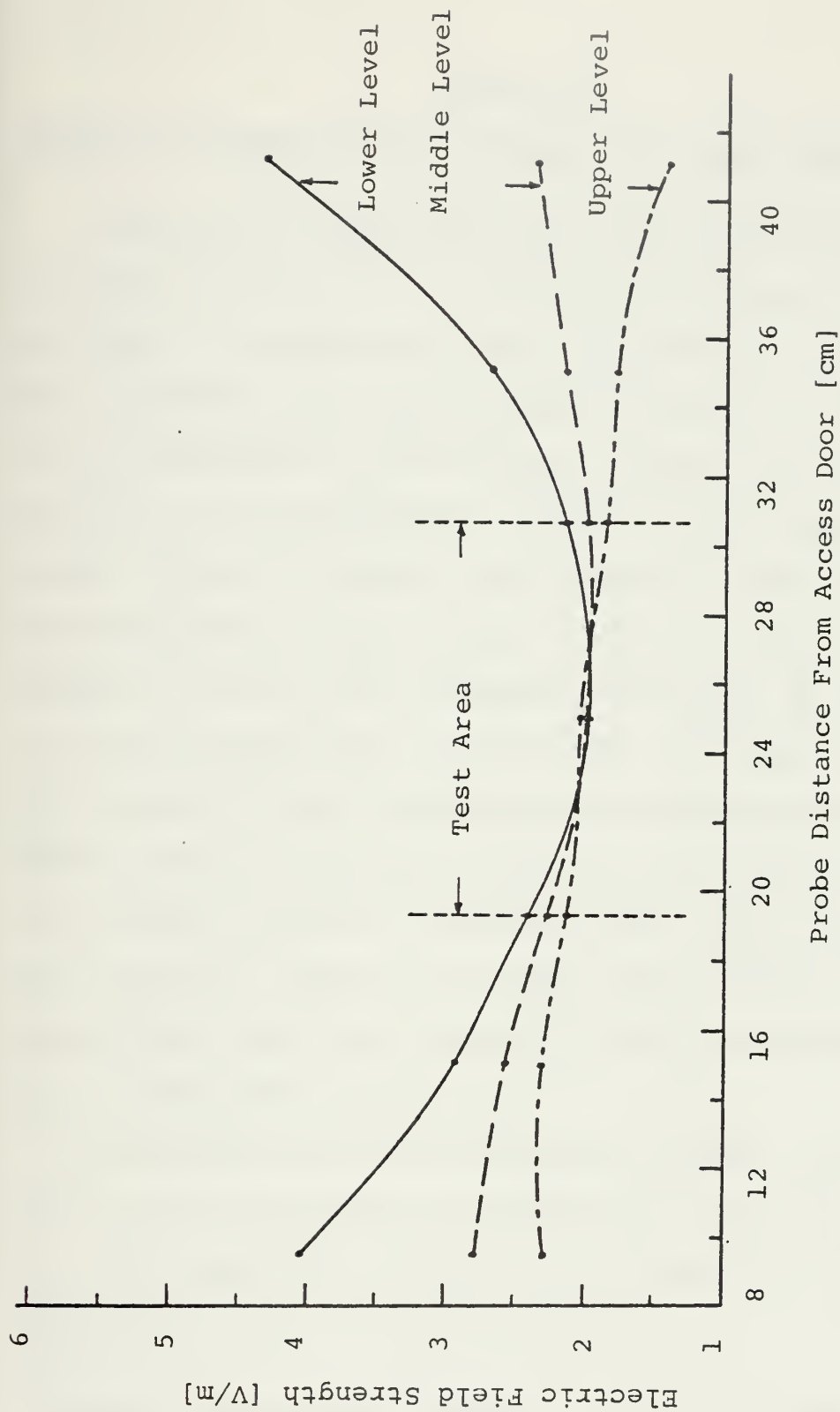


Figure B-8. Electric Field Distribution Inside Empty Cell at Frequency 700 MHz ( $E_{cal} = 3.25$  [V/m])





## APPENDIX C

### Example of Measuring the E Field Inside the (Empty) TEM Cell

A copy of the data sheet for the E field measurements is shown in Figure C-1. This case is for the empty cell (same procedure for loaded cell) at a frequency of 100 MHz using the calibrated small dipole probe, 976-4-034. The column "COL" corresponds to the columns, forward (F), middle (M) and back (B) of the positioning matrix shown in figure 17. The column "DISTAN." indicates the distance of the probe from the door opening. The columns "LEVEL 1", "LEVEL 2", and "LEVEL 3" are for the measurement planes  $\frac{3}{8}b$ ,  $\frac{1}{4}b$  and  $\frac{1}{8}b$ , as shown in figure 16, respectively. The subscripts 1, 2 and 3 used for the E fields also have the same meaning. Although the incident and reflected powers must be maintained at the same values, at the three planes and for all measurement positions, their values have been obtained to verify this assumption. (The small deviations which were measured, were due to instrument instability.)

Having obtained the probe output voltage for three levels and for all measurement positions the calculated E field,  $E_{cal}$ , was computed as follows (i.e., assuming the data of the fifth row of the table indicated by \*):

Incident power meter reading = -12.45

Dual Directional Coupler Attenuation = +22.85 dB (figure 19  
for  $f = 100$  MHz)



		P <sub>inc</sub> (dBm)			P <sub>ref</sub> (dBm)			FREQUENCY = 100 MHz (EMPTY CELL)										DATE: 27-AUG-1979		
COL.	DISTAN.	LEVEL			LEVEL			P <sub>NET</sub> (mW)	V <sub>1</sub> (mV) PROB	V <sub>2</sub> (mV) PROB	V <sub>3</sub> (mV) PROB	E <sub>1</sub> [V/m]	E <sub>2</sub> [V/m]	E <sub>3</sub> [V/m]						
		1	2	3	1	2	3													
F	10 cm	10.25	10.25	10.25	10.25	10.25	10.25	10.97	1	2.8	2	1.46	3	0.94	5.32	4.57	3.66			
F	15 cm	-	-	-	-	-	-		1	2.12	2	1.74	3	1.45	5.50	4.99	4.55			
F	#1	-	-	-	-	-	-		1	1.86	2	1.70	3	1.58	5.15	4.93	4.75			
F	#3	-	10.25	-	-	-	-		1	1.80	2	1.75	3	1.68	5.07	5.0	4.9			
*F	#5	-	-	-	-	-	-		1	1.84	2	1.75	3	1.63	5.13	5.0	4.83			
F	35 cm	-	-	-	-	-	-	1	2.04	2	1.74	3	1.45	5.40	4.99	4.55				
F	41 cm	-	-	-	-	-	-	1	2.75	2	1.36		0.90	6.27	4.41	3.59				
M	10 cm	10.25	-	-	-	-	-	10.97	1	2.83	2	1.48	3	1.02	6.36	4.60	3.32			
M	15 cm	10.25	-	-	-	-	-		1	2.12	2	1.75	3	1.45	5.50	5.0	4.55			
M	#11	10.25	-	-	-	-	-		1	1.88	2	1.76	3	1.63	5.18	5.01	4.93			
M	#13	-	-	-	-	-	-		1	1.76	2	1.75	3	1.70	5.01	5.0	4.93			
M	#15	-	-	-	-	-	-		1	1.84	2	1.71	3	1.63	5.13	4.94	4.83			
M	35 cm	-	-	-	-	-	-	1	2.03	2	1.68	3	1.45	5.39	4.90	4.55				
M	41 cm	-	-	-	-	-	-	1	2.74	2	1.35	3	0.93	6.26	4.39	3.64				
B	10 cm	10.25	-	-	-	-	-	10.97	1	2.94	2	1.40	3	1.02	6.48	4.47	3.82			
B	15 cm	-	-	-	-	-	-		1	2.14	2	1.72	3	1.46	5.53	4.96	4.87			
B	#21	-	-	-	-	-	-		1	1.88	2	1.73	3	1.63	5.18	4.97	4.83			
B	#23	-	10.25	-	-	-	-		1	1.75	2	1.70	3	1.70	5.0	4.93	4.93			
B	#25	-	-	-	-	-	-		1	1.84	2	1.71	3	1.65	5.13	4.94	4.86			
B	35 cm	-	-	-	-	-	-	1	2.02	2	1.69	3	1.45	5.37	4.91	4.55				
B	41 cm	-	-	-	-	-	-	1	2.74	2	1.30	3	0.89	6.26	4.31	3.57				
AVERAGE	10 cm	→							1.29	0.92	0.76			6.39	4.55	3.77				
	15 cm	→							1.12	1.01	0.92			5.51	4.98	4.56				
	#1,11,21	→							1.05	1.01	0.97			5.17	4.97	4.80				
	#3,13,23	→							1.02	1.01	1.0			5.03	4.98	4.92				
	#5,15,25	→							1.04	1.0	0.98			5.13	4.96	4.84				
	35 cm	→							1.09	1.0	0.92			5.39	4.93	4.55				
	41 cm	→							1.27	0.88	0.73			6.25	4.37	3.60				
										RELATIVE E field			E field measured							
										(E <sub>meas</sub> )										
										(E <sub>ref</sub> )										

Gen. Output Volts: 0.78  
 -- SET LEVEL : +11 dB  
 Directional Coupler: +22.85 dB  
 E<sub>ref</sub> = 5.20 [V/m]

PROBE NO: 976-4-034  
 READINGS FROM CALIBRATING CURVES:  $\frac{V_{probe}}{E_{ref}} = 7 \times 10^5$

Figure C-1. Tabulated Data for Mapping the Fields Inside the Empty Cell at Frequency 100 MHz by Using the 976-4-034 Dipole Probe



Therefore,

$$P_{in} = -12.45 \text{ (dBm)} + 22.85 \text{ (dB)} = 10.4 \text{ (dBm)}$$

By using

$$\text{dBm (power)} = 10 \log_{10} \text{ (mW)}$$

finally obtaining

$$P_{inc} = 10.97 \text{ mW.}$$

The same procedure should be followed for calculating the reflected power in mW and then subtract from the  $P_{inc}$ . But since the  $P_{ref}$  was insignificantly small, its calculation was omitted.

The calculated E field was found by applying equation (6)

$$\begin{aligned} E_{cal} &= 1.569 (P_n [\text{mW}])^{1/2} = 1.569 (10.97)^{1/2} \\ &= 5.20 \text{ [V/m]} . \end{aligned}$$

The measured electric field,  $E_{meas}$ , was calculated from the equation (8). The K factor was found from figure 18 at a frequency 100 MHz to be equal to  $7 \times 10^{-5}$ . Therefore for a value of probe output voltage, i.e., 1.84 mV,



$$\begin{aligned}
 E_{\text{meas}} &= (V_{\text{probe}}/K)^{1/2} = (1.84 \times 10^{-3} / 7 \times 10^{-5})^{1/2} \\
 &= 5.13 \text{ [V/m]} .
 \end{aligned}$$





## APPENDIX D

### Experimental Procedure for Determining the Best Type, Amount and Location of Absorbing Material Inside the TEM Cell

Figures D-1 through D-7 show samples of the obtained VSWR's and reflection coefficient distribution curves [ $\rho/\text{cm} = 0.1$ ] along the cell, for the type, amount and location of the absorbing material corresponding to the schematic diagram shown at each figure.



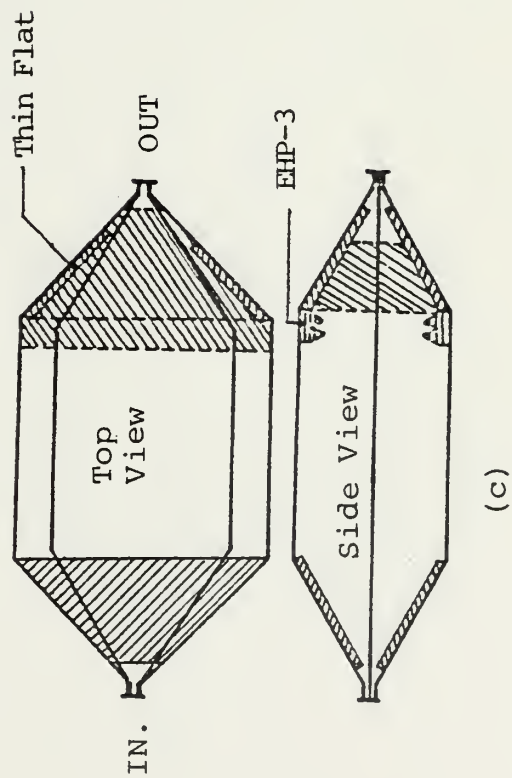
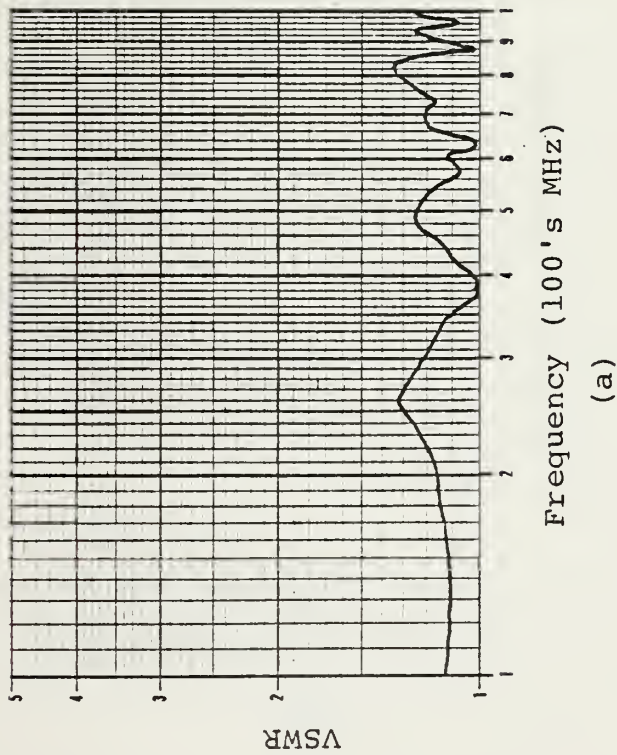
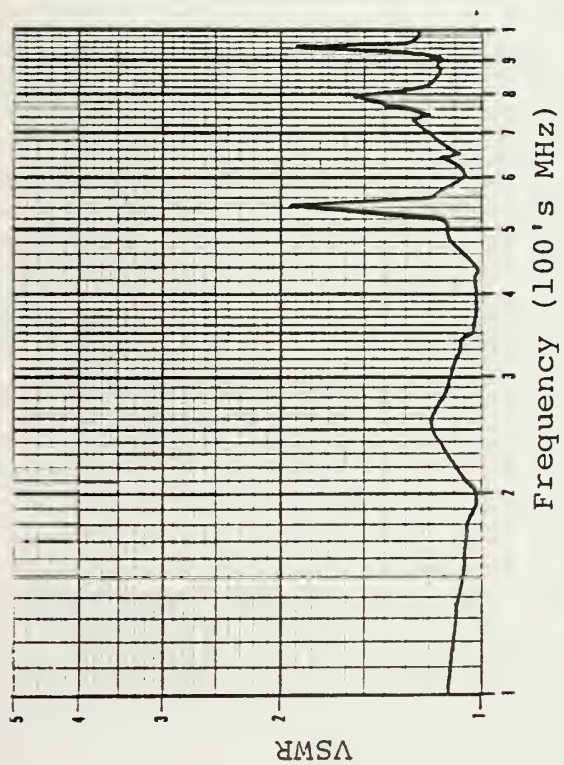
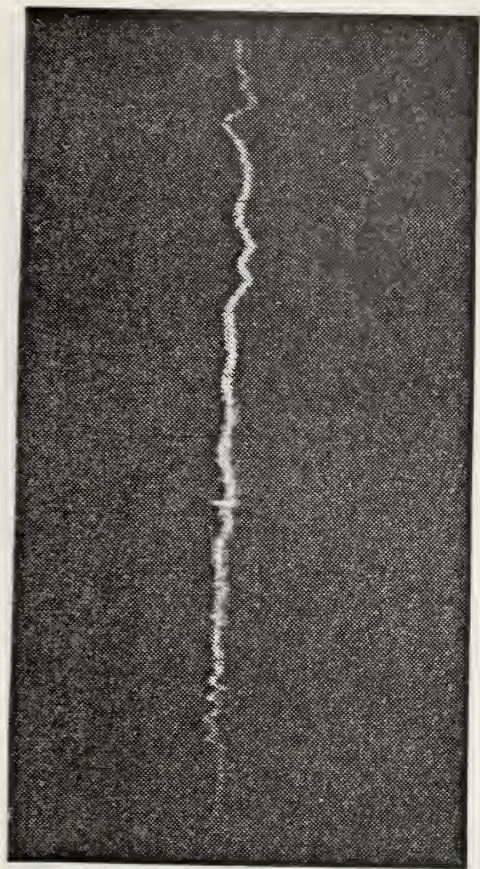


Figure D-1. Curves of VSWR (a) and Reflection Coefficient (b), for the Absorber Loaded TLM cell Configuration (c).

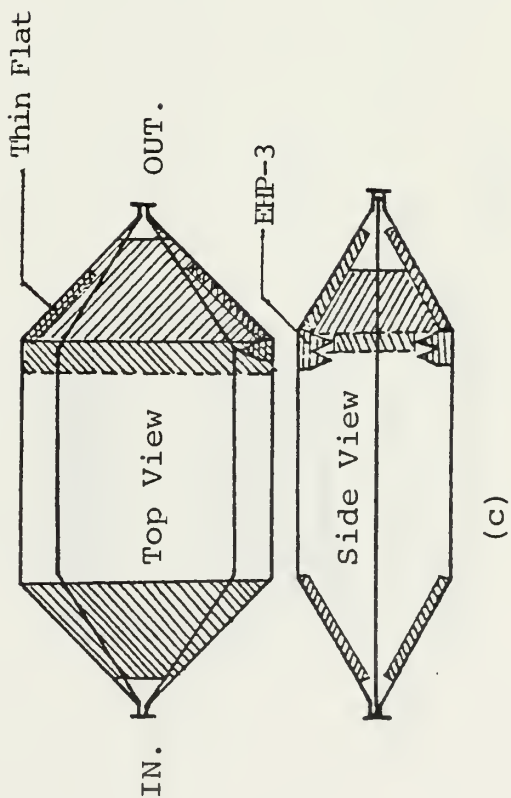




(a)



(b)



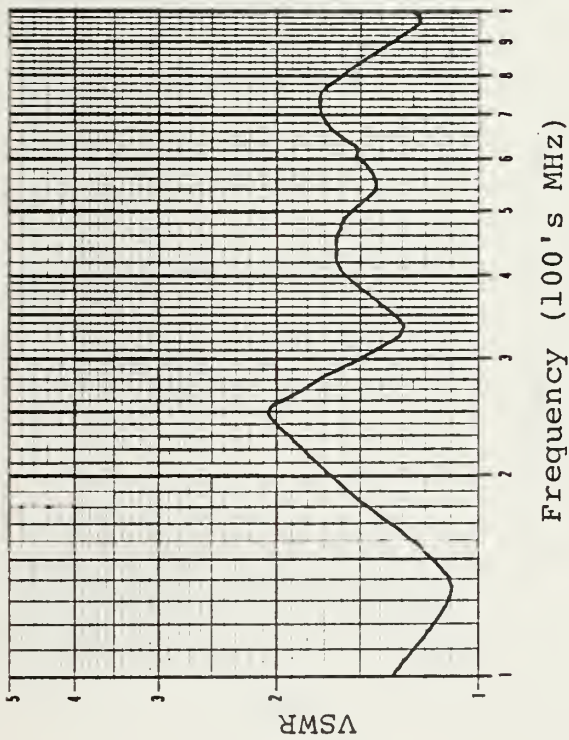
(c)

Figure D-2. Curves of VSWR (a) and Reflection Coefficient (b), for the Absorber Loaded TEM Cell Configuration

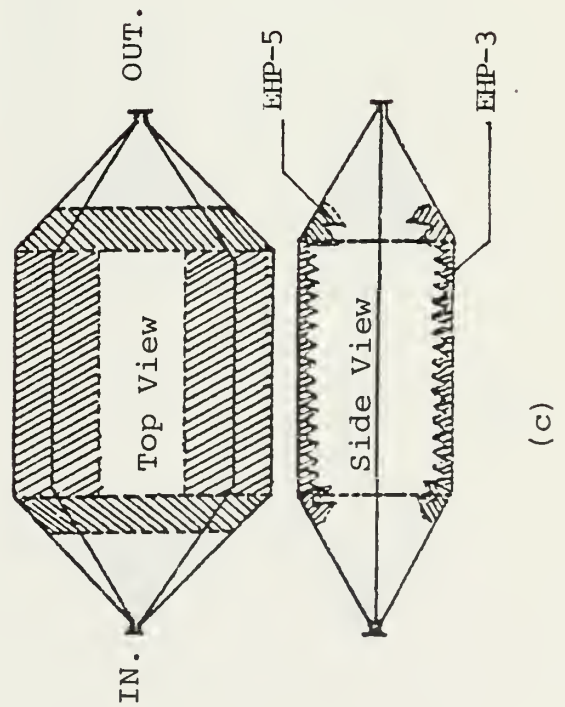








(a)



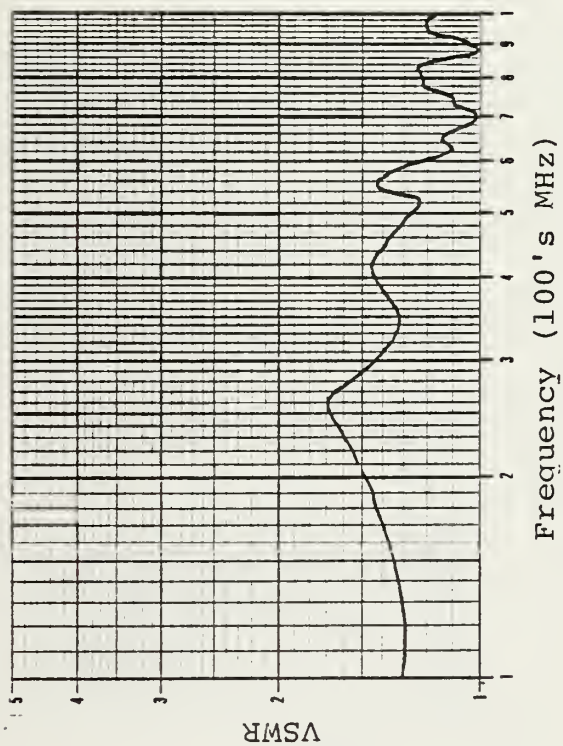
(c)



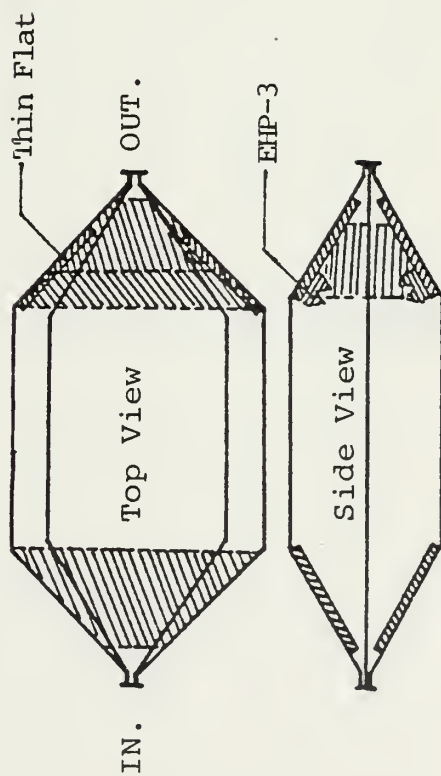
(b)

Figure D-3. Curves of VSWR (a) and Reflection Coefficient (b), for the Absorber Loaded TEM Cell Configuration (c)

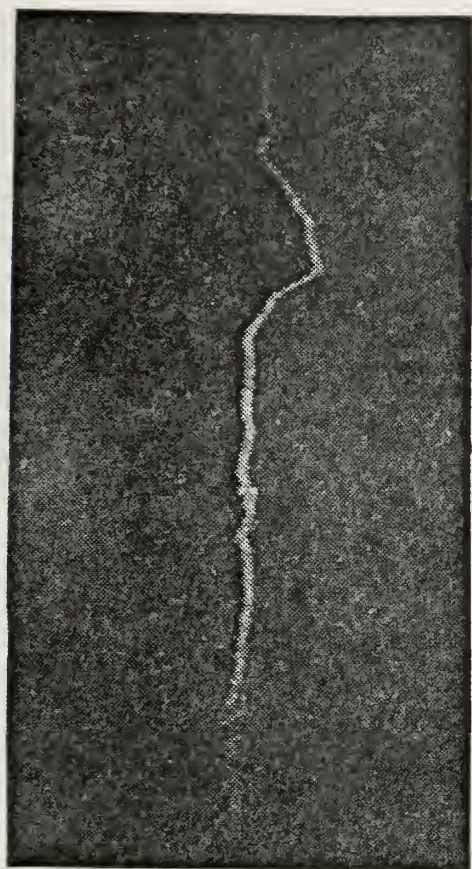




(a)



(c)

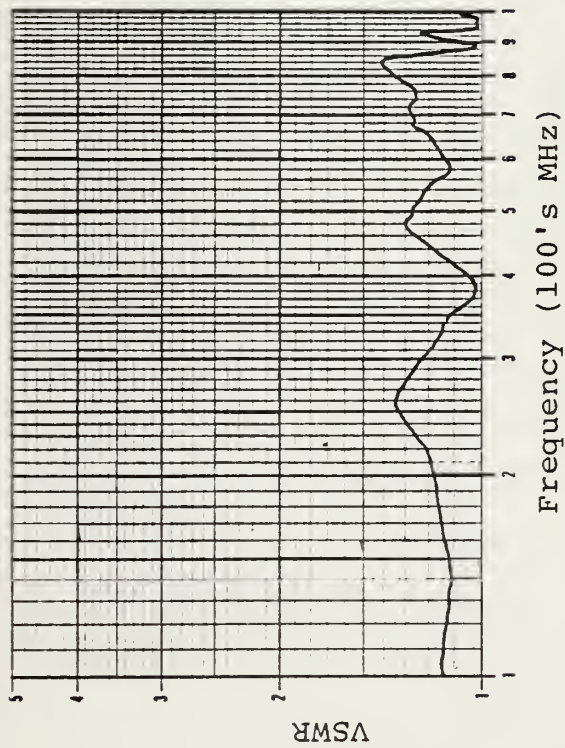


(b)

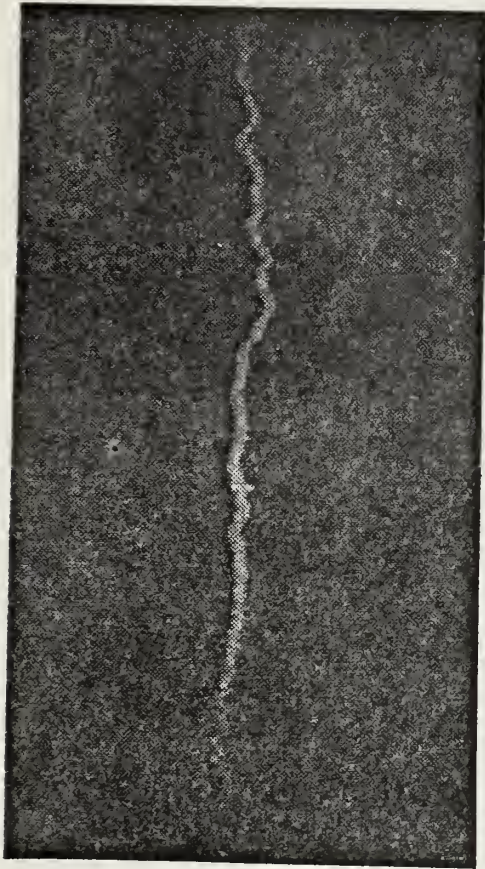
Figure D-4. Curves of VSWR (a) and Reflection Coefficient (b), for the Absorber Loaded TEM Cell Configuration (c)



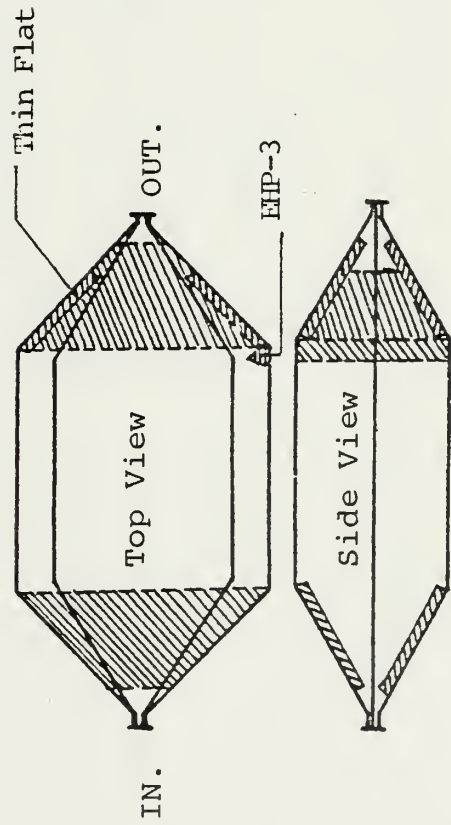




(a)



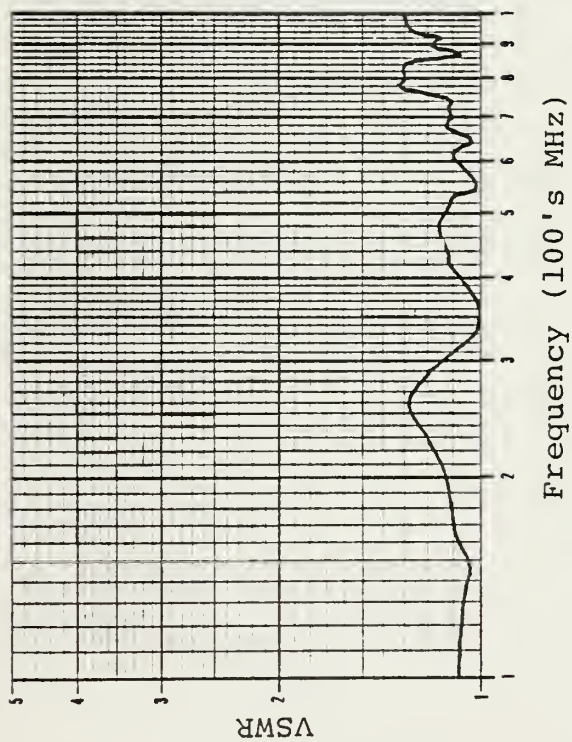
(b)



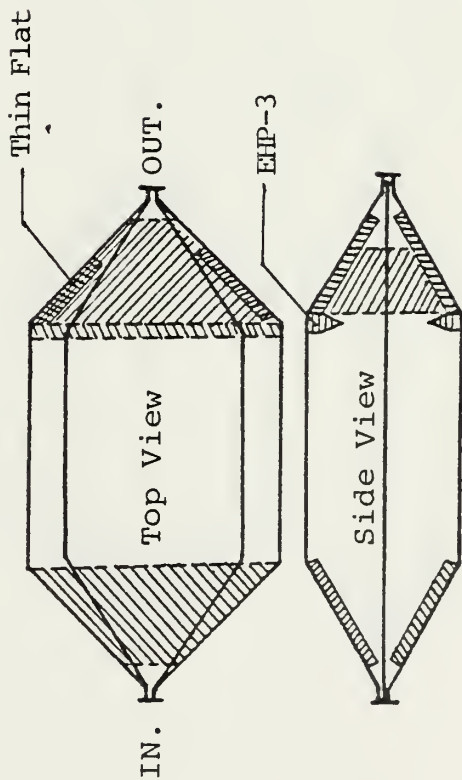
(c)

Figure D-5. Curves of VSWR (a) and Reflection Coefficient (b), for the Absorber Loaded TEM Cell Configuration (c)

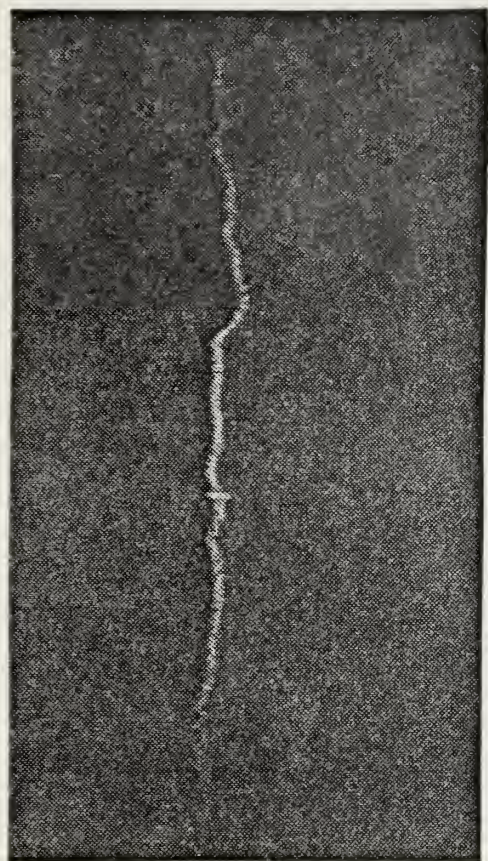




(a)



(c)

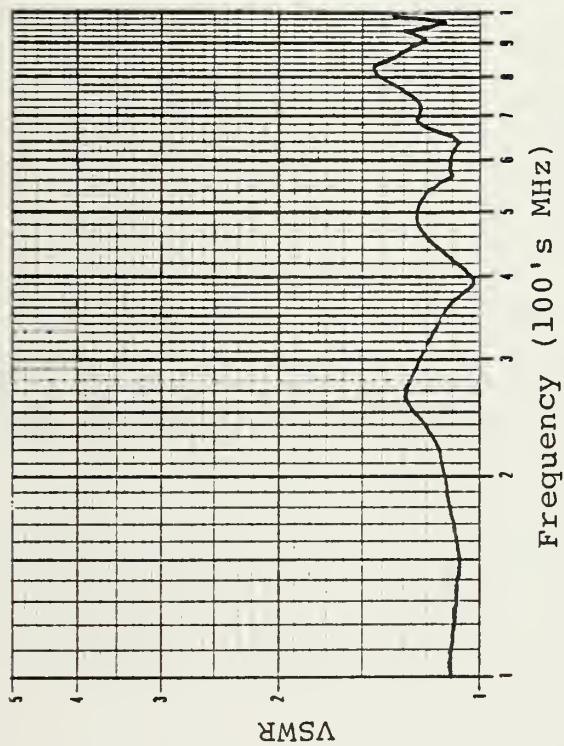


(b)

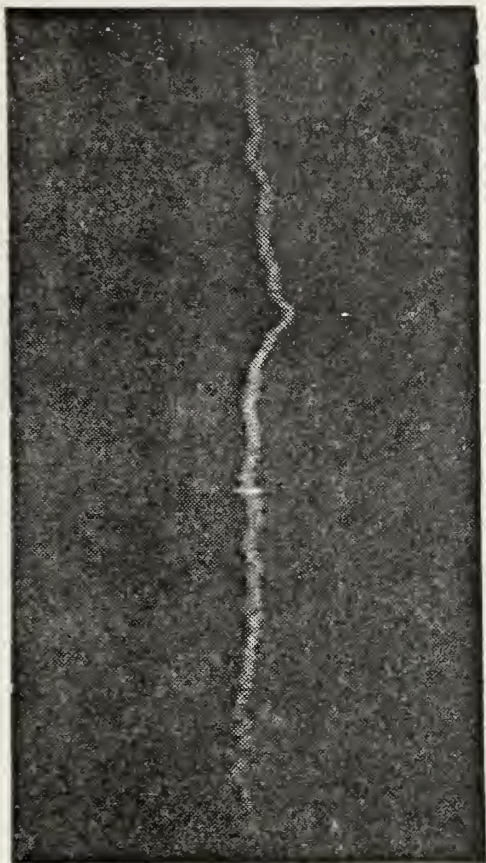
Figure D-6. Curves of VSWR (a) and Reflection Coefficient (b), for the Absorber Loaded TEM Cell Configuration (c)



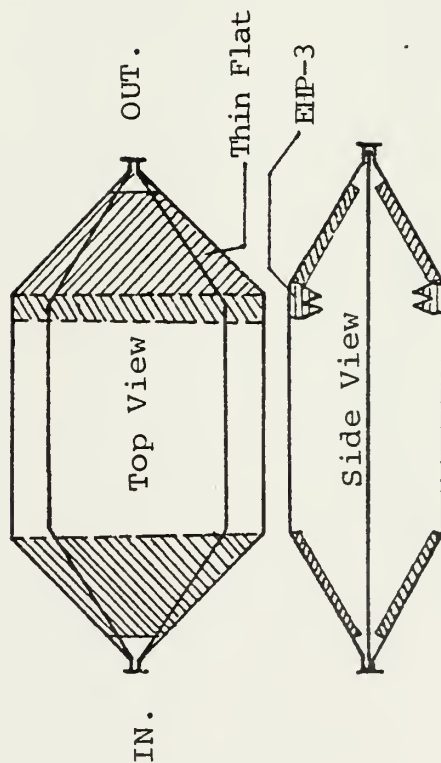




(a)



(b)



(c)

Figure D-7. Curves of VSWR (a) and Reflection Coefficient (b), for the Absorber Loaded TEM Cell Configuration (c)



## APPENDIX E

### Curves of Measured Electric Field Distribution Inside the Absorber Loaded TEM Cell

Figures E-1 through E-9 show the measured E field distribution inside the absorber loaded TEM cell, versus probe distance from the access door for the lower level at  $\frac{3}{8}b$ , middle level at  $\frac{1}{4}b$  and upper level at  $\frac{1}{8}b$  for frequencies 1 MHz, 3 MHz, 260 MHz, 400 MHz, 500 MHz, 675 MHz, 675 MHz for different power levels, 895 MHz with the access door closed and 895 MHz with the access door open. Again the Sandia 976-4-034 calibrated small dipole probe was used.



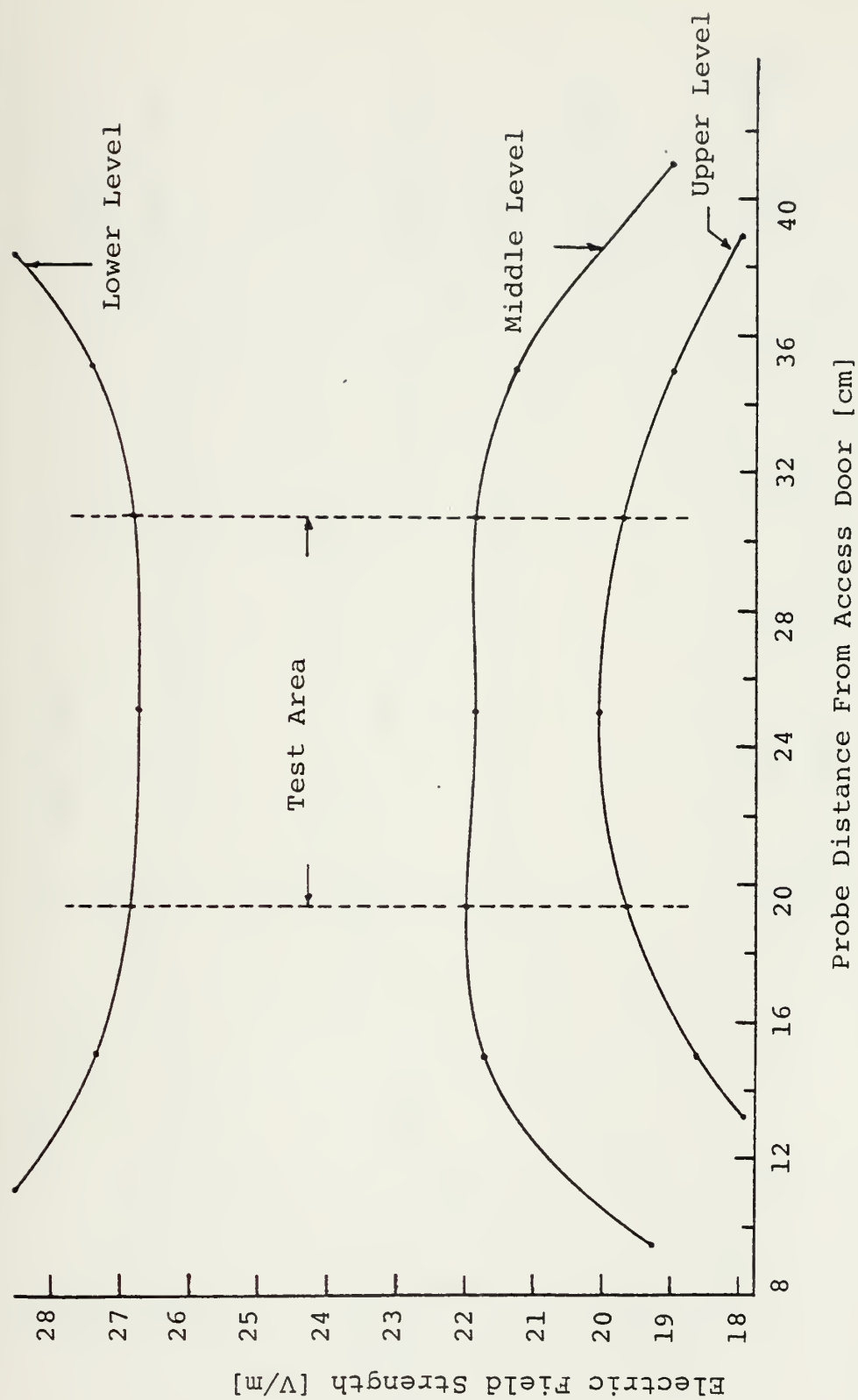


Figure E-1. Electric Field Distribution Inside Absorber Loaded Cell at Frequency 1 MHz ( $E_{cal} = 23.0$  [V/m])





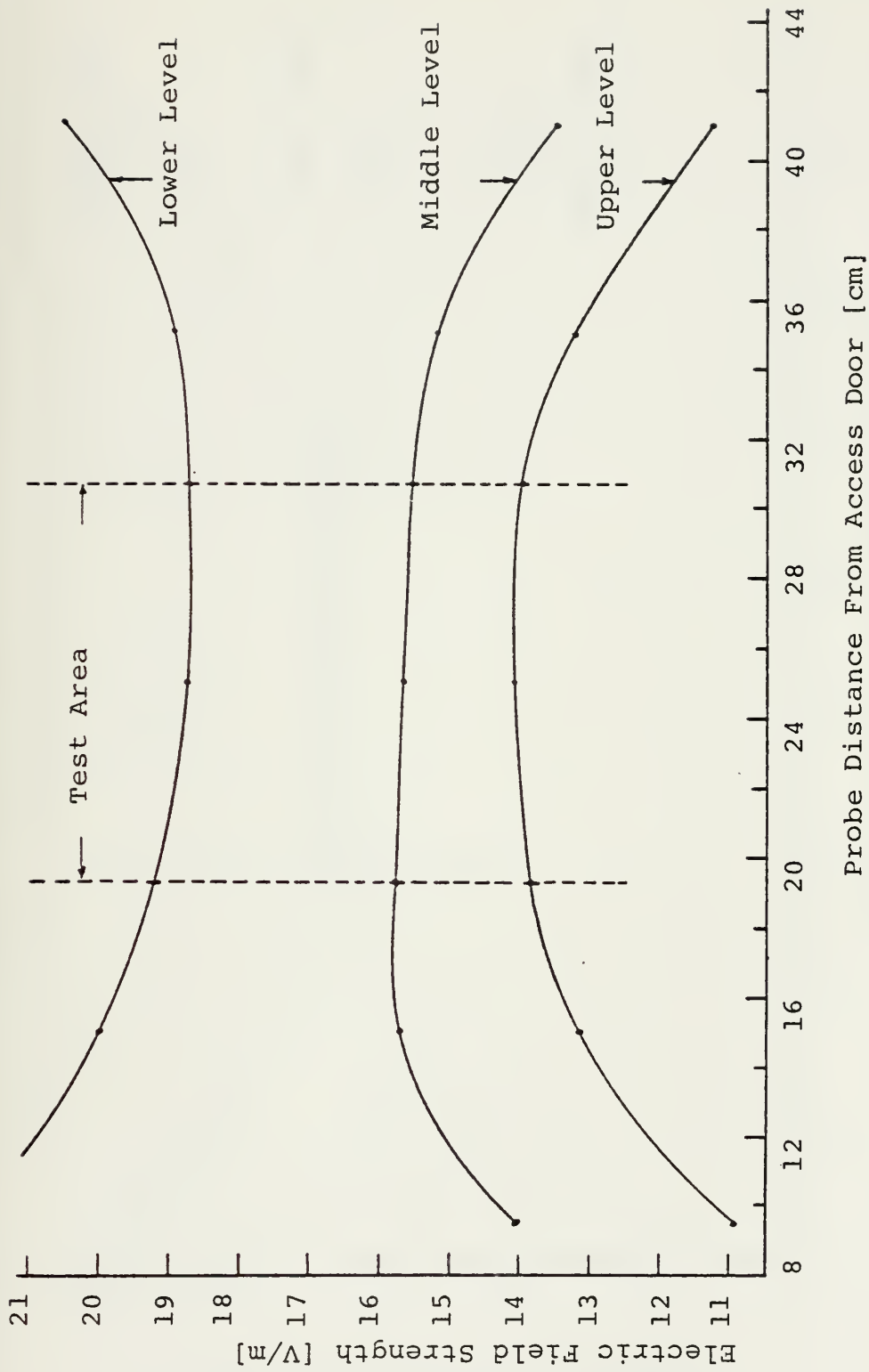


Figure E-2. Electric Field Distribution Inside Absorber Loaded Cell at Frequency 3 MHz ( $E_{cal} = 16.28$  [V/m])



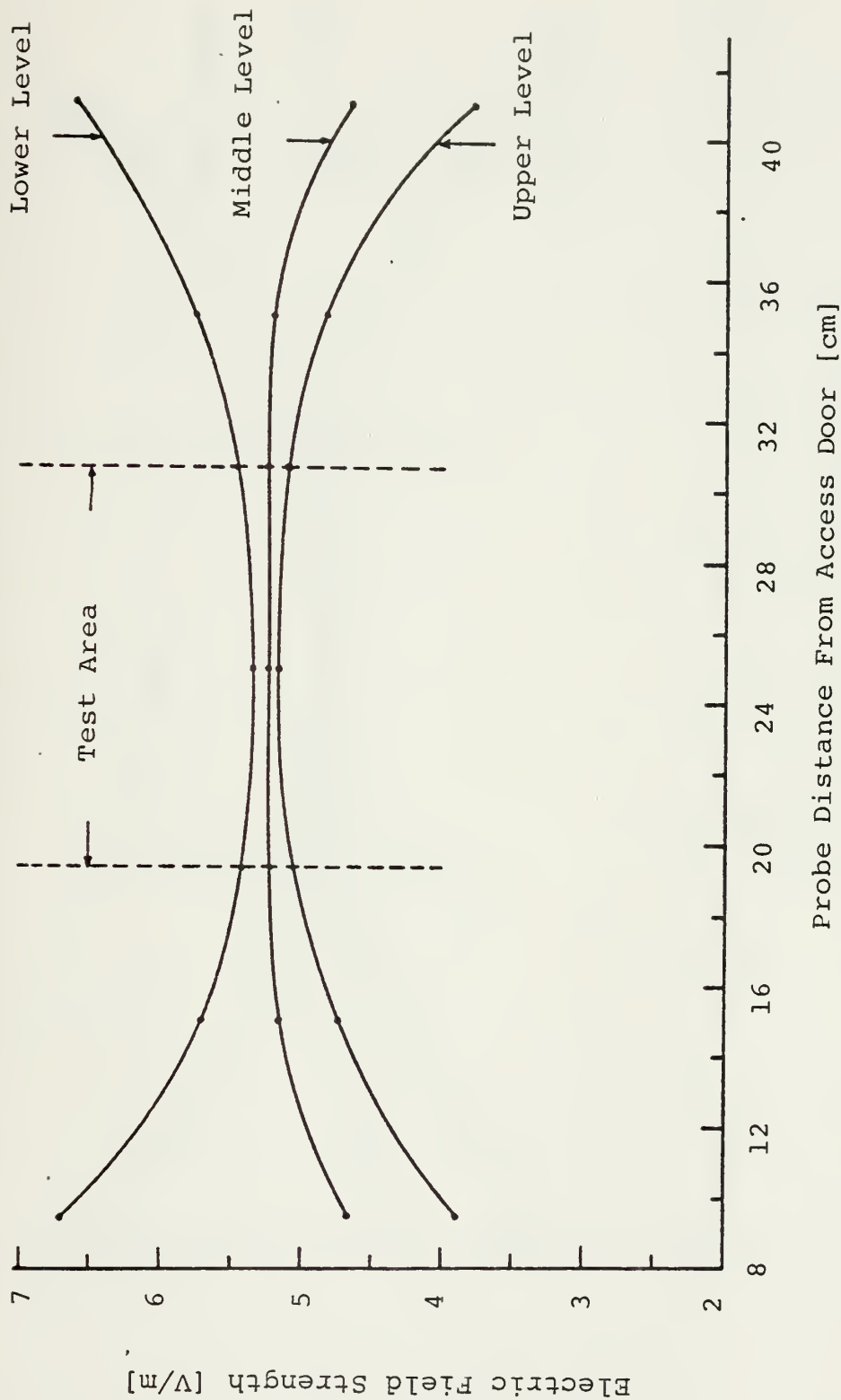


Figure E-3. Electric Field Distribution Inside Absorber Loaded Cell at Frequency 260 MHz ( $E_{cal} = 5.31$  [V/m])



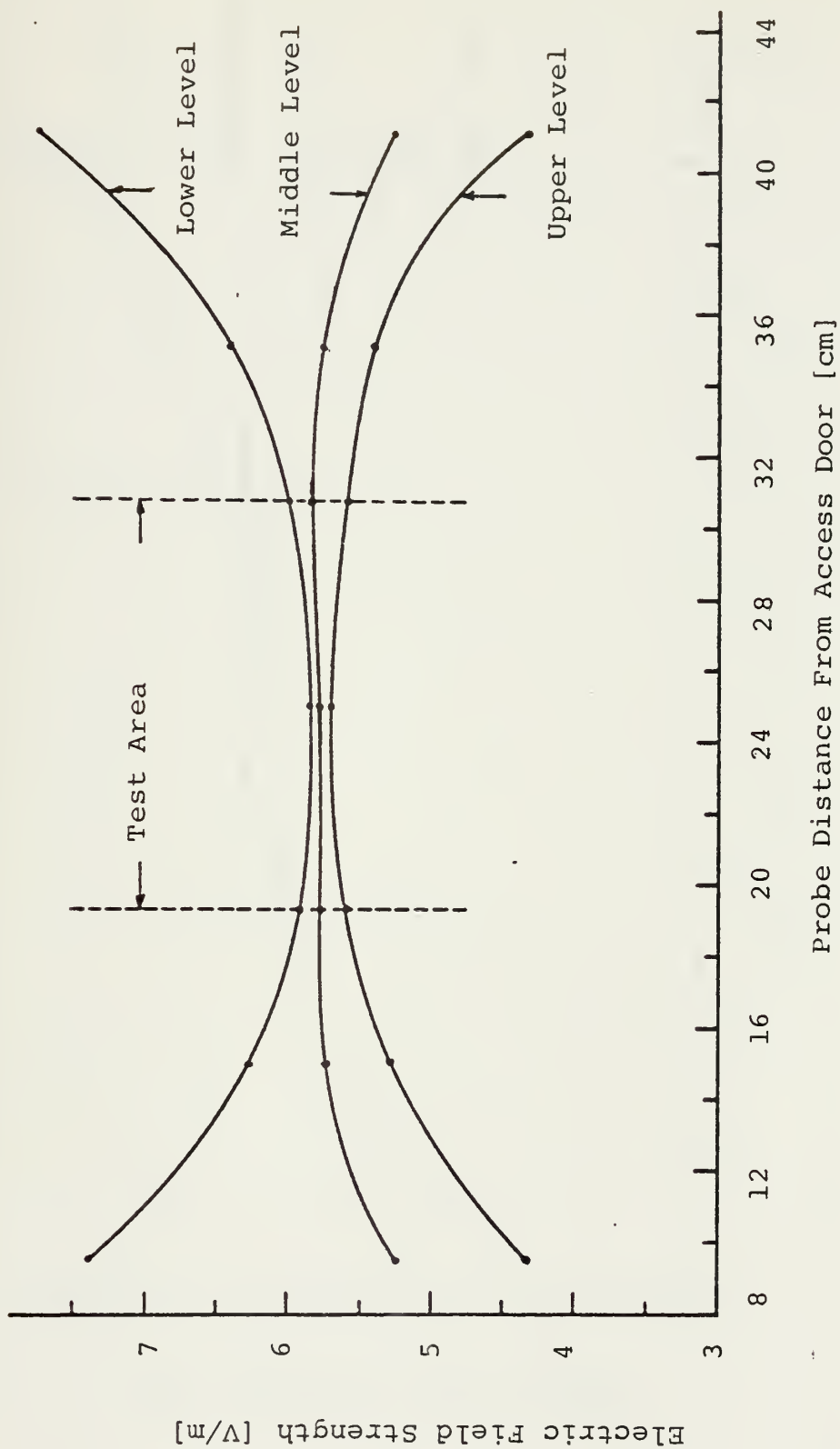


Figure E-4. Electric Field Distribution Inside Absorber Loaded Cell at Frequency 400 MHz ( $E_{cal} = 5.46$  [V/m])



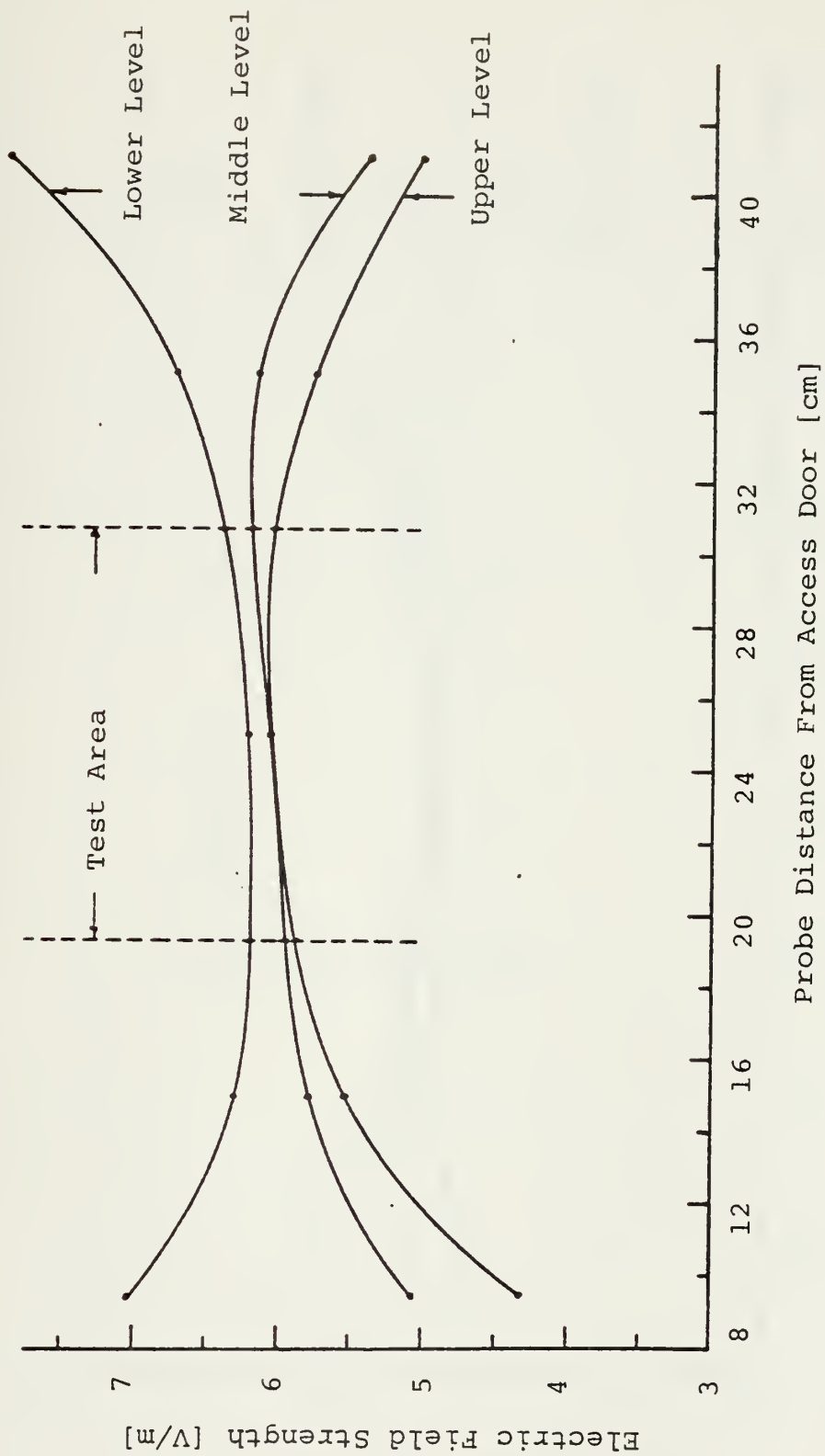


Figure E-5. Electric Field Distribution Inside Absorber Loaded Cell at Frequency 500 MHz ( $E_{cal} = 5.36$  [V/m])





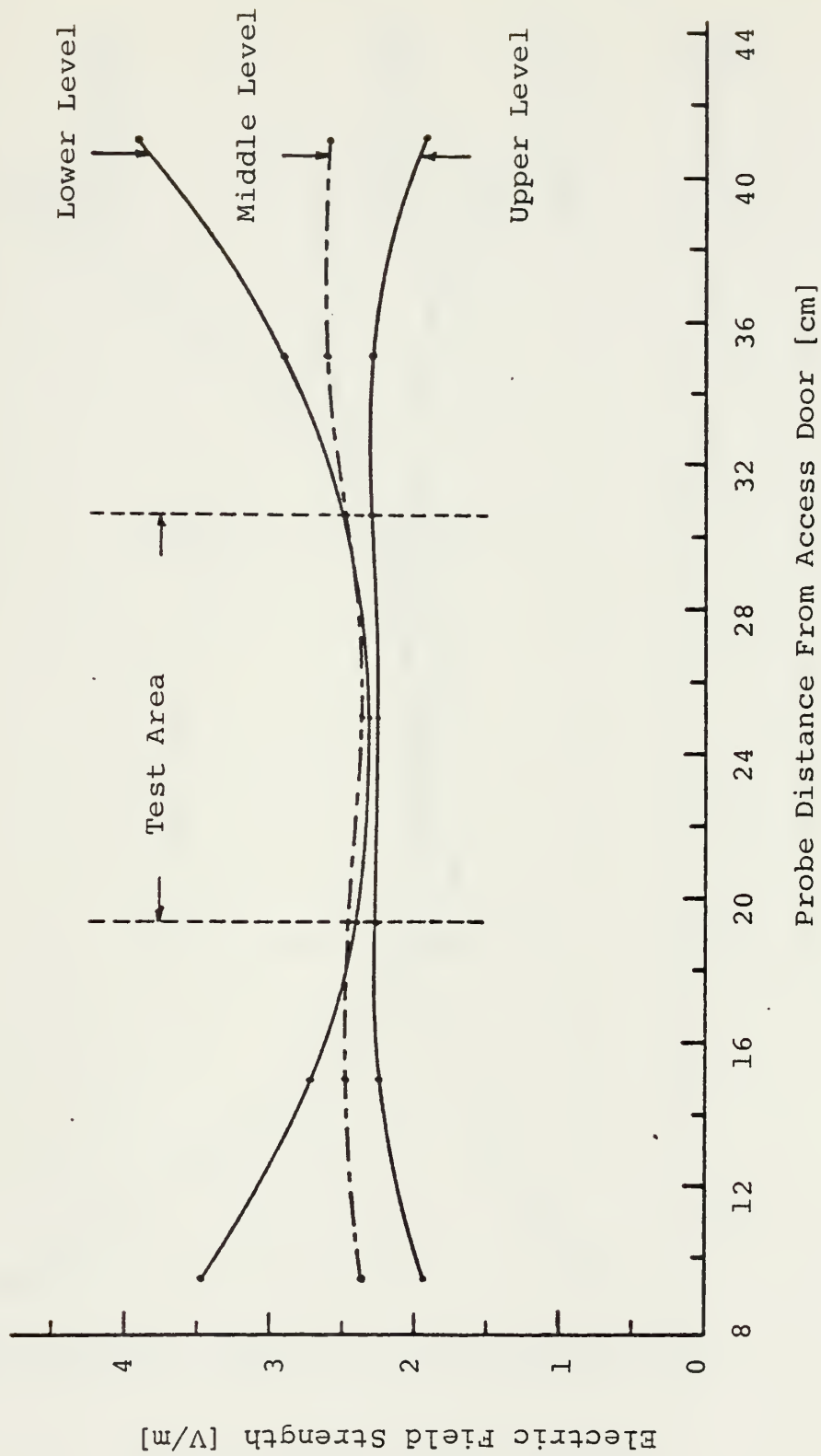


Figure E-6. Electric Field Distribution Inside Absorber Loaded Cell at Frequency 675 MHz ( $E_{cal} = 2.78$  [V/m])



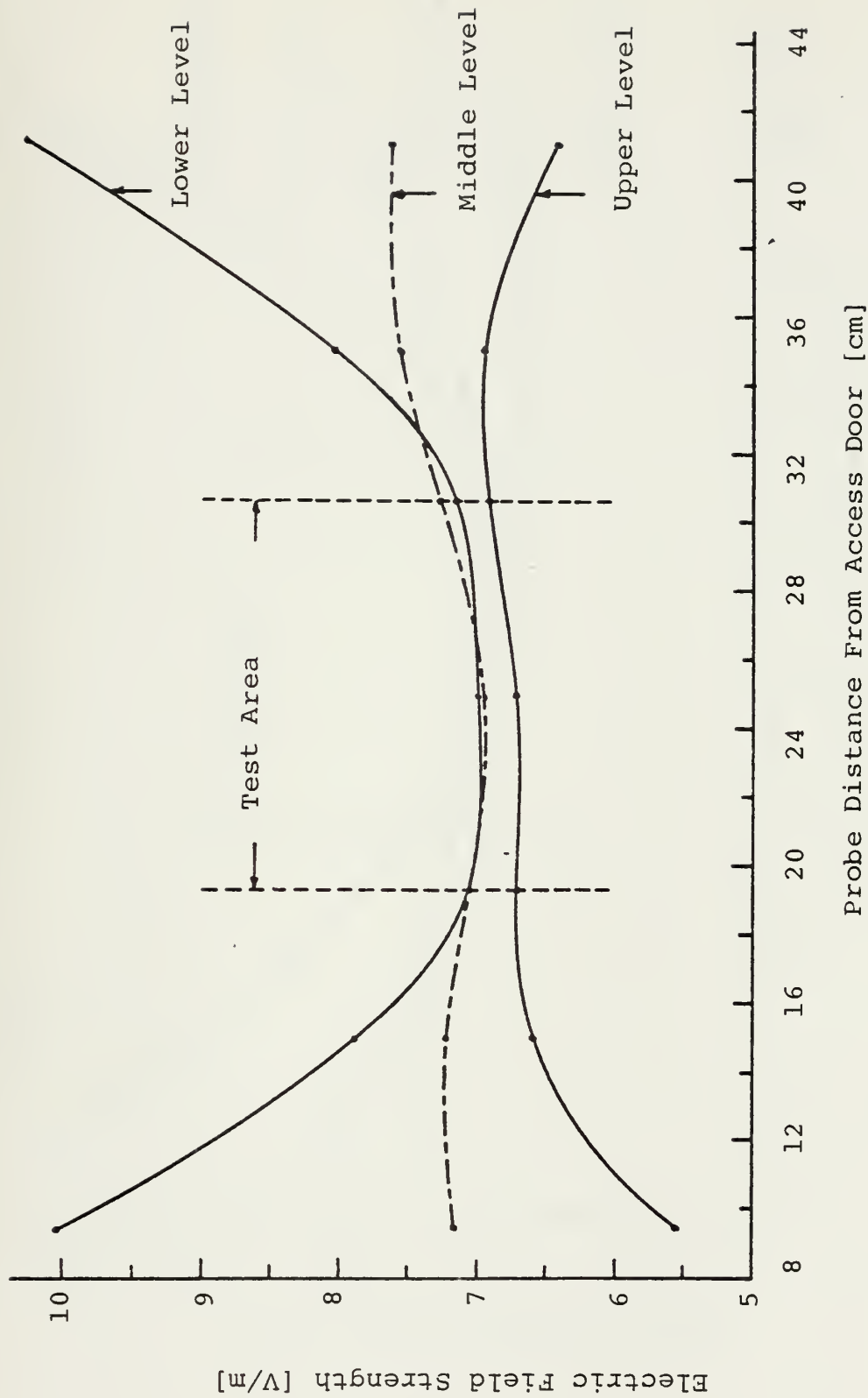


Figure E-7. Electric Field Distribution Inside Absorber Loaded Cell at Frequency 675 MHz ( $E_{cal} = 8.4$  [V/m])



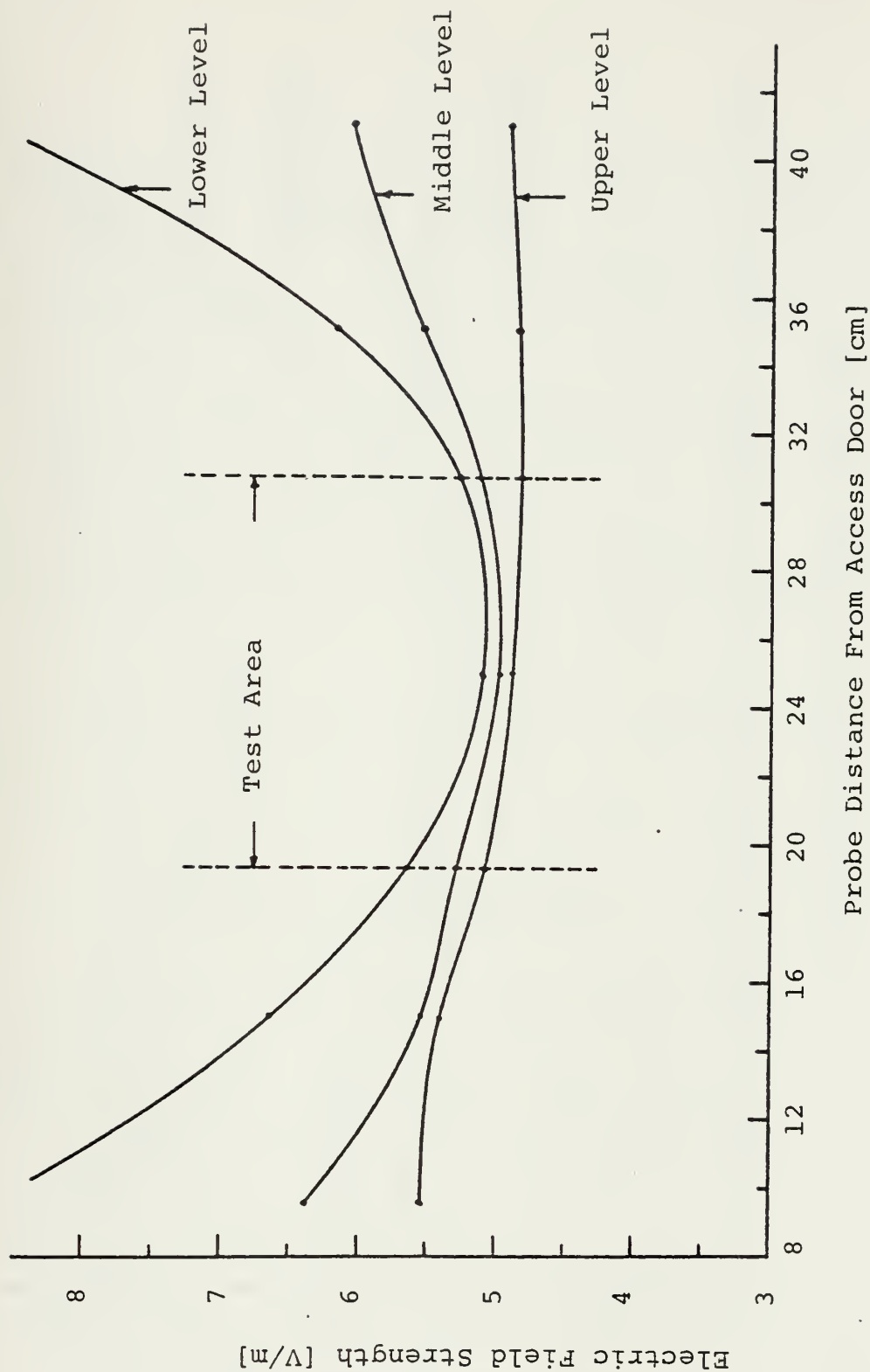


Figure E-8. Electric Field Distribution Inside Absorber Loaded Cell at Frequency 895 MHz ( $E_{cal} = 7.08$  [V/m], Access Door Open)





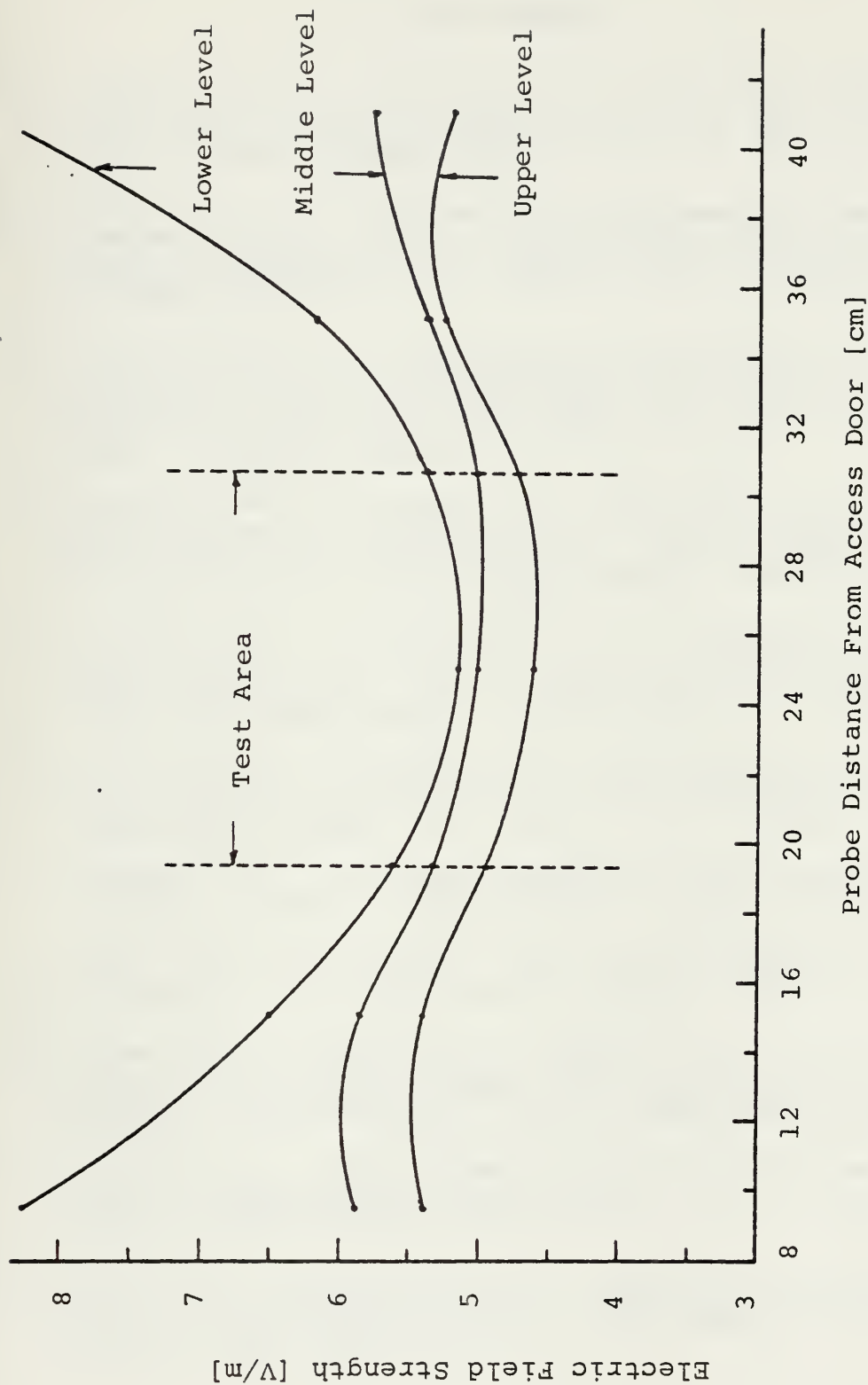


Figure E-9. Electric Field Distribution Inside Absorber Loaded Cell at Frequency 895 MHz ( $E_{cal} = 7.08$  [V/m], Access Door Closed)



## BIBLIOGRAPHY

1. Crawford, M.L., "Generation of Standard EM Fields for Calibration of Power Density Meters 20 KHz to 1000 MHz," NBSIR 75-804, January 1975.
2. Crawford, M.L., "Generation of Standard EM Fields Using TEM Transmission Cells," IEEE Transactions on Electromagnetic Capability, Vol. EMC-16, No. 4, pp. 189-195, November 1974.
3. Crawford, M.L., "Techniques for Measurement of Electromagnetic Radiation and Susceptibility of Electronic Equipment," EMC Symposium Digest, pp. 38-44, Montreux, IEEE 75 CH1012-4 Mont., May 20-22, 1975.
4. Crawford, M.L., Workman, J.L. and Thomas, C.L., "Generation of EM Susceptibility Test Fields Using a Large Absorber-Loaded TEM Cell," IEEE Trans. on Inst and Meas., Vol. IM-26, No. 3, pp. 225-230, Sept. 1977.
5. Crawford, M.L., and Workman, J.L., "Asymmetric Versus Symmetric TEM Cells for EMI Measurements," Conf Report IEEE Inter Symp on EMC, Atlanta, Ga., Jun 20-22, 1972.
6. Crawford, M.L., Workman, J.L., and Thomas, C.L., "Expanding the Bandwidth of TEM Cells for EMC Measurements," IEEE Trans. on EMC, Vol. EMC-20, No.3, August 1978.
7. Varnado, G.B., "The Electromagnetic Environments Simulator (EMES)," SAND 75-0412, November, 1975.
8. Seely, G.A., and Thomas, W.R., "Low Frequency Performance of the EMES Facility," SAI-78-700-AQ, 1978.
9. Brown, R.G., Sharpe, R.A., Hughes, W.L., Post, R.E., Lines, Waves, and Antennas, the Transmission of Electric Energy, Second Edition, 1973, by John Wiley & Sons, Inc.
10. Wheeler, H.A., "Transmission Lines with Exponential Taper," Proceedings of the I.R.E., Vol. 17, pp. 65-71, January 1939.
11. Gent, A.W., and Wallis, P.J., "Impedance Matching by Tapered Transmission Lines\*," JIEE London, Vol. 93, part IIA, pp. 559-563.



INITIAL DISTRIBUTION LIST

	No. Copies
1. Defense Documentation Center Cameron Station Alexandria, Virginia 22314	2
2. Library, Code 0142 Naval Postgraduate School Monterey, California 93940	2
3. Department Chairman, Code 62 Department of Electrical Engineering Naval Postgraduate School Monterey, California 93940	1
4. Hellenic General Navy Staff Department of Education c/o Embassy of Greece Naval Attache 2228 Massachusetts Avenue, NW Washington, D.C. 20008	4
5. Prfoessor Orestes M. Baycura, Code 62By Department of Electrical Engineering Naval Postgraduate School Monterey, California 93940	2
6. Dr. Richard W. Adler, Code 62Ab Department of Electrical Engineering Naval Postgraduate School Monterey, California 93940	10
7. Professor M.L. Wilcox, Code 62Wx Department of Electrical Engineering Naval Postgraduate School Monterey, California 93940	1
8. Professor S. Jr. Jaurequi, Code 62JA Department of Electrical Engineering Naval Postgraduate School Monterey, California 93940	15
9. Dr. M.L. Crawford, Code 723.03 Electromagnetic Fields Division National Bureau of Standards Boulder, Co. 90303	2



- |     |  |   |
|-----|--|---|
| 10. | Professor George Protopapadakis<br>Mitilinis 29<br>Athens, GREECE  | 1 |
| 11. | Professor F.J. Tischer, Code 62Ti<br>Department of Electrical Engineering<br>Naval Postgraduate School<br>Monterey, California 93940 | 1 |
| 12. | LCRD A. Psifias<br>A. Papagou 5<br>Zografou, Athens<br>GREECE  | 1 |
| 13. | Lieutenant Stavros I. Mpoukis<br>Kolokotroni 86<br>Korydallos<br>Athens, GREECE  | 5 |
| 14. | Dean of Research, Code 012<br>Naval postgraduate School<br>Monterey, Ca. 93940   | 1 |





Thesis

M88255

c.1

Mpoukis

186751

Design construction  
and evaluation of a TEM  
transmission cell for  
field probe calibration.

EM

Thesis

M88255

c.1

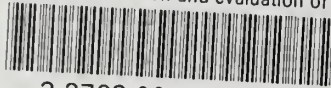
Mpoukis

136751

Design construction  
and evaluation of a TEM  
transmission cell for  
field probe calibration.

thesM88255

Design construction and evaluation of a



3 2768 001 91783 4

DUDLEY KNOX LIBRARY